NTNU
Norwegian University of Science and Technology

Faculty of Natural Sciences and Technology
Department of Chemical Engineering

DIPLOMA WORK 2008

Title: **Engineering Membrane Selectivity for CO_2 Separation**	**Subject (3-4 words):**
Author: **Hanne Skogestad**	**Carried out through:** **February 4 – July 20**
Advisor: May-Britt Hägg **Co-advisor:** **External advisor: Douglas Loy**	**Number of pages** **Hovedrapport: 134** **Bilag: 16**

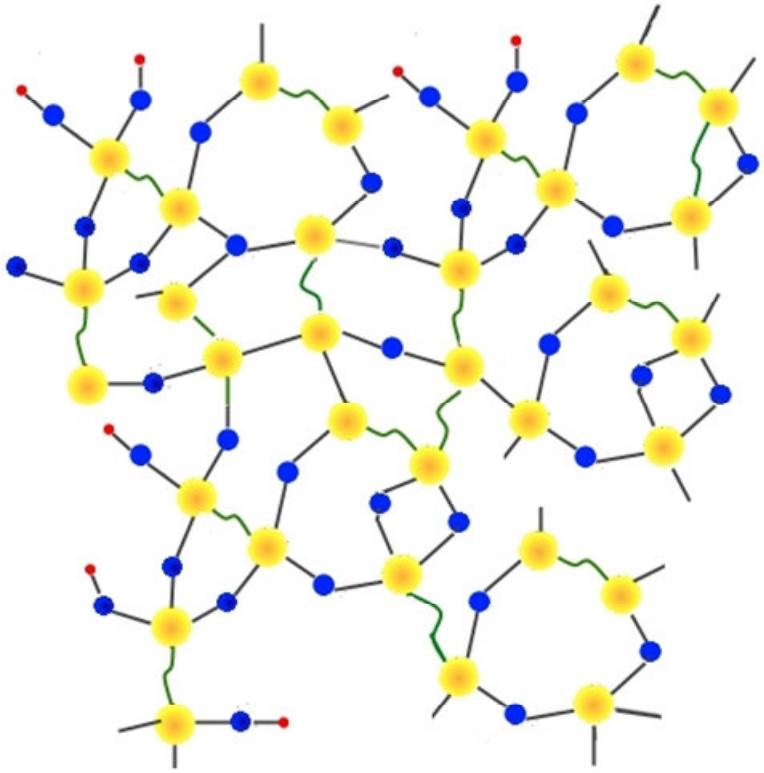

I declare that this is an independent work according to the exam regulations of theNorwegian University of Science and Technology

Date and signature: ...July 20, Hanne Skogestad.....

Abstract

Membrane technology has been ranked the most promising technology for CO_2 capture of flue gases. Bridged polysilsesquioxanes are organic-inorganic hybrid materials prepared by the sol-gel method that in previous studies have shown H_2/CO_2 selectivity in the 1300 range. However, the reproducibility of these membranes has been poorly and an investigation has therefore been conducted the spring 2008 at the University of Arizona at Tucson. The investigation included a study of the sol-gel solutions colloid growth over time, and their behavior at different coating methods. Bridged polysilsesquioxanes were prepared under different conditions and characterized afterwards. Sol-gels were made at different concentrations (0.05, 0.1, 0.2, 0.4, 0.5 and 0.6 M), different catalysts (HCl, NH_3, KOH), and with different solvents (water and tetrahydrafuran,). The sol-gel solutions were characterized by dynamic light scattering, scanning electron microscopy and atomic force microscopy, and the membranes were characterized by using optical microscopy. It was demonstrated that the colloids in the sol-gel solution continuously grow larger over time, until they reach gelation point. The largest particles were produced at the threshold concentration, the concentration at which the sol-gel is allowed to grow for more than one month. It was found that basic catalyst produce cluster of particles where as the acid-catalyzed sol-gels grow in chains. The solvent had no effect of the particle size, however it was established that tetrahydrafuran accelerated the gelation rate. Fluorescent monomer was added to the sol-gel solutions in order to determine if any coating had penetrated the support. Applying fluorescent monomer to the sol-gel solution contributed to the growth rate of the octane-bridged polysilsesquioxane, and also the particles grew larger. Furthermore, the addition of fluorescent monomer reduced cracking when applying the coatings. Spin coating was found to be the most suitable coating technique, and a speed at least of 5000 rpm had to be employed to avoid cracking.

Acknowledgements

My lab partner Zhe Li has been a tremendous help through out this project, not only in the lab but also with ideas and comments on my thesis. I want to thank Mike Keller for his creativity and willingness to always help. A big thanks to Jenny Taubert who always had time to share her thoughts, and to Beatrice Muriithi who helped with the dynamic light scattering and for taking the AFM pictures. Also, Jason Wertz, thanks for your help with the SEM, and for you and Dylan Boday for preparing the fluorescent monomer. An enormous thanks to Dr. Loy, who has helped in the end with the write-up, and for encouraging guidance through the year. At last I want to thank all you others from the Loy research group who has helped me and to Dr. Schrader for being responsible for my visit here.

Table of Contents

List of Tables

List of Figures

1.0 Introduction and motivation

Although there is not universal agreement on the cause, there is a growing agreement that global climate change is occurring, and many climate scientists believe that a major cause is the anthropogenic emission of greenhouse gases (GHGs) into the atmosphere. In 2007, the UN's Intergovernmental Panel on Climate Change (IPCC) concluded with more than 90% certainty that climate changes are mainly caused by human activity [1]. Carbon dioxide (CO_2) is identified to be one of the most important climate gases as the potential of reducing its emissions are huge. IPCC predicts that by the year 2100, the atmosphere may contain up to 570 parts per million per volume (ppmv) CO_2, causing a rise of mean global temperature of around 1.9°C and an increase in mean sea level of 38 meters [2]. The first global effort to reduce GHG has been realized in the Kyoto Protocol. The Kyoto Protocol is an international agreement linked to the United Nations Framework Convention on Climate Change. The key attribute of the Kyoto Protocol is that it sets binding targets for 37 industrialized countries and the European community for reducing greenhouse gas emissions [3]. The goal is to reduce the greenhouse gases with an average of five per cent against 1990 levels over the five-year period 2008-2012. Figure 1.1 represents the six largest emitters of carbon dioxide in 2003 (billions of metric tons).

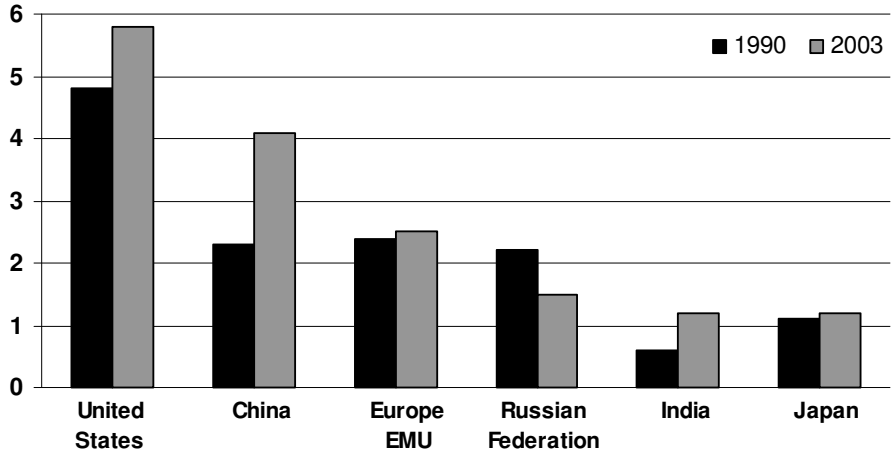

Figure 1.1. Six largest CO_2 emitters in 2003, billions of metric tons.
(Printed with permission from the *World Bank* [4])

If one is to consider carbon dioxide emissions *per capita* the picture is dramatically changed. Figure 1.2. represents the top six CO_2 emitters (billions of ton) when population is taken into account:

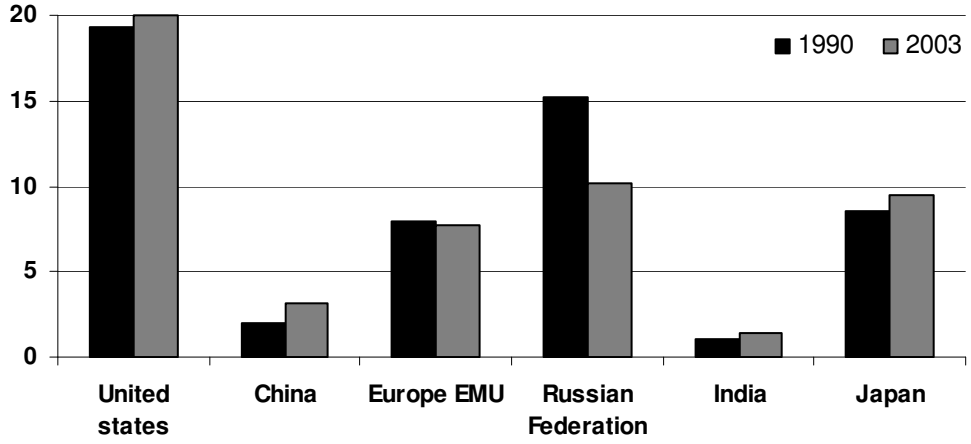

Figure 1. 2. World's six largest CO_2 emitters per capita
(Printed with permission from the *World Bank* [4])

Notably, the two world's largest green house emitters, the United States and China have not ratified the treaty.

Carbon dioxide emissions in industrial countries are mainly caused by the production of electricity and heat, manufacturing and construction, transportation, and other fuel combustion activities as can be seen in Figure 1.3.

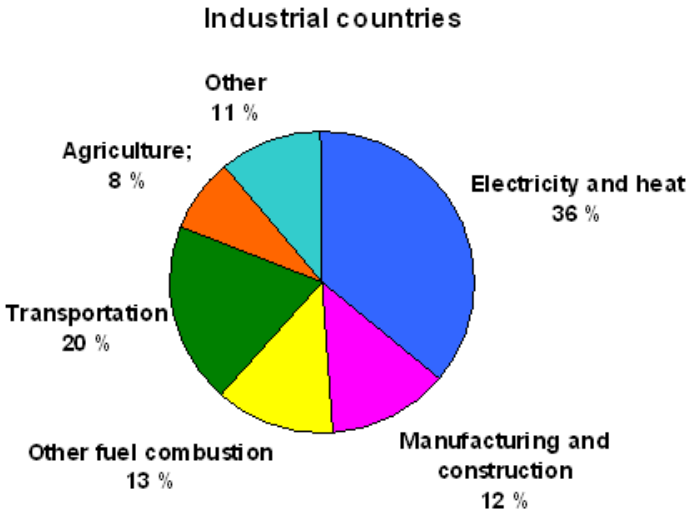

Figure 1. 3 CO_2 emissions by source in millions of metric tons of industrial countries, 2000
(Printed with permission from the *World Bank* [4])

Deforestation and the production of certain agriculture products are mainly responsible for the CO_2 emissions in the developing countries. As the living conditions are improving, electricity and heat generation is also an increasing source of emissions. Figure 1.4 shows the emissions by source for developing countries (2000) in millions of metric tons.

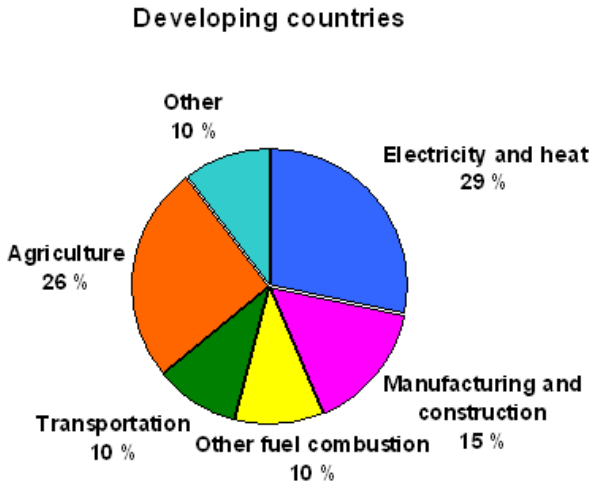

Figure 1. 4. CO_2 emissions by source in millions of metric tons, 2000
(Printed with permission from the *World Bank* [4])

Reducing CO_2 emissions from power plants is vital to reduce global warming, as approximately 30% of the world's emissions come from power plants. There are several existing technologies today, whereas absorption is by far the most used. However, due to the high energy cost associated with absorption, new, alternative solutions are being studied. The next section will focus on CO_2 capture technologies from flue gases.

1. 1 CO_2 removal from flue gases – A comparison of existing and novel technologies

One promising approach for reducing GHG emissions is carbon capture and sequestration (CCS). This concept allows for CO_2 to be captured from large point sources, such as power plants, and injected into geologic formations, for example depleted oil and gas fields, saline formations, and unmineable coal seams [5]. This approach would sequester the CO_2 for thousands of years [6]. One successful CCS project has been going on since 1996 by Statoil, which involves recovering the CO_2 in natural gas from the Sleipner Vest offshore gas field in Norway [7, 8]. The CO_2 is being reinjected it into a nearby aquifer under the North Sea at a rate of one million tons per year and the CO_2 migration is currently being monitored. CO_2 is also being injected into the ground in enhanced oil recovery (EOR) operations worldwide. The most extensive application of EOR is in the Permian Basin of west Texas, USA [9]. It is therefore technically possible to store CO_2 underground, however a geologically suitable location is essential.

CO_2 caption technology can be divided in three categories; Post-combustion, pre-combustion and oxy-combustion. Post-combustion capture involves the removal of CO_2 from the flue gas produced by combustion. For existing power plants which use air for combustion, typically a flue gas that is at atmospheric pressure and has a CO_2 concentration of less than 15% is generated. Consequently, the driving force for CO_2 capture from flue gas is low and creating technologies that are cost and energy efficient is challenging. Pre-combustion involves removing the CO_2 before the fuel is burned. This is done by reforming the natural gas with steam to produce CO_2 and hydrogen [10]. The hydrogen can then be used to produce useful energy or, as done today as feedstock for chemical production. The process is known as the synthesis gas approach and has the

advantage of using technology that is already in wide application, as natural gas reforming is deployed on a huge scale in the chemical industry. In oxy-combustion, the fuel is burned in an oxygen stream that contains little or no nitrogen [11]. This process is desirable as it produces a flue gas containing mostly CO_2 and water, and the water can easily be removed by condensation. A nice review on oxy-combustion has been given by Buhre et al. [12]. The rest of this chapter will focus on post-combustion capture as it has the greatest near-term potential for reducing GHG emissions.

Different methods for post-combustion CO_2 separation includes absorption, pressure- and temperature-swing adsorption, cryogenic distillation, membranes, and several other novel and emerging technologies. The most effective current method for CO_2 separation is absorption [13, 14], due to the well-established technology. Table 1.1 and 1.2 gives a typical flue gas composition for coal and natural gas fired power plants, respectively.

Table 1.1 Typical Untreated Flue Gas Composition from a Power Plant burning Low Sulfur Eastern Bituminous Coal [15]

Component	Concentration (by volume)
N_2	78-80%
CO_2	15-16%
H_20	5-7%
O_2	3-4%
CO	20 ppm
Hydrocarbons	10 ppm
HCl	100 ppm
SO_2	800 ppm
SO_3	10 ppm
NO_x	500 ppm

Table 1. 2. Typical Untreated Flue Gas Composition from a Power Plant burning Natural Gas [16]

Component	Concentration (by volume)
N_2	76%
CO_2	4%
H_20	7%
O_2	13%
CO	
Hydrocarbons	
HCl	
SO_2	0
SO_3	0

While the absorption method is currently the most effective for flue gases separation, the development of polymeric and inorganic membranes for membrane diffusion should result in membrane separation being more efficient than liquid absorption. Other novel methods such as carbonate-based systems, aqueous ammonia, solid sorbents, metal organic frameworks, enzyme-based systems and ionic liquids are emerging technologies that have demonstrated, either in laboratory or in the field, significant improvements in energy efficiency and cost over state-of-the art technologies. However, these methods are new and need to overcome various obstacles before they can be used in industry, which will be further discussed in the next section. All of the methods for CO_2 separation mentioned above can separate CO_2 to a satisfactory degree, depending on the conditions present in the flue gas stream. The challenge then, is to use a process that is cost effective at typical pressure, temperature, and composition of flue gas. Another important term is the energy penalty of capture technology. The energy penalty is defined as the reduction in net power output of the capture plant compared to the reference plant (no CO_2 capture) for equal fuel inputs [17]. In other words, it is how much energy that is lost due to the CO_2 capture, and is an important parameter when comparing different CO_2-capture technologies. Today, it is commonly agreed that not just one technology will be the winning one, but a hybrid system of the most common technologies.

1. 1. 1. Methods for CO_2 separation

Amine Absorption process

The most commonly used CO_2 separation technology, and the state-of-the-art technology, is amine absorption. In the CO_2 amine absorption processes, an amine is used that reacts with CO_2, but not with any other components of the flue gas stream. Amines react with CO_2 to form water soluble ammonium carbonate, thus the process is able to capture CO_2 from streams with a low CO_2 partial pressure, but due to absorption thermodynamics, the capacity is limited. Some commonly used amines are monoethanolamine (MEA) and methyldiethanolamine (MDEA). The carbonate solution is typically pumped to a regeneration column, where the CO_2 is reheated and moved from the solution. The energy demand of the physical absorption process is predominantly due to compression of gas and pumping of solvent [15]. Chemical absorption processes need heat for regeneration, which strongly depends on type of solvent and solvent concentration in the aqueous solution.

Advantages to Absorption

The amine for CO_2 separation can be regenerated and recycled, thus reducing the cost of material. Also, the separated CO_2 stream from the regeneration column is of high purity. An exact percentage is not reported, but most amine absorption processes deliver a stream with purity higher than 95%. Another advantage offered by absorption is the need for human operators is minimized. Continuous monitoring and automation is sufficient, and proper instrumentation and surveillance [18] minimize labor cost. Yet another advantage to amine absorption is that it is so well known, and promising new solvents are currently being developed.

Disadvantages to Absorption

While absorption does have strong advantages the total cost (including addition of new solvent and other operating and maintenance costs) is relatively high, about \$14/ton CO_2 separated [19]. It imposes an energy penalty of 25% to 37% on power plants burning coal [20], and in addition to high regeneration costs, approximately 1. 6 kg of solvent are lost for each ton of CO_2 separated [18]. Also, a solvent that meets the Norwegian Pollution Control Authority (Statens forurensnings tilsyn, SFT) requirements is yet to be found. Today, there is no solvent that meets both the specifications of high purity separation and environmental friendliness. Improvements to amine-based systems for post-combustion CO_2 capture are being pursued by a number of process developers; Fluor [21], Mitsubishi Heavy Industries (MHI) [22], and Cansolv Technologies [23]

Adsorption

In adsorption processes one or more components of gas or liquid stream are adsorbed on the surface of a solid adsorbent (i.e. carbon fiber composite molecular sieve (CFCMS) or a solid amine sorbent, HCS^+ (thioformyl ion)) and a separation is accomplished. Due to interactions between CO_2 and the sorbent, CO_2 molecules are attracted and trapped by surface groups of the sorbent. Many solids have the capability to selectively adsorb CO_2 into small cracks, pores, or just onto their external surfaces under specific temperature and pressure conditions. The two main methods for adsorption are pressure swing adsorption (PSA) and temperature swing adsorption (TSA). It has been established that PSA is superior to TSA due to its lower energy demand and higher regeneration rate [24].

Advantages to Adsorption

Adsorption only requires vessels capable of withstanding small pressure changes. Unlike competing technologies, adsorption does not suffer from corrosive solutions like the amines, neither does it need to withstand large temperature changes, like cryogenic processes. Also, the energy cost for adsorption is approximately \$7/ton CO_2 removed at CO_2 concentrations of 28–34 mole %. However, the cost is approximately four times

greater with lower concentrations of CO_2 (10–11.5 mol%), typically found in flue gases [19].

Disadvantages to Adsorption

Due to the fact that adsorption operates best under low concentrations of CO_2 (i.e. between 0.04% and 1.5% [25]), the process is unfavorable as a stand-alone since most power plants have higher concentrations of CO_2, approximately 15% [26].

The second drawback for adsorption is that available sorbents are not selective enough for CO_2 separation from flue gases. Because the sorbents' ability is usually based on pore size, gases smaller than CO_2 can also penetrate the pores. N_2 is the gas that most commonly fills up pore space in sorbents. For some types of adsorbents, this facilitates the adsorption process, but only up to a point. When the pores are full (blocked), CO_2 cannot effectively interact with sites located within the adsorbent [27]. Research to develop sorbents capable of selectively binding CO_2 is underway [28].

Another drawback is that adsorption is slow. For typical materials, the residence time for maximum adsorption depends on the sorbent, but 20 minutes is a reasonable estimate [29]. When dealing with large volumes of flue gas, as in a power plant, this is too slow to be practical.

Despite these disadvantages, physical adsorption can play a satisfactory role in a hybrid system. Since it requires a low concentration of CO_2 for optimum performance, it could be placed after another separation process.

Membrane Diffusion

Membranes can be inorganic, polymeric, solid or liquids [30]. Industrial applications are currently dominated by polymeric membranes. However, new applications such as fuel cells, membrane reactors and other high-temperature separation have resulted in the accelerated development of inorganic membranes.

Inorganic or polymeric membrane separation processes are expected to be more efficient then conventional CO_2 separation processes due to their low energy requirements. In a power plant, the flue gases are sent at atmospheric pressure into a chamber that is divided

by a membrane; the CO_2 passes through the membrane into another part of the chamber where it is collected at a lower pressure (typically 10% of the feed pressure).

Advantages to Membrane Diffusion

Membrane separation processes provide several advantages over other conventional separation techniques [31]. First, the membrane process is a feasible energy-saving alternative for CO_2 separation, since it does not require any phase transformation. Second, the necessary process equipment is very simple with no moving parts, compact, relatively easy to operate and control, and also easy to scale-up. When it comes to simplicity, membranes are by far the superior of existing technologies. While pressure swing adsorption (PSA) requires the equipment for swinging pressure and cryogenic distillation must endure extreme temperatures, the only equipment necessary for membrane separation is the membrane and a compressor. The flue gases must be compressed before separation, but this compression is much smaller than that necessary for PSA. Membranes require no additional chemicals in contrast to absorption, and it has no energy efficiency limitations (i.e. azeotrops). Another big advantage is that membranes offer an easy scale up and high process flexibility, as membranes modules can be added in parallel.

Disadvantages to Membrane Diffusion

The biggest challenge with membranes is the limited experience that is offered today due to the fact that gas membranes are of new technology. Also, up-scaling represents a linear relationship between energy requirement and CO_2-removal as opposed to amine absorption. The problem with membrane technology for removing flue gases is that the flue gases enter the membrane unit at atmospheric pressure. To obtain the requirements of purity that industry require, a large amount of energy is needed for vacuuming the permeate. In fact, if a CO_2 purity of 99% is needed, membrane technology will not be able to compete with state-of-the-art absorption technology. An alternative to pressurizing the flue gas it to position the membrane directly after the combustion chamber. Inorganic membranes can handle the high temperature and pressures that occur after the combustion chamber, however these membranes are also much more cost extensive.

Also, flue gases contain sulfates, particles and water which must be removed prior to the membrane unit. Another challenge is to obtain high selectivity and permeability for CO_2. Currently, it is a trade-off; membranes that are very selective are not very permeable, while permeable membranes allow other gases besides CO_2 to permeate, requiring a secondary separation.

Many organic membranes do not perform well at high temperature which is typical of flue gases exiting the stack. High resistant polymers can be applied up to a temperature of 400°C [32], or at best 600°C [33], however inorganic membranes can resist temperatures as high as 4000°C [32].

Conventional polymeric membranes consisting of either thin, nonporous polymeric membranes or microporous membranes have not demonstrated both high selectivity and economically feasible permeability [34]. Sandia National Laboratory studied the separation properties of bridged polysilsesquioxanes with various bridging groups, spray coated on alumina supports. The membrane showed selectivity in the 1300 range (single gas tests) for H_2/CO_2 and H_2/CH_4, and good permeability was also obtained. The bridging group act as facilitated transport agents and may selectively permeate CO_2 by means of a reversible reaction of CO_2. Other gases, such as nitrogen and methane, will permeate exclusively by the solution-diffusion mechanism. However, good reproducibility has not obtained with these membranes which has been the purpose for this master thesis conducted at the University of Arizona, Tucson during the spring 2008 (see Appendix 1 for full project description). This research has been focused on preparing hybrid organic-inorganic films bearing amine or urea functionalities in organic bridging groups as carbon dioxide selective membranes. This project investigated bridged polysilsesquioxanes [35] (Figure 1.5) because their intimate mixing of organic and inorganic phases at the molecular level permit fundamental studies in structure property relationships to be performed. Sol-gel polymerization chemistry of amine, urea and hydrocarbon bridged polysilsesquioxanes were investigated as means to asymmetric coatings.

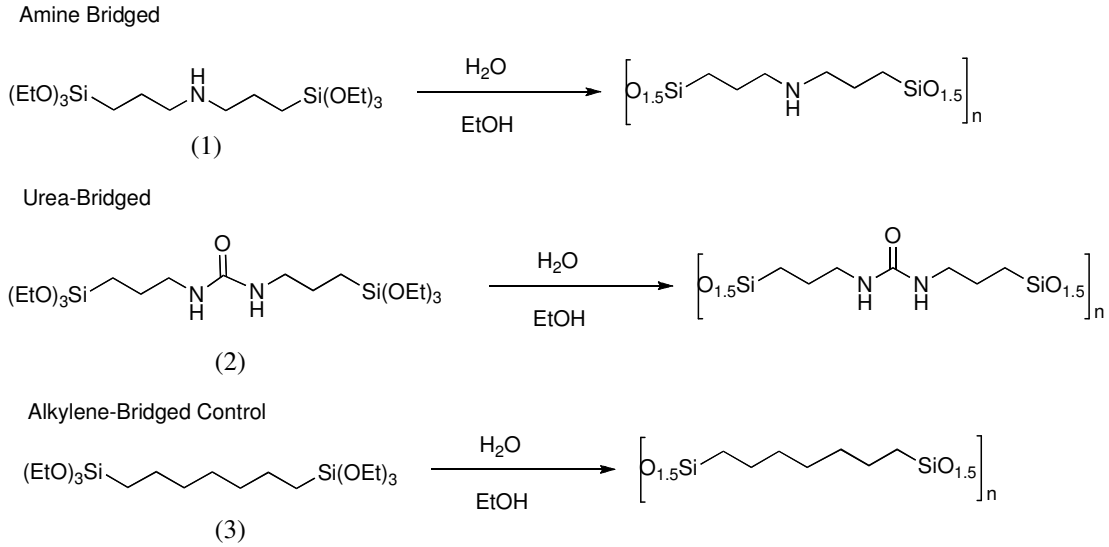

Figure 1. 5. Sol-gel polymerization of bridged monomers (1-3)

Because the bridged polysilsesquioxanes are highly cross-linked materials, their membranes are too brittle without some support. Therefore, the bridged polysilsesquioxanes were prepared on porous zirconia and alumina membranes. The size of the bridged colloids as a function of polymerization pH, monomer concentration and monomer type was monitored over time with dynamic light scattering, to make sure that good reproducibility of the membranes were obtained. In order to ensure that the membrane was located only on top of the support, the hybrid colloid was prepared with a small amount of a fluorescent co-monomer (Figure 1.6). Any material that had penetrated into the support would show up when exposed to ultraviolet lighting. Microscopic inspection of the cross-sections was also preformed to detect destructive characterization.

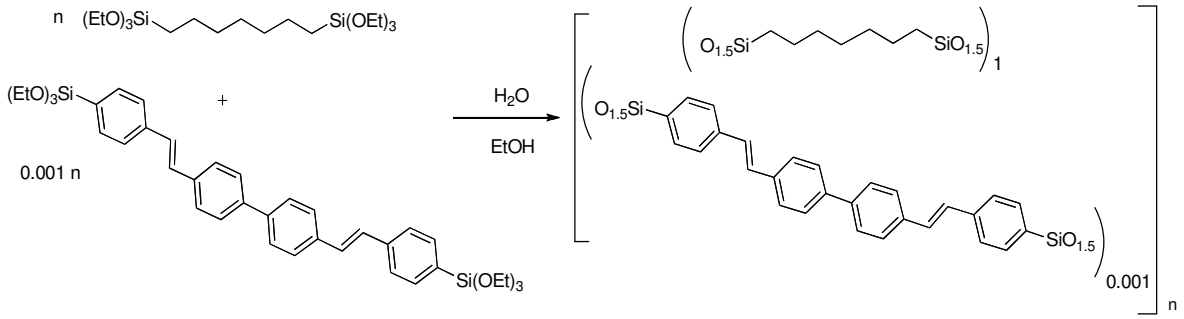

Figure 1.6. Sol-gel polymerization of colloid with blue fluorescent dye bridged monomer to image hybrid thin film in asymmetric membranes.1+

The next section will involve emerging technologies which have demonstrated, either in laboratory or in the field, significant improvements in efficiency or/and cost over state-of-the-art technologies. A good survey has been given by Figueroa and al. [36]

Cryogenic Distillation

To perform cryogenic separation, all components of the flue gas except for N_2 and CO_2 have to be removed prior to cooling. When all other gases and particulates are completely removed, the remaining gas is sent into a cryogenic chamber where the temperature and pressure are at such conditions that it causes the CO_2 to liquefy. Under the right pressure and temperature conditions, CO_2 will condense while N_2 remains as a gas. This distillation allows N_2 to escape through an outlet at the top of the chamber while the highly concentrated liquid CO_2 can be collected at the bottom of the chamber [37].

Advantages and Disadvantages to Cryogenic Distillation

The advantage of cryogenic distillation is that it produces liquid CO_2, immediately ready for transport via pipeline or tanker for sequestration. Also, the CO_2 recovery is very high and a CO_2 purity after distillation can exceed 99.95% [38].

However, the cryogenic process is extremely energy intensive. The energy required to keep the system cool makes the current process cost ineffective. Another factor is that the cryogenic process cannot be used alone as NO_X, SO_X, H2O, and O_2 must all be removed from the flue gas prior to the CO_2 separation. The cost for cryogenic distillation is predicted by lab-scale experiments to be approximately \$33/ton CO_2 separated (7). This can be compared to the absorption cost of \$14/ton CO_2 removed and adsorption's \$28/ton CO_2 (as stated previously).

Cryogenic distillation is quite new and has room for improvement and optimization. Lowering the energy required and eliminating the limitations of the process is in focus of current research.

Hydrate Formation and Dissociation

Hydrates are structures in which water forms a cage with cavities where small gases such as CO_2 can be trapped. The structure resembles ice, and hydrates are formed over 4 atm and below 10°C [13]. One method for separating CO_2 from flue gases is to use hydrate formation separation. A maximum of 8 CO_2 molecules can be trapped in a cage of 46 water molecules. This gives a fraction of CO_2/H_2O of 0.148 but a weight fraction of 0.31 g CO_2/g H_2O [39]. Water readily forms hydrates with CO_2 and allow the waste gases to escape.

The advantage to using hydrate formation for separating CO_2 from flue gas is that it may not be more energy intensive than traditional technology (chemical absorption, PSA, etc.). In fact, this technology has shown to have an energy penalty as small as 6% to 8% and the U.S. Department of Energy (DOE) considers this the most promising long-term CO_2 capture technology identified to date [20]. Furthermore, the hydrates can be easier to transport than CO_2 gas.

Due to the requirement of very high pressures (~ 88.8 atm [13]), the hydrate formation technology is not yet feasible. In addition, the flue gas must be at 8°C, which means an additional amount of energy is needed. Hydrates are known to plug pipelines in natural gas transport, and there is a risk that hydrates will plug the equipment in a power plant. Mechanisms to prevent hydrate plugging must be set in place for this method to function properly in a plant application. The hydrate separation could also highly benefit from increasing the conversion rates, as the highest rate obtained so far is approximately 35%. Better heat transfer could increase the efficiency of hydrate separation. Other major areas of improvement are how to remove the heat of formation and how to keep a steady flow despite multiple phases (liquid CO_2, hydrate, liquid water, and ice) [40].

Carbonate-based systems

Carbonate systems are water-soluble carbonates which react with CO_2 to form bicarbonates, that when heated, reverts back to CO_2 and carbonate. The University of Texas at Austin is developing a system based on K_2CO_3, in which the capacity of the solvent is enhanced with catalytic amounts of piperazine (PZ) [41, 42]. This system has an absorption rate 10-30% faster than a 30% solution of MEA and exhibit favorable

equilibrium characteristics. It has shown to have a 5% lower energy requirement with a higher loading capacity of 40% vs. 30% for the MEA system.

Aqueous ammonia

Ammonia and its derivatives react with CO_2 via various mechanisms [43], one of which is the reaction of ammonium carbonate, CO_2, and water to produce ammonium bicarbonate (equation 1.1). Since this reaction has a lower heat of reaction than the amine-based system, energy savings can be made in the regeneration process. Other advantages include high potential for CO_2 capacity, lack of degradation during absorption/regeneration, tolerance to oxygen in the flue gas, and the ability for regeneration at high pressures. Also, there exists a possibility to simultaneously remove CO_2, SO_2, NO_x, plus HCl and HF that may exist in flue gas. However, there are concerns about ammonia's high volatility, and the flue gas must be cooled to the 15-27° C range to enhance the CO_2 absorption of the ammonia and, to avoid vapor emissions during the absorption process. There are also concerns that ammonia will be lost during regeneration. Further investigations include process optimization to increase CO_2 loading and the elimination of ammonia vapor losses during operation.

$$H_2O + CO_2 \rightleftharpoons H_2CO_3 + NH_3 \rightleftharpoons NH_4HCO_3 \overset{NH_3}{\rightleftharpoons} (NH_4)_2CO_3 \qquad (1.1)$$

Metal Organic Frameworks

A new class of hybrid materials built from metal ions and organic bridging ligands which exhibit well-defined coordination geometry, are known as metal organic frameworks (MOFs). The structures are built with carefully sized cavities that can adsorb CO_2 and have shown higher CO_2 storage capacity than both zeolites and carbon materials [44]. Also, the heat required for recovery for the adsorbed CO_2 is low. Over the last years, numerous MOFs with different chemically and structally properties have been developed, one of the most promising one being from the National Energy Technology Laboratory

(NETL) [45]. There remain further investigations of the stability over thousand of cycles and the effect of impurities at typical flue gas temperature and pressure.

Enzyme-based systems

Living systems have the capacity to capture CO_2 which is the basis for enzyme-based systems. By mimicking the mechanism of mammalian respiratory systems, CO_2 capture can be achieved. One process developed is the hollow fiber contained liquid membrane (HFCLM) configuration with carbonic anhydrase (CA) [46] where CO_2 is transported across the membrane as HCO_3. CA (a biocatalyst) is contained in a hollow fiber liquid membrane and has demonstrated a potential removal of CO_2 of 90% at laboratory-scale. Some technical challenges exists; pore wetting, surface fouling, loss of enzyme activity, long-term operation, and scale-up, all which are currently being addressed.

Ionic liquids

Ionic liquids (IL) include a broad range of salts, normally containing an organic cation and either an organic or inorganic anion. They can dissolve gaseous CO_2 and are stable up to several hundreds Celsius. Their ability to handle high temperatures makes it possible to recover CO_2 from flue gases without any cooling, also, the these are physical liquids so small amounts of heat is required for regeneration. ILs can have high viscosities which can be an issue in practical applications, also ionic liquid cleanup after extraction is a key area of need for further work [47], as many ILs are toxic. Also, the present cost of the ILs is too high for commercial applications [48].

1. 1. 2. Ranking of Technologies

A survey completed by Aaron et al. [49] ranked membranes as the most promising individual method for CO_2 separation of flue gases. The same conclusion was also drawn by Gottlicher et al. [19] in a survey where 300 articles on CO_2 removal from fossil-fuelled power generation systems were reviewed, comparing 60 different alternatives for CO_2 capture in power plants. A recent review prepared by Yang and coworkers [44] have come to the same conclusion. The decision is based on the fact that membranes require little energy for operation, are space-saving, and metallic and ceramic membranes

can handle high temperatures and do not need a cooler after the combustor chamber. Also, membrane separation units are predicted to be easy to integrate into existing power plants, allowing current plants to remain in operation. The only drawback to membranes such as described by Aaron et al. is that they are still at the research and development stage, and also no material has been found to operate at the high temperatures from a combustion chamber. Since membrane technology is highly dependant on the process, the cost is largely unknown.

Furthermore, Aaron et al. conclude that the second most promising process is absorption. The conditions are relatively easy to meet for absorption and regeneration, causing the energy penalty to be fairly low. Since absorption is a well-established process, much is known about it, guiding further research and improvement. Developing new solvents that are resistant to degradation and not corrosive to the equipment are necessary. Also, easier regeneration and faster loading are issues to be resolved prior to the industrial use of absorption. Aaron et al. recognize that absorption could be the preferable method for separating CO_2 if the Mitsubishi [40] and Econamine FG processes are as efficient in application as they have been in pilot testing. At last, the authors recognize that a hybrid system will probably be the best solution for the future. One system developed by Pederson et al. [50] is a concept where the flue gas will be passed through a bundle of membrane tubes while an amine solution flows through the shell side of the bundle. In this case CO_2 will pass through the membrane and be absorbed in the amine, while impurities will be blocked from the amine. In this way the amine loss will be decreased as a result of a stable salt formation. Whether membrane separation can stand alone as a CO_2 capture process for flue gas or whether it may have to be part of a hybrid separation system remains to be investigated further.

2. 0 Membrane Types and Transport Mechanisms

The scope of this chapter will be on the various transport mechanisms in membranes followed by a classification of different membranes.

A membrane may be defined as a permselective barrier between two homogeneous phases [51]. The membrane acts as a semi-permeable barrier and separation occurs due to the membrane control over the rate of movement of various molecules between two liquid phases, two gas phases, or a liquid and a gas phase (Figure 2. 1)

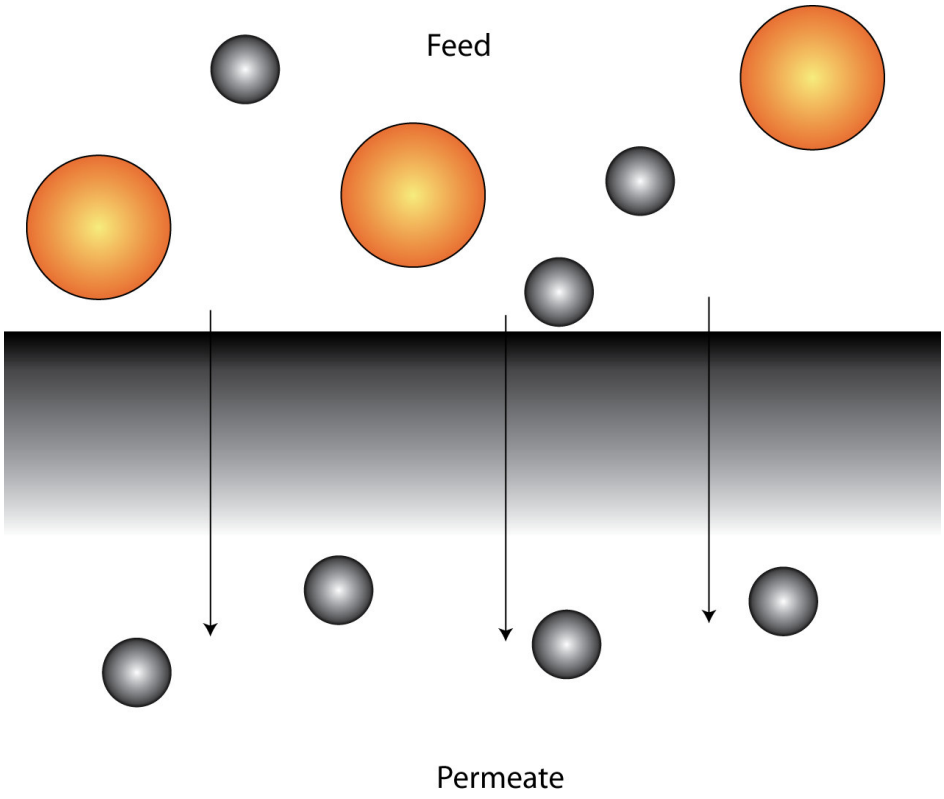

Figure 2. 1. Cartoon of a membrane

Important membrane terminology includes feed, permeate, retenate, selectivity, permeability and permeance. The upstream side is considered the feed, and membranes

are characterized by the fact that the feed stream is divided into two streams, the retenate and the permeate, where the permeate side is the downstream.

For a mixture consisting of components A and B the selectivity factor is given by the concentrations of A and B in the permeate over the concentration of A and B in the feed (equation 2.1)

$$\alpha_{A/B} = \frac{y_A / y_B}{x_A / x_B} \qquad (2.1)$$

Permeability (P), or more precisely permeability coefficient, is a partial-pressure and thickness-normalized productivity of a polymeric gas separation membrane (eq. 2.2)

$$P = J \times l \qquad (2.2)$$

where J is the gas flow per unit pressure and l the membrane thickness.

Permeance is closely related to the permeability, however, permeance, has only partial-pressure normalized flux. It should be mentioned that there exists a disagreement in the membrane field weather to use permeability or permeance when discussing membrane productivity [52].

2. 1 Transport in membranes

A molecule is transported across a membrane due to a driving force acting on it. Two main driving forces are important in membrane processes, the chemical potential difference and the electrical potential difference. The extent of the force is determined by the difference in potential across the membrane (ΔX), divided by the membrane thickness (l):

$$\text{Driving force} = \frac{\Delta X}{l} \qquad (2.3)$$

Particles are transferred from a high potential region to a low potential region until an equilibrium is reached, which is known as passive transport. To keep a constant flow though the membrane, an external force needs to be applied to the system. There exists a proportionality relationship between the flux (J) and driving force (X):

Flux (J) = proportionality factor (A) * driving force (X) (2.4)

where A is a measure of the resistance exerted by the membrane when a given force is acting on this component.

For a gas separation process assuming perfect mixing, pressure is the driving force and the transport depends on the diffusivity of the gas through the membrane (D_{AB}) and the solubility of the gas (S). The resistance is a function the membrane thickness. The combination of the diffusivity and the solubility is known as the permeability of the gas, P_i. The flux (J) is given by the Fickian diffusion equation, eq. 2.5 [51]

$$J = \frac{D_{AB}S}{l}(x_{r,i}p_h - x_{p,i}p_l) = \frac{P_i}{l}(x_{r,i}p_h - x_{p,i}p_l) \quad (2.5)$$

where p_h is the pressure on the feed side (high pressure), p_l is pressure on the permeate side (low pressure), x_r and x_p are the fractions of component *i* on the feed and permeate side, respectively.

2. 1. 1 Transport of gases through porous membranes

Gas transport through porous membranes may occur via different mechanisms (Figure 2.2). A brief description of the commonly occurring mechanisms is given below:

(a)Molecular diffusion (convective flow): In molecular diffusion, the mean free path of the gas molecules is smaller than the pore size [53]. Gas molecules collide exclusively with each other and seem to ignore the existence of the membrane. Diffusion occurs primarily through molecule–molecule collisions and no separation is obtained between the gas components [51]. The driving force is the composition gradient. If a pressure

gradient is applied in such pore regimes, laminar flow occurs, as given by Poiseuille's equation. Such transport is often referred to as Poiseuille flow or viscous flow [53].

(b) *Knudsen diffusion*: When the mean free path of the gas molecules is greater than the pore size, Knudson diffusion is dominant. In such situations the collisions of the molecules with the pore wall are more frequent than the collisions among molecules. Separation selectivities with this mechanism are proportional to the ratio of the inverse square root of the molecular weights [51].

(c) *Surface diffusion*: Surface diffusion occurs when the permeating species exhibit a strong affinity for the membrane surface and adsorb along the pore walls. In this mechanism, separation occurs due to differences in the degree of adsorption of the permeating species. Surface diffusion often occurs in parallel with other transport mechanisms such as Knudsen diffusion [54, 55]

(d) Capillary condensation: Capillary condensation is one form of surface flow where one of the gas components is a condensable gas. At certain pressures, the pore gets completely filled by the condensed gas. Due to the formation of menisci at both ends of the pore, transport can take place through hydrodynamic flow driven by capillary pressure difference between the two ends. In theory, capillary condensation can be used to achieve very high selectivities, as the formation of the liquid layer of the condensable gas will block and prevent the flow of the non-condensable gas [56-58].

(e) *Molecular sieving*: When the pore size becomes comparable to the molecular size, separation occurs due to the fact that some molecules are too big to pass through the pores. This type of diffusion is a strong function of molecular shape and size, pore size, and interactions between the pore wall and gas molecules. This type of mechanism is dominant in microporous zeolite membranes and carbon molecular sieves [54, 57].

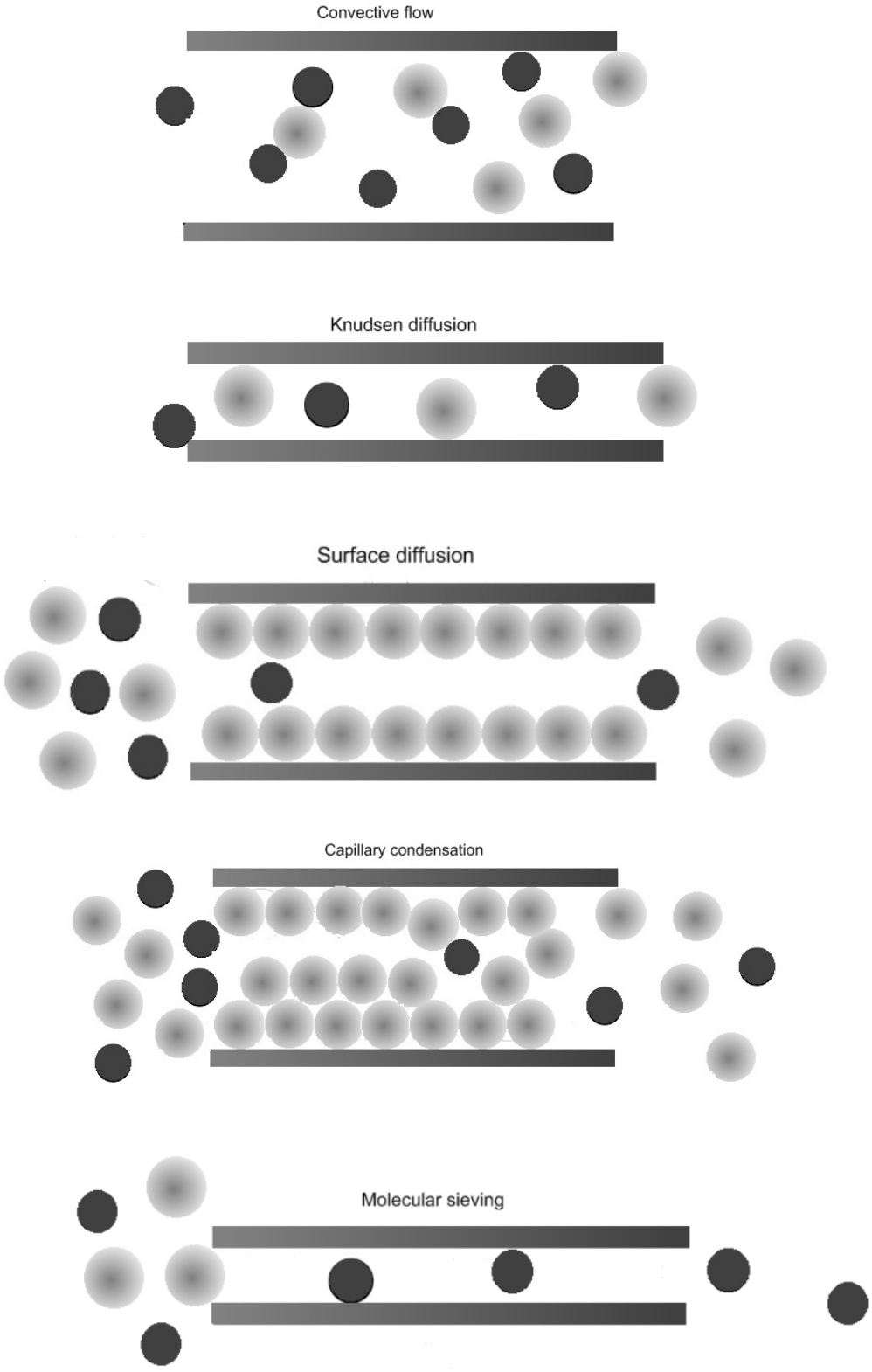

Figure 2. 2. Different types of transport in porous membranes

2. 1. 2 Transport of gases through dense membranes

When the sizes of molecules are in the same order of magnitude, porous membranes cannot be used to achieve separation as the separation mechanism is based on different sizes of the molecules. Instead, dense membranes must be applied. The transport of gas in a nonporous membrane can be described in terms of the solution-diffusion mechanism

Permeability (P) = Solubility (S)*Diffusivity (2. 6)

The solution-diffusion is widely accepted to be the main mechanism of transport in dense membranes [31, 54, 59]. This mechanism is generally considered to be a three-step process. In the first step the gas molecules are absorbed by the membrane surface on the upstream end. This is followed by the diffusion of the gas molecules through the material matrix. In the final step the gas molecules evaporate on the downstream end. For ideal systems, the solubility is independent of the concentration and the sorption isotherm is linear (i.e. Henry's law). This is a common feature for elastomers. For glassy polymers, the solubility of gas often deviates from Henry's law and the sorption isotherm is described by the dual sorption theory. The dual-sorption theory is a combination of Henry's law and Langmuir expressions [51].

2. 1. 3 Fixed site carrier membranes

Another form of passive transport is "facilitated" transport or "carrier-mediated" transport. In this case the transport of a component across a membrane is enhanced by the presence of a mobile or fixed carrier. The carrier interacts specifically with one or more specific component in the feed and an additional mechanism results in an increase in transport. In facilitated transport, components can be transported against their chemical potential gradient. In this case transport proceeds in a co-current or counter-current fashion, with the driving force being the chemical potential gradient of the second component. Another way a component can be transported against its chemical potential gradient is when energy is added to the system, for example by means of a chemical reaction [51]. The total flux of a permeant A will be the sum of Fickian diffusion (Eq. 2.5) and the carrier-mediated transport [60]:

$$J_A = \frac{D_A}{l}(c_{A,0} - c_{A,l}) + \frac{D_{AC}}{l}(c_{AC,0} - c_{AC,l}) \qquad (2.\ 7)$$

$$c_A = S_A p_A \qquad (2.\ 8)$$

The first term in the equation (2.7) is the Fickian diffusion (D_A) and the second term represents the carrier mediated diffusion (D_{AC}). The concentrations of component A and the carrier are denoted c_A and c_{AC}, respectively, where 0 represents the feed side and l the permeate side.

Facilitated transport membranes for gas separation was first introduced by Ward and Robb by impregnating the pores of a microporous support with a carrier solution [60]. The membrane demonstrated excellent separation abilities, with a separation factor of 1500 reported for CO_2/O_2. However, serious problems have been detected with the carrier-mediated membrane; Degradation problems such as the loss of the carrier component due to evaporation or entrainment with the gas stream additionally the carrier can become deactivated. To overcome these problems the use of ion exchange membranes as support has been introduced. To solve the stability problem further modifications have been added. By introducing carriers directly into polymer membranes, the carriers are covalently bonded with the polymer and problems with evaporation and entrainment are resolved. This results in a lower mobility of the carriers, but the fixed-site-carriers (FSC) are favorable when stability is considered. A method to improve the mobility and efficiency of the FSC membrane has been attained by the introduction of water swollen FSC membranes. The diffusivity of a swollen FSC membrane shows diffusivities between that of a mobile and fixed carrier.

2. 2 Types of Membranes

Membranes can be classified by nature, i.e. biological or synthetic membranes. The two types differ completely in structure and functionality [51]. The scope of this section will be on synthetic membranes, which further can be divided into organic (polymeric or liquid) and inorganic (glass, ceramic, metal, molecular sieves and mixed matrix) membranes.

Another way of classifying membranes is by morphology or structure. The membrane structure determines the separation mechanism and hence the application. The solid synthetic membranes can be divided into symmetric and asymmetric membranes, and both categories can be subdivided into dense or porous. The separation through a dense membrane is dependent on the solution/diffusion or the facilitated transport mechanism. The separation in porous membranes is either a result of Knudsen diffusion, surface diffusion, molecular sieving or a combination of these.

The symmetric membrane ranges in a thickness between 5-200 micrometers, and the resistance is a function of the total membrane thickness An asymmetric membrane consist of a very thin dense toplayer (thickness of 0.1-0.5 micrometers) over a porous substructure (thickness 50-150 micrometers). Further development of an asymmetric membrane is a composite membrane, where the dense toplayer is made from a different material than the support. In this way, the each layer can be optimized independently to obtain optimal membrane performance with respect to selectivity, permeation rate, and chemical and thermal stability.

There are several important factors when choosing a membrane: processability, cost, mechanical/chemical stability, and most importantly, selectivity and permeability. The relationship between the selectivity and permeability for various gas pairs was suggested by Robeson as an “upper bound trade-off curve” [61]. It can been seen that all polymeric materials were found to lie under a straight line defined as the upper bound, but molecular sieves are not bound to this limit [62], as can be shown in Figure 2. 3.

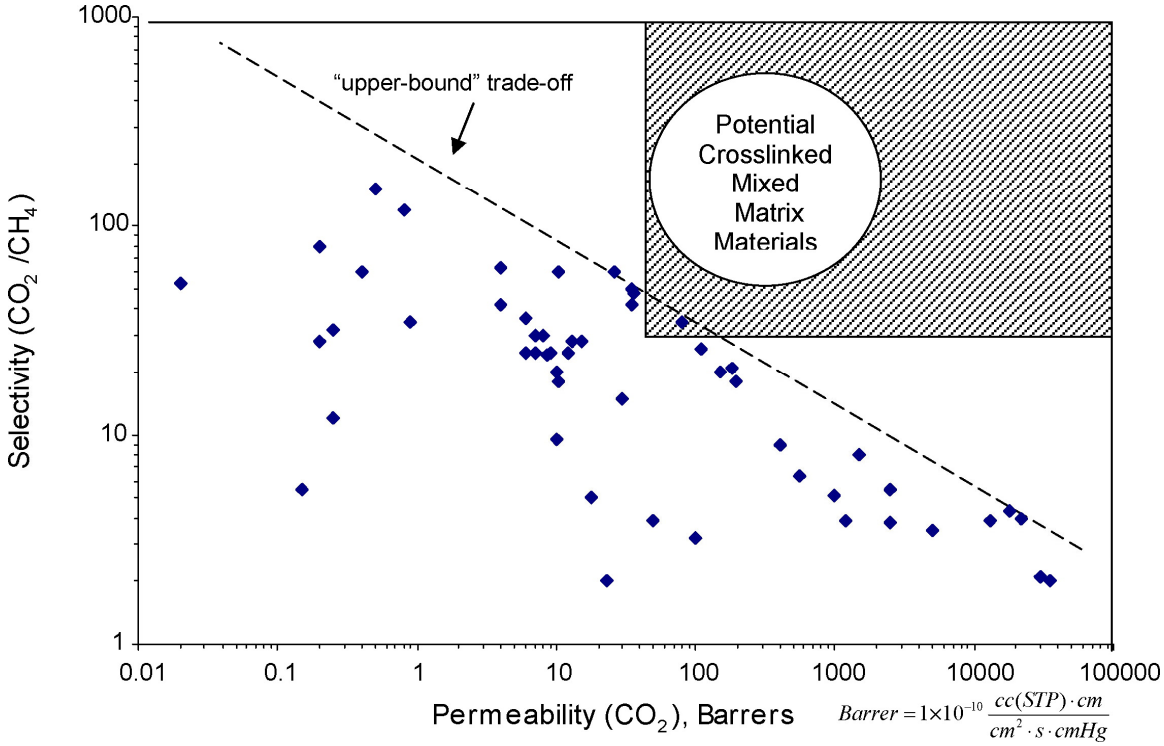

Figure 2. 3. Robeson "upper bound" curve for CO_2/CH_4 separation (From Hillock et al. [63], printed with permission from Elsevier Limited)

The processability is simply how easily the membrane is made. Polymeric membranes are made by casting or spinning, and inorganic membranes are usually made from the sol-gel process (chapter 3.1). As mentioned earlier, high selectivity and high permeability can never be obtained simultaneously, however, some membranes show better properties than others. The stability of a membrane is how well it behaves under different pressure, temperatures and chemicals. Different membranes have good qualities in different areas, but no membrane today has shown good qualities in all.

2. 2. 1 Inorganic membranes

Inorganic membranes have been developed as an alternative to polymers due to their specific properties; they can withstand harsh environments like high temperatures, high pressure and aggressive chemicals. Polymeric membranes will never exceed a temperature limit of 600°C, but inorganic membranes can withstand much higher temperatures [51]. The efficiency of polymeric membranes decreases with time due to

fouling, compaction, chemical degradation and thermal instability. Due to this limited thermal stability and susceptibility to abrasion and chemical attack, polymeric membranes have not found application in separation processes where hot reactive gases are encountered [64]. This has resulted in a shift of interest toward inorganic membranes. Nevertheless, for gas separation processes, inorganic membranes are expected to cost between one and three orders of magnitude more per unit of membrane area compared to polymeric membranes. With this in mind, it is reasonable to expect that these membranes will be used only in areas where cost per unit membrane area is secondary to performance, like sensors or specialty separations that are not feasible with current membranes [62].

Inorganic membranes are increasingly being explored to separate gas mixtures. Not only do they exhibit superior chemical and thermal properties, inorganic membranes usually have much higher gas fluxes compared to polymeric membranes [64].

There are basically two types of inorganic membranes – dense and porous. Porous inorganic membranes include ceramic membranes, such as alumina, silica, titania and glass and porous metals, such as stainless steel and silver. These membranes exhibit high permeabilties, but low selectivties.

Dense inorganic membranes are highly specific in their separation behaviors, for example Pd-metal based membranes which are hydrogen specific and metal oxide membranes which are oxygen specific. To meet the dual requirements of high selectivity and high peremabilities, inorganic composite membranes have been introduced [65, 66].
The preparation of inorganic membranes includes a variety of methods; extrusion, powder suspension, molten salt inclusion, phase separation and leaching, nuclear track etching, dynamic deposition, anodic oxidation, pyrolysis, particle dispersion/slip casting and pyrolysis. Inorganic (ceramic) membranes offer many advantages, however they suffer from a few limitations at the present state of technology. Burgraaf [67] list these advantages and disadvantages

Table 2. 1. Advantages and Disadvantages of Inorganic (Ceramic) membranes

Advantages

1. High temperature stability
2. Mechanical stability under large pressure gradients (noncompressible)
3. Chemical stability (particularly in organic solvents)
4. No ageing, long lifetime
5. Rigorous cleaning operation allowable (steam sterilization, high backflush capability)
6. (Electro) catalytic and electrochemical activity easily realizable
7. High throughput volume and diminished fouling
8. Good control of pore dimension and pore size distribution

Disadvantages

1. Brittle character needs special configurations and supporting systems
2. Relatively high capital installation costs
3. Relatively high modification costs in case of defects
4. Sealing technology for high-temperature applications may be complicated

Next, an overview of types of inorganic membranes is given.

Glass membranes

Glass membranes are usually made from Pyrex or Vycor, both containing SiO_2, B_2O_3 and Na_2O. The membranes are made by heating them to a temperature between 1300-1500°C and then slowly cooling them to 500-800°C [51]. At this stage a phase separation occurs. Demixing occurs into two phases, one phase that consists mainly of SiO_2, and one phase that contains mostly B_2O_3. The B_2O_3 phase is soluble in acids, and can therefore be dissolved to make pores in the micrometer to nanometer range. Glass membranes can easily be changed to perform different types of separation by modifying their surface.

Ceramics

Ceramics are formed by the combination of metal with a non-metal in the form of an oxide, nitride or carbide. Ceramic membranes represents the main class of inorganic membranes with aluminum oxide or alumina (γ-Al_2O_3), zirconium oxide or zirconia (ZrO_2), and silicon oxide or silica (SiO_2) as the most important representatives. The last,

more commonly known as glass, is mainly prepared by techniques involving leaching on demixed glasses but can also be prepared by the sol-gel method. The sol-gel method (chapter 3. 1) is also used for preparing alumina and zirconia membranes. The valence electrons of the metal part are retained by the nonmetal atoms resulting in a highly stable bond and consequently these materials are highly thermally and chemically resistant. Ceramics can withstand extreme temperatures (above 4000°C) and are therefore very suitable for gas separation occurring at high temperatures or membrane reactors [51]. Also, they show superior chemical stability, and can generally handle any pH and organic solvent. They can be cleaned with any cleaning agent, allowing strong acid and alkali treatment. Ceramics are characterized as hard and brittle materials.

Metal membranes

Metal membranes are dense and usually consist of thin metal plates of palladium or alloys of palladium and silver or copper. Because palladium is so brittle, alloys are necessary. Alloys may also give higher permeability than pure palladium. These metals/alloys are only permeable to atomic hydrogen, which implies that palladium has superior selectivity of hydrogen over all other gases [68-70]. Originally used in the form of relatively thick dense metal membranes, the self-supporting thick membranes (50–100 micrometers) have been found unattractive because of the high costs, low permeance and low chemical stability. Instead, current Pd-based membranes consists of a thin layer (<20 micrometers) of the palladium or palladium alloy deposited onto a porous ceramic or metal substrate [71, 72].

Molecular sieving materials

Molecular sieving materials have a very defined pore structure and rely primarily on differences in molecular size and shape to achieve separation [62]. Important molecular sieves are carbon sieves and zeolite sieves. Zeolites are microporous aluminasilicates, and the structure consists of a three-dimensional network of SiO_4 and AlO_4 tetrahedra [51]. These membranes are highly stable, and can handle high temperatures, pressures and highly sorbing materials [62]. Also, these membranes are not restricted by Robeson's "upper bound" and lie beyond it, as shown in Figure 2.3. However, these

membranes are fragile, expensive and difficult to process and are today not commercially significant.

Mixed matrix membranes (MMM)

A mixed matrix membrane consists of a polymeric material filled with inorganic fillers or particles (Figure 2.4). The bulk phase (phase A) is typically a polymer; the dispersed phase (phase B) represents the inorganic particles, which may be zeolite, carbon molecular sieves, or nano-size particles The inorganic material is introduced to enhance mechanical properties as well as separation properties compared to polymers. At the same time, the fragility inherent in the inorganic membranes may be avoided by using a flexible polymer as the continuous matrix. In contrast to the conventional mixed matrix membranes, a novel MMM design has been proposed using non-porous nano-size particles [73]. The function of the fillers is to systematically direct the molecular packing of the polymer chains, hence enhancing the separation properties of glassy polymeric membranes. This approach is partly motivated by the unique transport characteristics of poly(4-methyl-2-pentyne) (PMP), which is a reverse-selective glassy polymer. By incorporating nonporous particles, having dimensions comparable to those of individual polymer chains, the manner in which these pack can be regulated and thereby favorably manipulate molecular transport and selectivity.

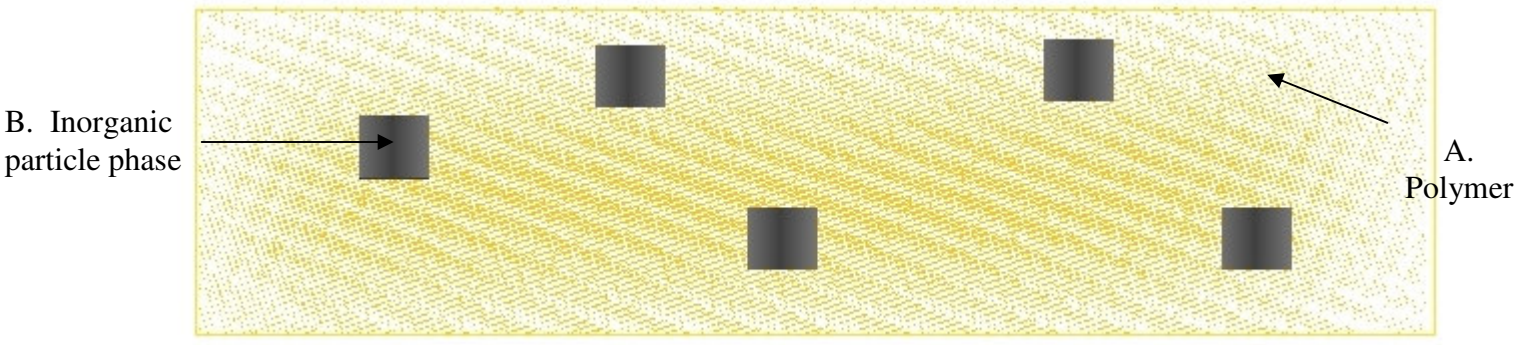

Figure 2. 4. Cartoon of mixed matrix membrane

2. 2. 2 Polymeric membranes

Preliminary criteria for selecting polymeric materials for gas separation are based on chemical resistance, sorption capacity and good mechanical strength [74]. However, key important factors for selecting polymeric materials are: (a) intrinsic membrane properties, (b) ability of the polymer to resist swelling induced plasticization, and (c) ability to process the polymer into a useful asymmetric morphology. It is important that a polymeric membrane has a large molecular weight to prevent brittleness. With that in mind, polymers are good in the way that they are easy and cheap to process, have a good permeability and have a relative high chemical stability. They do however, come short when it comes to selectivity. Therefore, the break-through for polymeric membranes came with the asymmetric/composite membranes, increasing both permeance and selectivity.

3. 0 Production and Characterization of Membranes

In chapter 2.0 it was shown that a large number of materials can be used as the basis for membrane preparation. The scope of this chapter will be the production and characterization of membranes with an emphasis on sol-gels processing.

3. 1. The Sol-Gel Process

This section covers the basics of sol-gel chemistry. First, a short overview will be given followed by a more detailed description of each of the different steps in sol-gel processing.

Different processes for producing functional oxide layers includes glass melting, ceramic powder methods and sol-gel. The last has the advantages of potentially higher purity, homogeneity and lower processing temperatures [75]. Two different routes are widely used in the sol-gel processing, the colloidal suspension route and the polymeric gel route [32]. Both routes use a precursor which may be hydrolyzed and polymerized. The essential parameter to control is the hydrolysis rate with respect to the condensation rate [67]. The colloidal suspension route is based on colloid chemistry in aqueous media where a precursor with a fast hydrolysis rate is reacted with water. The polymeric route its concerned with chemistry of metal organic precursors in organic solvents where the hydrolysis rate is kept low by adding successively small amount of water and by choosing a precursors which hydrolysis relatively slowly [76]. The most commonly used precursors are metal alkoxides [77], however other precursors like nitrates [75] and metal salts [76] can be used. Both routes can be used to prepare supported ceramic membranes where the porous structure is influenced by the different steps involved in the process.

A *sol* is a dispersion of colloidal particles in a liquid, and a *colloid* is a solid particle with at least one spatial dimension between 1-1000 nanometer [78]. A precise definition of a *gel* does not exist, however one definition given by Hench, defines a gel as a network with pores of submicrometer dimensions and polymeric chains whose average

length is greater than a micrometer [75]. A gel can be obtained by network growth from an array of discrete colloidal particles (Figure 3.1).

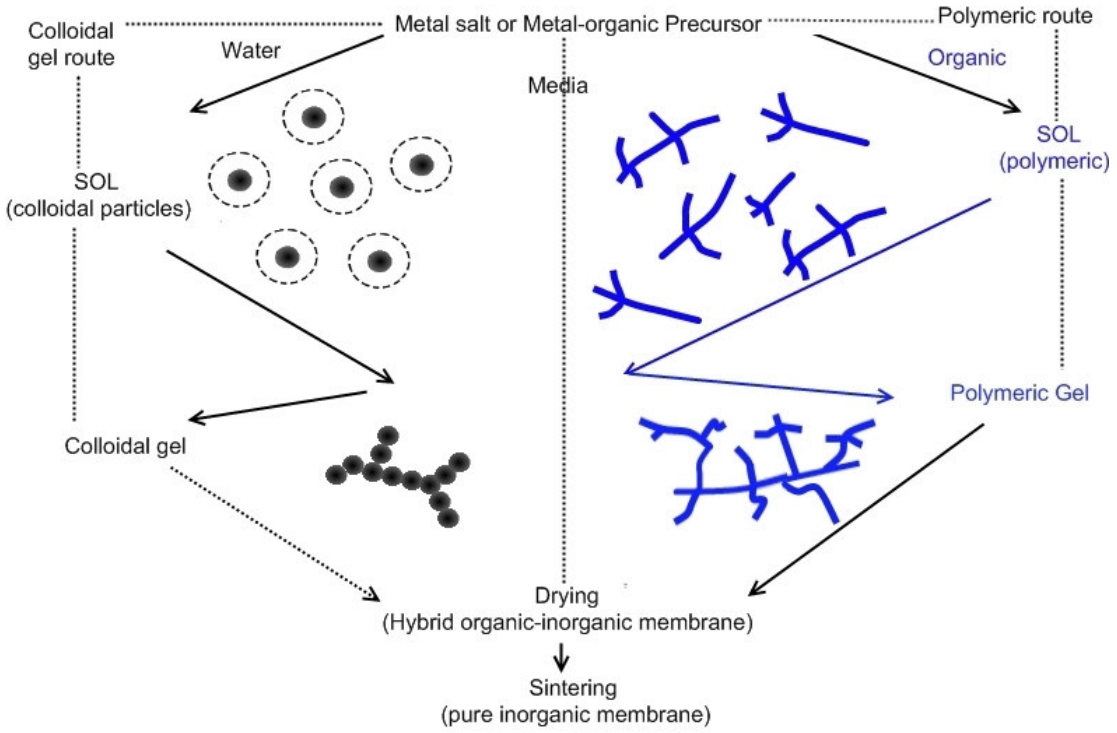

Figure 3. 1. Scheme of sol-gel routes.

The first step when preparing membranes by the sol-gel process is the preparation of a sol using molecular precursors, either a metal salt or metal organics [76]. In both cases condensation reactions occur at the sol stage with formation of colloids or clusters which interconnect and form the gel. The final gel is greatly dependant on the category of the precursors used in the process, as sols and gels evolve differently depending on the precursors used. By using different precursors, catalysts and solvents, the final membrane pore structure can be tailored to fit many needs. Depending on whether the colloid or polymeric method is used, two main structures of gels can be formed:

Physical gels in which steric or electrolytic effects in the sol dominate gel formation. The way individual particles can be arranged during the process is the main characteristic of how the gel is formed. These gels are formed in aqueous media.
Polymeric gels in which the gel formation is determined by the relative rates and extent of chemical reations. In this case organic media are preferred.

In the colloidal route, a precipitate of gelatinous hydroxide or hydrated oxide particles is formed which is peptized in a subsequent step to a stable colloidal suspension [67]. The particles sizes range from 5-15 nanometer which form loosely bound agglomerates with sizes ranging from 5-1000 nanometers. A gel can be formed by increasing the suspension concentration or by manipulating the surface charge of the colloids, as this causes the colloid particles to connect and form interlinked chains of particles or agglomerates. The pH and the nature of the electrolyte are important parameters concerning the gelling point and volume as they decide the mutual repulsion force.

In the polymeric route, two chemical reactions take place [67]:

1. The partial hydrolysis of the metal organic compound which introduces the active functional OH group attached to the metal atom.
2. These then react with each other or with other reactants to form a polymeric solution which further polymerizes to form a solution of organic-inorganic polymeric molecules.

The final result of this process is an interlinked network, a gel. As the gel is formed continuously in the liquid, it changes form and continue to shrink, and it is not necessary to remove the liquid as in the colloidal route. According to Brurggraaf [67], the water can be supplied in three different ways: (1) by slowly adding water to an alcoholic solution of the alkoxide, (2) *in-situ* production of H_2O through an esterfication reaction by adding an organic acid to the alkoxide solution, (3) dissolving an alkaline base or a hydrated salt into the alkoxide solution in alcohol. At last, by changing the nature of the catalyst used for the polycondensation/polymerization reaction the structure of the gel can be changed significantly. The rest of this chapter will focus on the sol-gel of silica as are they are the most common and in the interest of this research project.

Hench recognizes there are seven steps involved in making sol-gel derived silica monoliths [75].

Step 1: *Mixing*. When using the colloidal suspension route, the sol is made by mixing colloidal particles in water at a pH that prevents precipitation. When preparing a sol by the polymeric route, a liquid alkoxide precursor such as $Si(OR)_4$ is hydrolyzed by mixing with water (eq. 3.1)

Hydrolysis:

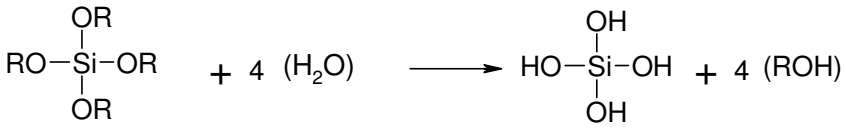

$$Si(OR)_4 + 4(H_2O) \rightarrow Si(OH)_4 + 4(ROH) \qquad (3.1)$$

The hydrated silica tetrahedral interact in a condensation reaction (eq 3.2) forming $\equiv Si-O-Si\equiv$ bonds.

Condensation:

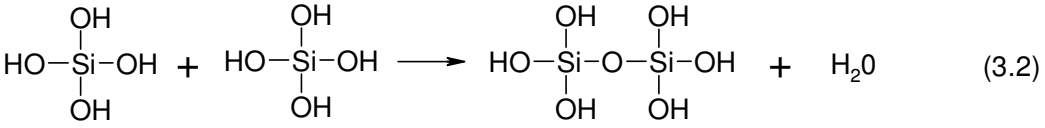

Further polycondensations reactions leads to a linkage of additional Si-O-Si bonds which results in a SiO_2 network (eq. 3.3). Water and the alcohol expelled from the reactions remains the in the pores of the network.

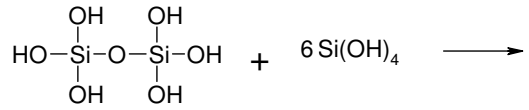

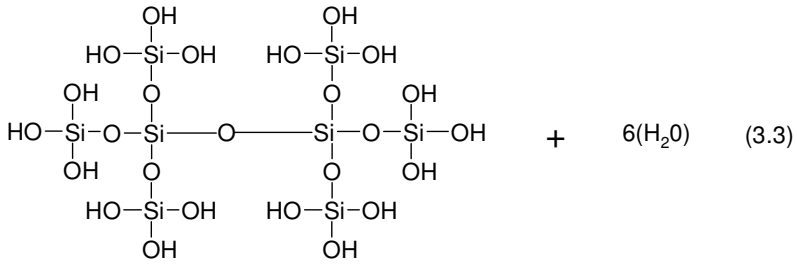

When the SiO_2 network reaches a significant size by condensation and hydrolysis, the formation of colloid particles will occur which will eventually result in a sol. The size of the sol particles and the cross-linking within the particles depend upon among others the pH and the ratio between water and monomer.

Step 2: *Casting*. At this point the sol is a low-viscosity liquid and can therefore be cast into a mold.

Step 3: *Gelation.* As the colloidal particles and condensed silica species grow together they form a three-dimensional network. The properties of the gel are dependent on the size of particles and the extent of cross-linking prior to gelation. At the point of gelation the viscosity of the gel increases greatly and a solid object results in the shape of the mold. With appropriate control, fibers can be pulled or spun as gelation occurs [75].

Step 4: *Ageing.* The ageing of a gel is the process where the cast object is completely immersed in a liquid for a period of time. The time period can be hours to days, and during ageing the gel densifies as the localized solution undergo polycondensation. Reprecipitation of the gel network increases the thickness of the interparticle necks and decreases the porosity. At this point the gel strength has increased preparing the gel for the drying process where the gel can suffer from cracking due to the evaporation of solvent.

Step 5*: Drying.* Drying involves removing the solvent and water from the pore network. Depending on the drying process, the final result will be either an aerogel or a xerogel. Drying at ambient pressure by thermal evaporation leads to shrinkage and the gel is referred to as a xerogel. When the pore liquid is removed as a gas phase under supercritical conditions, the network does not collapse and a low density aerogel is produced.

Step 6. *Dehydration or Chemical Stabilization.* Some sol-gel routes require chemical stabilization by removal of surface silanol (Si-OH) bonds from the pore network so the surface does not rehydroxylate. This results in a chemically stable, porous solid. Porous gels made in this way are optically transparent and can with some modifications be used as exceptional optical components when impregnated with optically active polymers such as fluors, wavelength shifters, dyes or nonlinear polymers [79, 80].

Step 7. *Densification.* When the gel is exposed to higher temperatures (above its glass transition temperature, Tg), the pores are eliminated and the gel undergoes further densification. The densification temperature of the gel is mainly dependent on three parameters; the dimensions of the pore network, the connectivity of the pores, and the surface area.

Details of six of these seven sol-gel processing steps follow. As mentioned earlier, the emphasis is on sol-gel derived silica made by the alkoxide process under ambient pressure.

3. 1. 1 Hydrolysis and Polycondensation.

At the time of gelation, much of the structure of the gel is established. Subsequent processes such as ageing, drying, stabilization and densification all depend upon the formed at gelation. The structure of the gel is determined in part by the relative rates of hydrolysis and condensation, and therefore understanding the kinetics of theses two processes and the ratio of their rate constants (k_h/k_c) is crucial for determining the gel structure. The kinetics of hydrolysis and condensation are complex processes as many species are present in the solution and the two processes are occurring simultaneously. Some key parameters are temperature, nature and concentration of electrolyte (acid, base), type of solvent and type of precursor. Another important parameter is the nature of alkoxide groups on the silicon atom. In general, it can be said that the longer and bulkier the alkoxide group, the slower the rate constant. For example, in the case of the hydrolysis of $Si(OR)_4$, $k_H = 51\times10^{-3} L\cdot mol^{-1}\cdot s^{-1}\cdot\left[H^+\right]^{-1}$ for R = C_2H_5 and $k_H = 3\times10^{-3} L\cdot mol^{-1}\cdot s^{-1}\cdot\left[H^+\right]^{-1}$ for R = $(CH_3)_2CH(CH_2)_3CH(CH_3)CH_2$ [75].

3. 1. 2 Gelation

The gelation point or gelation time (t_{gel}) is known as the point where the sol becomes a gel, more specifically it is the point where the gel can support a stress elastically. The change is gradual as more and more particles collide and become interconnected, and there is no precise point where the gelation point occurs. For this specific project,

gelation was determined to be the point at which the solution would no longer flow when the vial was tilted at a 90º angle.

3. 1. 3 Ageing

A gel will continue to change structure and its properties as longs as it is kept in its pore liquid. The gel will experience changes in its physical properties like pore size, porosity and surface area. Four processes can occur singly or simultaneously, including polycondensation, syneresis, coarsening and phase transformation.

Polycondensation reactions, equation 3.3, continue to occur within the gel network as long as neighboring silanols are close enough to react. This effect results in the increase of the connectivity of the network as well as its fractial dimension.

As mentioned earlier, syneresis is the spontaneous shrinkage of the gel and the resulting expulsion of liquid from the pores. The extent of syneresis is different depending on weather the gel is colloidal or polymeric. In aqueous gel systems, the structure is controlled by the balance between electrostatic repulsion and attractive van der Waals forces. The extent of shrinkage can be controlled by additions of electrolyte. In an organic media, syneresis is attributed to formation of new bonds through condensation reactions which increases the bridging bonds and cause contraction of the gel network. According to Vysotskii and al. [81], the rate of contraction of silica gel during syneresis has a minimum at the isoelectric point, and for silica this point is pH equal to 2.

The last aging process that will be described is “Ostwald ripening” or “coarsening.” Due to the fact that smaller particles experience a higher activity in a solution, the dissolved material will diffuse from smaller to larger particles [78]. The process will continue until there’s only “one large particle left” meaning complete phase separation has occurred. Since the solubility of silica increases at high pH, so does the rate of coarsening [75].

The aging process can be affected or altered by different parameters, like time, temperature and pH. During aging, the gel experiences changes in most of its physical properties. Since the condensation reactions creates additional bridging bonds, the gel

exhibits an increase in stiffness as well as the elastic modulus, the viscosity and the modulus of rupture. It has been shown from West et al. [82] that the gel strength increases logarithmically with times between 1-32 days, and for this reason it is advisable to age large monolithic gels before drying to reduce the chance of cracking.

3. 1. 4. Drying

According to Hench [75], it has been generally accepted since the time of Sherwood [83-86] that there are three stages of drying. In the first stage, the gel experiences a decrease in volume equal to the loss of solvent from evaporation. The gel is deformed due to the large capillary forces, and causes shrinkage of the gel. At this point, the strength of the gel has increased greatly due to the greater packing density of the solid phase, just enough to resist further shrinkage. At this state, the capillary forces reaches a maximum, and unable to compress the gel any further, drainage of the pores takes place which is the onset of stage 2. Through surface films, the liquid flows to the surface and evaporates. When there is very little liquid left, the surface films can no longer perform the transport work and the only way for the residue to escape is by evaporation from within the pores and diffusion of vapor to the surface. This is known as stage 3 and continues until equilibrium is reached, depending on the ambient conditions. During drying, cracking can occur in either stages but most commonly is happens in stage 2. The possibility of cracking at this point is great due to high stresses and low strain tolerance of the material. As mentioned earlier, due to large capillary forces created from small pores, the gel can experience cracking during drying. It is therefore crucial to control the drying process by decreasing the liquid surface energy by addition of surfactants, or eliminate the very small pores. Another option is to perform hypercritical evaporation which avoids the solid-liquid interface. A third option is to obtain monodisperse pore sizes by controlling the rates of hydroloysis and condensation, as differences in evaporation causes stresses. If the evaporation is even, the stress on the network is negligible

3. 1. 5. Stabilization

As all gels are thermodynamically unstable, chemical and thermal modifications must be done to create a gel that is kinetically stable in ambient environment. Due to the large concentration of silanol groups on the pore surfaces, the gel must be chemically and thermally stabilized. Chemical stabilization involves the reduction of silanol concentration at the surface so that the gel does not rehydroxylate. Thermal stabilization is reducing the surface area so that the gel at a given temperature can be used without undergoing reversible structural changes. The two processes are dependent of each other as surface silanol groups and chemisorbed water have an extreme effect on the structure.

3. 1. 6. Densification

The last step in the sol-gel process is densification. Densification occurs between 1000 and 1700 Cº depending on the size of the pores and the material. The temperature at which the onset of densification occurs is strongly determined by the amount of water in the silica gel, as the water concentration highly affects the viscosity of the melt. It has been shown by Nogami and Moriya [87] that a gel prepared in acid experiences a higher surface area and water content than the same gel prepared in base, and this results in the acid-catalyzed gel starts to densify approximately 200 Cº lower the gel prepared in base. Gels have a higher specific surface area, and thus higher free energy than glasses, and the driving force for sintering is the reduction of surface area. The final result of the densification of sol-gel is indistinguishable from those of a melt-derived glass [75].

3. 1. 7. Summary

The sol-gel method is a process where the structure of the material can be controlled on a nanometer scale, even from the earliest stages of processing. Some advantages of the sol-gel process include higher purity and homogeneity and a lower processing temperature may be used. The chemistry behind each sol-gel process step is established, however understanding the molecular reaction mechanism and the thermodynamics and kinetics of sol-gel systems is insufficient.

The last section gave a general overview of the sol-gel process, the next section will focus on bridged polysilsesquioxanes, their preparation, application and properties.

3. 2. Bridged Polysilsesquioxanes

Organic-inorganic hybrid materials are attractive materials as they combine the advantages of inorganic and organic components. Bridged polysilsesquioxanes (BPs) are a hybrid material which consists of a variable organic bridging group and two or more trifunctional silyl groups [35], SiX_3, where X denotes hydrolysable groups which mostly are alkoxy groups. The organic bridging group (R) is linked to two or more Si atoms by Si-C bonds (Figure 3.2). The organic bridge, also known as the spacer, can be varied in length, rigidity geometry of substitution and functionality. Bridged polysilsesquioxanes are linked together in a three-dimensional network where the organic and inorganic parts are mixed on the molecular level [88]. One of the advantages of these materials is the possibility varying the organic bridging group which can give rise to a variety of bulk properties, such as porosity, thermal stability, refractive index, optical clarity, chemical resistance, hydrophobicity and dielectric constant [35]. The polysilsesquioxanes can be prepared as gels, films or fibers. Applications range from optics, coatings, catalysis, and separation media. The different types of organic bridging groups represent a vast population, and typical groups are rigid arylenic, acetylenic and olefinic to flexible alkylenes ranging from 1-14 methylene groups. They also include a variety of functionalized groups such as amines, ethers, sulfides, phosphines, amides, ureas, carbamates and carbonates. In addition, bridging groups have included organometallics in which the metal is part of the bridge or pendant to the bridge.

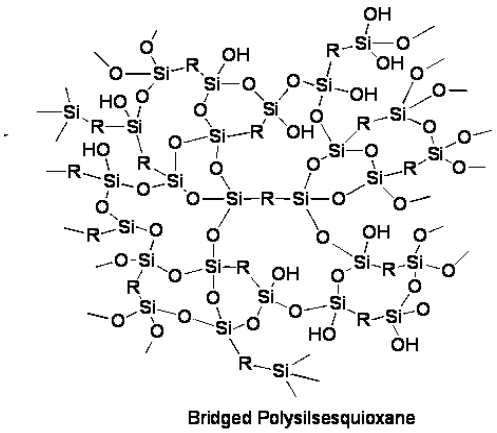

Figure 3. 2. Bridged polysilsesquioxane network

3. 2. 1 History

Bridged polysilsesquioxanes have been known and used since the 1950's [89], primarly as coupling agents [90], surface modifiers, coatings [91] and as components for adhesive formulations. In the early 1990's, studies were carried out to see if the porosity of BPs could be controlled at the molecular level [92]. Theses investigations lead into a new area where new properties could be controlled, such as the optical, thermomechanical and chemical properties of the BPs.

3. 2. 2. Sol-Gel Processing of Bridged Polysilsesquioxanes

Preparation

Bridged polysilsesquioxanes (BPs) are prepared by the sol-gel method (see chapter 3.1) which offers a number of advantages like low processing temperature, high homogeneity of the final products, creating materials with desired surface properties and a variety of pores [88]. The resulting product is a function of all synthesis conditions; type and concentration of precursor, type and concentration of catalyst, type of solvent, temperature, time of ageing, mode of drying, etc.

The basic steps in the sol-gel process involve the hydrolysis of molecular precursors followed by polycondensation reactions. Further the sols undergo ageing and finally the sol-gel process is completed by drying. The hydrolysis and condensation reactions leads to a viscous liquid composed of polymers, oligomers, aggreagates and

solvent, more commonly known as a sol. As the hydrolysis and condensation reactions continue, individual particles are joined together by siloxane bonds which eventually leads to the formation of a giant cluster across the flask. At this stage, the sol experiences a high viscosity and low elasticity and the sol will not pour even if it is tipped at a 90° angle; This point is described as the gelling point. The sol-gel polymerizations of the BPs are usually rapid (minutes to hours) and form irreversible gels.

The organic bridging group usually represents 40-60 wt % of the network [35]. The reactions are usually carried out in the same alcohol generated by the hydrolysis or in tetrahydrofuran. There have also been cases where the sol-gel has been prepared in nonpolar solvents like toluene through a transesterification reaction between the triethoxysilyl groups and anhydrous formic acid [93]. At least three equivalents of water must be added to the reactions while the three other equivalents are self-produced by the hydrolysis. As with silica gels, the molar ratio between water and silica can have an influence of the final material. The sol-gel reactions are usually acid or base catalyzed, all though there are cases where fluoride catalysts have been used [35]. Typically, hydrochloric acid is used as the acid catalyst and ammonium hydroxide, sodium hydroxide and potassium hydroxide are commonly used as basic catalysts. The final material structure is greatly dependent on the type of catalyst used; When acid is used the final result is usually a lower-crosslinked gel that easily compacts under drying, resulting in a microporous structure. Basic catalysts produce mesoporous structures after drying due to the formation of clusters which pack to form mesopores [94].

The substituents can effect the sol-gel formation in various ways as they can sterically hinder the hydrolysis and condensation reactions and influence the presence of intramolecular condensations. Cyclization reactions are bottlenecks in the sol-gel formation and can even prevent the formation of gels. When intramolecular condensations leading to carbosiloxane rings occur, the polymer growth dramatically decreases. These cyclization reactions only come important with monomers containing one-four methylene repeating units in the bridging group [95], or with bridged groups with cis substitution geometries [96]. It has been found that these cyclic structures are incorporated in the final gels and it is expected that this will contribute to the bulk properties of the gel [35].

After the gels are formed, they undergo ageing and then drying. Ageing (see chapter 3.1.) is important to control as is has shown to have a substantial effect on the final porosity and texture of the BPs gels. The influence of ageing has been investigated by Cerveau and al. [97]. During the ageing step, the solid undergoes a reorganization of the structure which changes the pore size distribution and influences the specific surface area.

Drying is the process where removal of water is performed. Three different drying methods are commonly used: (1) involves air-drying, washing with water followed by drying, (2) is the so called solvent-exchange method were the polymerization solvent is exchanged with a solvent with a lower dielectric than that from slow air drying, and (3) involves replacing the original solvent with supercritical carbon dioxide extraction and then slowly venting the gas [98]. The types of gels that are formed by using (1) and (2) are called xerogels, and gels dried with method (3) are called aerogels. Xeorogels usually exhibit specific area up to 1000 m^2/g, however aerogels can have specific surface area much higher than $1000m^2/g$. Due to the low monomer concentrations the gels can lose as much as 80-95% of their volume with air drying. This shrinkage can result in collapse some of the pores, but most BPs remain porous with surface area between 200-1200 m^2/g.

The sol-gel process of BP's offer a number of advantages and disadvantages. Dabrowski et al. [88] have listed some advantages and disadvantages from the point of view of potential applications in the field of adsorption:

1) The synthesis can be performed under *chemie douce* conditions, such as atmospheric pressure and low temperature
2) The products can be made pure as it is possible to achieve high purity of the precursors.
3) Homogeneity of the final gel can be obtained
4) Gel properties can be tailored by using the proper synthesis conditions, i.e. particle size, pore size, porosity and surface functionalities.
5) Pores sizes can be controlled by using entrapped organic moieties as templates, but the most effective way of controlling the porosity is by changing the flexibility of the bridging group [35].

6) Functional groups can be introduced on the surface by co-condensation of the monomer with a functional group carrier instead of grafting these groups after the synthesis.

Unfortunatly the sol-gel processing of BP's suffer from some limitations:

1) Precurors are relatively expensive and many are not commercially available.
2) The process is sensitive to moisture
3) If a monolith is desired, the process is not suitable for large scale production, as the process is time consuming due to the ageing and drying requirements.

Some of the limitations can be overcome by optimizing the sol-gel process of BPs and taking advantage of these materials in fields where they would reveal properties not attainable by other synthetic approaches [94].

3. 2. 3 Porosity

Since porosity is a key parameter for BPs used as catalysts, membranes and adsorbents materials, high surface areas and control over the pore size are important goals. The porosity of theses materials is a function of the compliance of the network which is affected by the degree of condensation and the flexibility of the organic bridging group. By changing the type and length of the bridging group, various porosities can be obtained. It was found that by increasing the length of a carbon backbone chain in a series of basic catalyzed alkylene-bridged polysilsesquioxanes, the porosity decreased from a specific surface area of 729 m^2/g (two methylene units) to 94 m^2/g (10 units) [88].

In some cases it is desirable to make nonporous gels, such as chemical barriers, dense membranes and optical coatings. This is attainable by using acids as catalysts which can lead to the collapse of the porosity and thus nonporous gels or thin films. Non-porous xeorogels are produced if the number of carbon atoms in the organic bridging group is more than five, however, xerogels synthesized in the alkaline medium with the same number of carbon atoms results in a porous structure with a high specific

surface area. When base is used as the catalyst, a less compliant network is formed as the base usually provides a more condensed network and more rigid bridging groups. In this manner the porosity is more often retained after drying, in comparison with acid. Alkylene bridged polysilsesquioxanes prepared with base catalyst and bridging groups up to 10 carbons in length give rise to mesporous xerogels (20 Å < mean pore diameter < 500 Å [99]. The mean pore diameter have been shown to be proportional to the length of the bridging groups [35]. The prevention of network collapse during drying can be obtained by using unsaturated or aromatic spacers instead of alkylene ones.

BPs with different bridging groups have been examined extensively by Cerveau et al. [100]. They found an enormous difference in the properties of the solid depending on the chemical structure of the organic moieties. It was reported that systems with rigid bridges gave hydrophilic materials with high values of specific area, while as more flexible groups produced dense, hydrophobic structures. As mentioned earlier, it is not only the organic precursor that decides the final material, but also the kinetic parameters such as type of catalyst, type of solvent, concentration of monomer and catalyst, ageing and drying.

Pore templating

Porosity can also be obtained by pore templating, a process where the organic group is used as the template for the porosity. In templating, the organic group occupies space until it is removed by calcinations, chemical oxidation, chemical rearrangements, or hydrolysis [35]. The process will leave a pore that is approximately about the size and shape as the organic molecule. Alternatively, the porosity can be controlled by cleaving, chemically modifying or partly removing the organic bridging group.

3. 2. 4 Thermal stability and Mechanical Properties

In general, bridged polysilsesquioxanes offer high thermal stability. For example, the alkylene-bridged polysilsesquioxanes are stable over 400°C, and the phenylene-bridged can resist temperatures as high as 500°C. There is less information to be found about their mechanical properties, however, some highly branched polysilsesquioxanes known

as “star-gels” have been characterizes as compliant gels or glasses [93]. The dynamic mechanical properties of epoxy-bridged polysilsesquioxanes have been studied by Dynamic Mechanical Analysis (DMA) [101].

The most common application for BPs have been for surface modifications as coupling agents, especially those with sulfides in the bridging group with silica-filled rubber [90]. Because BPs bridged with alkylene [95], ether [102] and urea [103] form relatively hard films, they can be used to protect easily scratched surfaces. These types of coatings can also be used as protective layers for metals, microelectronic applications like low k dielectrics and photoresists. They have also been used in biological manners, such as encapsulating sol-gel networks for enzymes and cells. Bridged polysilsesquioxanes can also be used in optics, by incorporating dyes into the sol-gel matrix waveguides, lasers, light-emitting diodes, and nonlinear optical materials can be obtained [104].

Bridged polysilsesquioxanes can exhibit high surface areas and can contain a variety of chemical functionalities. This combination makes them excellent for separation media, such as chromatographic supports for High-Performance Liquid Chromatography (HPLC) and membranes. BPs bridged with phenylene have shown to be good sorption materials for the removal of aromatic compounds from aqueous solutions [105, 106], and ethylene bridged BPs with amino groups in the surface have shown an affinity for adsorbing organic compounds (n-hexane, n-heptane, benzene, cyclohexane, acetonitrile and triethylamine) from the gas phase [107]. BPs have also shown high protonic conductivities for fuel cell membranes [108]. Bridged polysilsesquioxanes been used as pore templates in inorganic membranes [77] and as a structural material [109].

The high surface area and chemical functionality also makes BPs attractive as catalyst supports. By varying the bridging group, the selectivity and reactivity can be tailored. Different bridging groups have been used for catalyst supports, however the most common use of BPs in catalysis is as an agent for attaching highly dispersed catalysts to a solid support of another material. A heterogeneous catalyst of chromium(III)-bridged polysilsesquioxanes, was prepared for liquid phase partial oxidation of alkyl aromatic substrate s [110].

Bulk properties of BPs such as porosity and high surface area can also be taken advantage of as metal adsorbents. For example, bridged polysilesquioxanes with thiocarbamate bridging groups have been used to adsorb metals such as silver [111], rare earth elements [112] and gold, palladium, and platinum [113].

3. 2. 5. Summary

Bridged polysilsesquioxanes are hybrid organic-inorganic materials where the organic and inorganic parts are mixed on the molecular level. The materials can be produced as dense films to high surface area structures and applications range from coupling agents to separation media. They are prepared in a single step in contrast to many silica systems which undergo surface modifications in a subsequent step. The easy preparation method combined with a high range of applications make these attractive materials for the future.

3. 3 Characterization of membranes

The characterization of membranes can be preformed by numerous methods. Some common techniques include scanning electron microscopy (SEM), bubble-point method, mercury intrusion porometry, permeation measurements, gas adsorption-desorption and solute rejection measurements [51]. The methods above can be divided in two groups: Structure-related parameters and permeation-related parameters. Structure-related parameters include determination of pore size, pore size distribution, top layer thickness and surface porosity analysis. Permeation-related parameters are based on determination of the actual separation parameters using components that are more or less retained by the membrane. As for the characterization of sol-gels it is important to know the sizes of the colloids and one useful method to study the growth of particles over time is by dynamic light scattering (DLS). In this chapter, only the following will be considered: SEM atomic force microscope (AFM), gas adsorption-desorption, gas testing and dynamic light scattering

3. 3. 1 Scanning electron microscopy

Scanning electron microscopy allows a clear view of the overall structure of a microfiltration membrane. By visual inspection, the top surface, the cross-section and the bottom surface can all be clearly observed. Also, any asymmetry in the morphology can be seen. In addition, the porosity and the pore size distribution can be estimated from the resultant images.

Electron microscopy can be divided in two groups: scanning electron microscopy (SEM) and transmission electron microscopy (TEM). Only SEM will be considered in this section. The resolution of simple electron microscopy lies in the 10 nanometer range, whereas the pore diameters of microfiltration membranes are about 5 nanometers.

The principle behind scanning electron microscopy is that a beam of electron hits the membrane sample, known as primary electrons, and electrons are then reflected off the surface (or actually liberated from atoms on the surface), collected at a detector and this determines the image (what seen on the screen). When a membrane is placed under the electron beam, charges can be built up at the surface and the membrane can be damaged due to the high accelerating voltage. By coating the sample with a fine conducting layer of gold, carbon or platinum the problem can be avoided, however this must be carefully carried out as poor coating techniques gives rise to artifacts.

3. 3. 2. Atomic Force Microscopy (AFM) [78]

The Scanning Tunneling Microscopy (STM) is a new generation of advanced instruments that allows for surfaces to be investigated at a molecular level. The STM consist of a probe (sharp, thin metal tip) which is mounted on a piece of piezoelectric ceramic material and placed a couple of nanometers away from a conductive surface. By forcing on a given potential it is possible to make electrons “jump” from the surface to the metal probe (tunneling effect). If the electric current is kept constant while the probe is being moved across the surface the vertical movement of the probe can be recorded with a precision of a few Ångstøm.

A type of STM is the Atomic Force Microscopy (AFM) which consists of a cantilever that scans the surface while recording the interactions between the tip of the probe and the surface which results in a topographic image of the surface.

3. 3. 3 Gas adsorption-desorption

Gas adsorption-desorption is a technique used to determine pore sizes and pore size distribution in porous materials. By measuring the adsorption-desorption isotherm as a function of relative pressure (i.e. the ratio between the applied pressure and the saturation pressure), the pore sizes and pore size distributions can be calculated from predicted models.

The adsorption and desorption isotherm is determined by using an inert gas, usually nitrogen. The method is carried out by filling the smallest pores with low pressure, and then increasing the pressure further so larger pores will be filled, almost reaching the saturation point. The total pore volume is determined by the quantity of gas adsorbed near the saturation pressure. At the saturation pressure, the pressure is decreased and desorption occurs. The desorption and adsorption curves are generally not identical due to the hysteresis effect. The main problem with this method is the difficulty in relating the pore geometry to a model which allows for the pore size and the pore size distribution to be determined from the isotherms.

3. 3. 4. Gas testing

Gas testing allows the actual membrane performance to be tested (Figure 3.3). The selectivity, permeability and permeance can be measured. Also, the mechanical strength can be measured by increasing the pressure until the membrane collapses. Gas testing can be carried our in two ways, single gas tests or mixed gas tests. In single gas tests, one gas is applied on the feed side of the membrane and the rate of permeation of this gas is measured. In order to determine selectivity the permeation rate of one gas is compared to another. In mixed gas tests a gas chromatograph (GC) must be used to analyze and determine the composition of the permeating gas. From the flux and composition, the selectivity, permeability (permeance) can be calculated. A slightly lower selectivity is usually observed in mixed gas tests than is calculated in single gas tests

Figure 3. 3. Gas Permeation rig

3. 3. 5 Dynamic Light Scattering (DLS)

In an asymmetric membrane it is vital that the dense layer does not sieve into the porous support. Sol-gel chemistry produces colloids of different sizes and it's therefore important to control the particle sizes. A powerful tool to characterize the structure and dynamics for polymer solutions with gels is Dynamics Light Scattering (DLS), sometimes referred to as Photon Correlation Spectroscopy or Quasi-Elastic Light Scattering. This technique allows measurements of particles sizes typically in the sub micron region and can measure down to sizes as small as 0.6 nanometers. A brief introduction to the theory behind DLS will be given in the next chapter.

Figure 3. 4. Image of a Dynamic Light Scattering apparatus

Brownian Motion

DLS measures the Brownian motion and relates this to the size of the particles. Brownian motion is the random movement of particles due to the bombardment by the solvent molecules that surround them. A large particle will exhibit a slower motion then a smaller one. The smaller particles are more influenced by the movement of the solvent molecules and move more quickly. It is important that the temperature is stable as convection currents can cause the movement of particles and will ruin the correct interpretation of size in a DLS measurement. The velocity of the Brownian motion is defined by the translation diffusion coefficient (D).

The Hydrodynamic Diameter

The actual size of the diameter is calculated from the translation diffusion coefficient by using the Stokes-Einstein equation (3. 4);

$$d(H) = \frac{kT}{3\pi\eta D} \qquad (3.\ 4)$$

where

d (H) = hydrodynamic diameter

D = translational diffusion coefficient

k = Boltzmann's constant

T = absolute temperature

η = viscosity

The theory of DLS is based on spherical particles, therefore the diameters obtained by this technique is the diameter of a sphere that has the same translational diffusion coefficient as the particle. Other significant factors that affect the diffusion speed (besides the temperature) are ionic strength of medium and surface structure.

The ions that are present in the medium and the total ionic concentration can affect the particle diffusion speed by changing the thickness of the electric double layer known as the Debye length (K^{-1}). For that reason a particle will seem larger in a low conductivity medium since it will produce an extended double layer of ions around the particle. On the contrary a higher conductivity media will suppress the electrical double layer and the measured hydrodynamic diameter. A way around this problem is adding a small amount of salt which will suppress the electrical double layer and ensure that the hydrodynamic diameter reported is valid. As for the structure surface of a particle it can affect the diffusion speed and likewise change the apparent size of the particle. For example, an adsorbed polymer layer projecting out into the medium will reduce the diffusion speed more than if the polymer is lying flat on the surface. In conclusion it is important to realize that the nature of the surface of the polymer, as well as the ionic concentration of the medium can affect the polymer confirmation which in turn can change the apparent size by several nanometers.

Light Scattering Theories

Two different light scattering theories exist depending on the size range of particles, Rayleigh and Mie theory. Rayleigh theory is used if the particles are small compared to the wavelength of the laser used, typically less then d = λ/10 or around 60 nanometers for a He-Ne laser. For small particles the polarized laser will illuminate the particle

isotropic, meaning the scatter will be equal in all directions. From the Rayleigh approximation it is recognized that the scattered intensity is proportional to the hydrodynamic diameter to the power of six, and that it is inversely proportional to the wavelength to the power of four, or more precisely; $I \propto d^6$ and $I \propto \frac{1}{\lambda^4}$, where I is the intensity of the scattered light, d is the particle diameter and λ is the laser wavelength. From this it can be seen that a 50 nanometer particle will scatter as 10^6 or one million times as much light as a 5 nanometer particle. This is probably the biggest flaw of the DLS measurements since there is a great danger that larger particles will swamp the scattered light from the smaller ones.

Mie Theory provides a rigorous solution for the calculation of particle size distributions from light scattering data and is based on Maxwell's electromagnetic field equations. It predicts scattering intensities for all particles, small or large, transparent or opaque within the following assumptions:

- The particles being measured are spherical
- The suspension is dilute, such at the scattered light is measured before it is re-scattered by other particles.
- The optical properties of the particles and the medium surrounding them is know
- The particles are homogeneous

Correlation Function

Since the particles in a dispersion exhibit constant, random Brownian motion, this will cause the intensity of scattered light to fluctuate as a function of time. To deal with this, the system contains a correlator that is designed to compare the signals and measure the degree of similarities of two signals at varying time intervals. The correlator in the instrument will construct a correlation function G (τ) of the scattered intensity:

$$G(\tau) = < I(t).I(t+\tau) > \qquad (3.5)$$

where τ is the time difference or the sample time of the correlator.

To obtain the size of the particles, various algorithms must be preformed on the correlation function; The mean size or z-average diameter is provided by fitting a single exponential to the correlation function This approach will also present an estimate of the width of the distribution or the polydispersity index. This method is known as the intensity size distribution since it is obtained form a plot of the relative intensity of light scattered by particles in various size classes. If the intensity distribution shows s tail of more than one peak, then Mie theory can be used to convert the intensity distribution to a volume distribution. This will give a more realistic view of the importance of the tail or second peak present. As mentioned earlier, one of the drawbacks with light scattering is the fact that the intensity distributions can show faux distributions. To overcome this problem other distributions can be calculated, the volume and number distributions. The difference between intensity, volume and number distributions can best be illustrated by a simple example: If a sample consists of two equal populations of spherical diameters of 5 and 50 nanometers, the number distribution will display two peaks positioned at 5 and 50 nanometer of a 1:1 ratio. If the number distribution is converted to a volume distribution, the two peaks will shift to a 1:1000 ratio due to the fact that the volume of a sphere is $4/3\pi\ (d/2)^3$. An intensity distribution would show a 1:1000000 ratio between the two peaks according to Rayleigh's approximation which states the intensity of scattering is proportional to d^6. The three different distributions are given in Figure 3.5.

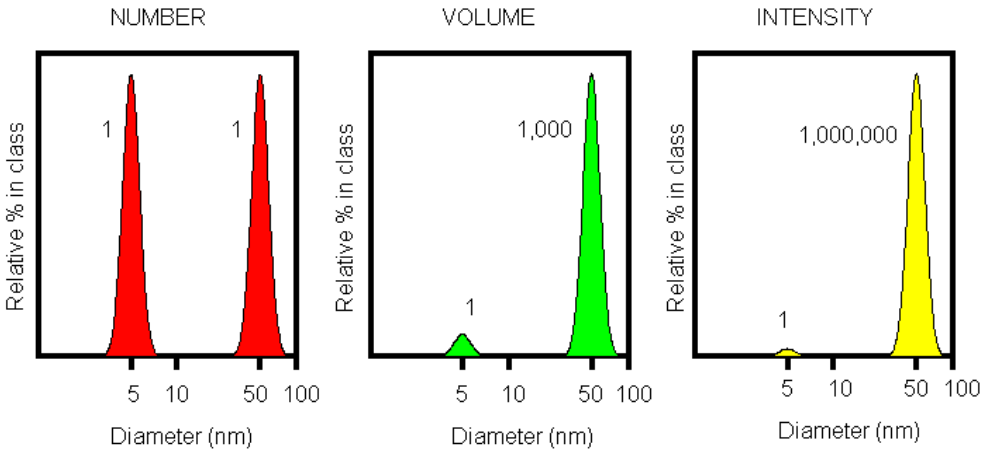

Figure 3.5. Number, volume and intensity distributions of a bimodal mixture of 5 and 50 nanometer particles present in equal numbers.

As can be seen from Figure 3.5, the volume and number distributions give a much more accurate result, however, since they are calculated from the intensity distributions an error here will results in an error to the 3^{rd} power for the volume distributions and an error to the 6^{th} power for the number distributions. The results of this can be seen as fluctuations in the volume and number data, and the results from these distributions should be used with care.

Dynamic Light Scattering Instrument

A typical light scattering instrument consists of six main components as can be demonstrated in Figure 3. 6 (denoted 1-6). The light source used to illuminate the sample is a laser (1). The sample is contained in a cell (2) which most of the laser beam passes through, however some light is scattered by the particles within the samples at all angles which a detector (3) measures. The detector position can be at various angles, however typically 90 degrees is used. It is important that the scattered light lie within a specific range for the detector to successfully measure it. Too much light will cause the detector to become saturated and therefore an attenuator (4) exists to overcome this problem. The attenuator can control the amount of light that is permitted through the sample. If the sample is concentrated, the attenuator will reduce the intensity of scattering, or if the sample consists of very small particles or samples of low concentration, the attenuator will allow more laser light through the sample. Furthermore, the scattered intensity signal us passed to a digital processing board knows as the correlator (5). As mentioned, the correlator compares the scattering intensity at successive time intervals to derive the rate at which the intensity is varying. Finally the correlator information is passed to a computer (6) where the software will analyze the data and derive size information. A typical light scattering instrument is given in Figure 3.6.

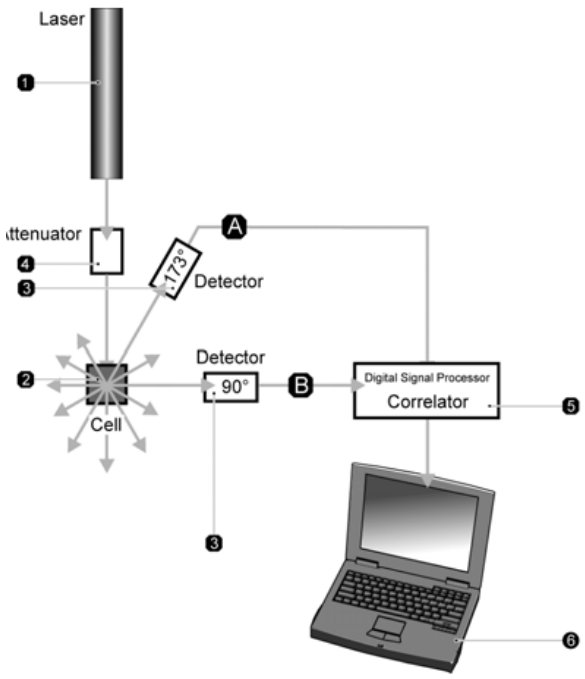

Figure 3. 6. Typical dynamic light scattering apparatus

3. 4 Coating techniques

In this section different coating techniques will be discussed with an emphasis on the preparation of ceramic membranes.

A major break-through in membrane development was made when the asymmetric membrane was introduced. The asymmetric membrane consists of a thin dense top layer over a porous support of the same material. Another step forward was the development of the composite membrane where the top layer and the sub layer are made from different materials. To apply the thin dense top layer upon a support numerous techniques can be applied:

- dip coating
- spray coating
- spin coating
- slip casting
- interfacial polymerization
- in-situ polymerization
- chemical vapor deposition
- sputtering

The preparation of porous, inorganic membranes can be done in a manner of ways depending on the desired membrane material and the pore size. Since many membranes are multilayered composite membranes, different method may be used to prepare the support material and the separation layer. Preparation of thin film membranes include chemical vapor deposition (CVD), sputtering and spray pyrolysis.

CVD involves the deposition of a component in the vapor state on a substrate by means of a chemical reaction. For example, Gavales and al. [114] deposited SiO_2 films within the wall of porous Vycor tubes by SiH_4 oxidation in opposing reactant geometry. SiH_4 was passed inside the Vycor tube while O_2 was passed outside and reacted within a narrow front inside the tube wall to form a thin SiO_2 film. Once the pores were plugged, the reactants could no longer reach other and the reaction stopped.

Sputtering is a technique where a target is bombarded with energetic particles, causing surface atoms to be ejected and then deposited on a substrate close to the target. This method have been used by Gryaznov et al. [115] which deposited thin films of binary and ternary alloys of palladium with manganese, cobalt, ruthenium, tin and lead on asymmetric membranes, porous stainless steel sheets and oxide supports by the sputtering technique.

Spray pyrolysis involves spraying a solution of metal salts into a heated gas stream where it is pyrolyzed. This method has been successfully applied for the production of fine metals or metal oxide particles. Li et al. [116] obtained a Pd-Ag alloy membrane on the surface of a porous alumina hollow fiber by spray pyrolysis of a Pd $(NO_3)_2$ and $AgNO_3$ solutions on a H_2-O_2 flame.

The rest of this chapter will focus on the three techniques used in the project.

Dip Coating

The biggest advantage of dip coating is its simplicity: An asymmetric membrane is immersed in the coating solution containing the polymer, the concentration of the solute in the solution being low (often less than 1%). When the asymmetric membrane is removed from the bath containing the coating material and the solvent, a thin layer adheres to it. The film is then put to dry (often in an oven) where the solvent evaporates

and where crosslinking occurs. The crosslinking contributes the coating layer to become attached to the sub layer.

Spin coating

A widely used method to produce thin and uniform polymer films is spin coating. A solution is placed onto a solid substrate which is then rotated and the solution is spread out and covers the substrate due to the centrifugal force. Due to the spinning, the solvent evaporates and after a certain time of spinning a residual solid covers the substrate. Factors influencing the final film thickness include spinning speed, concentration of the polymer solution, and molar mass of the polymer used [117]. According to Dunkel [118], for a moderate concentrated solution the film thickness is directly proportional to the concentration. However, deviations from this proportionality have been observed for high and low concentrations [119]. The spinning process can be divided into fours steps.

Step 1 is the deposition of the coating fluid onto the substrate. The deposition of the coating solution can be performed in various manners; by using a nozzle and pouring the coating solution, by using a pipette and dropping the fluid or by spraying the solution onto the surface. Usually a substantial excess of coating solution is applied.

Step 2 involves accelerating the substrate up to its final, desired, rotation speed. Fluid is expelled from the surface by rotational motion and due to the initial depth of the fluid on the surface spiral vortices may be present during this stage. At last the substrate reaches its desired speed and the fluid is thin enough that the viscous shear drag exactly balances the rotational accelerations.

Step 3 is when the substrate is spinning at a constant rate and fluid viscous forces dominate fluid thinning. Edge effects are often seen because the fluid flows uniformly outward, but must form droplets at the edge to be flung off. Depending on the surface tension, viscosity, rotation rate, etc., there may be a small bead of coating thickness difference around the rim of the final substrate. However, if the liquid exhibits Newtonian viscosity and if the fluid thickness is initially uniform across the wafer,

theoretically the fluid thickness profile and any time should be uniform and leading to a uniform final coating.

Step 4 is when the substrate is spinning at a constant rate and solvent evaporation dominates the coating thinning behavior. At this point, the coating gels because the solvent is removed.

Step 3 and 4 occur simultaneously throughout all times, however the viscous flow effects dominate early on while the evaporation process dominates later. When the spinning is stopped, some applications require post-treatment like heating.

Slip-casting of ceramic membranes

Slip casting is probably the most widely used technique for preparing metallic oxide and ceramic membranes. When preparing ceramic membranes the porous support system it is necessary to prepare a stable slip (suspension) and the sol-gel technique is frequently used for this purpose (see chapter 3.1). The dispersion media, which in most cases is water or alcohol, sieves into the pores created by capillary forces. As the solid particles are retained at the interface of the support, they form a gel by the sol-gel mechanism. In this process it is important that the sol-gel mechanism starts immediately so that the particles do not penetrate the pores of the support system [67]. As a result of this, the slip must be close to its gelling state and the concentration cannot be too low. Membrane thickness is controlled by the dipping time, slip concentration, and the pore size of the support [64].

4. 0 Experimental

This chapter will cover the experimental section (sol-gel polymerizations, dynamic light scattering, SEM, AFM) together with a description of the apparatus.

4. 1 Sol-gel polymerizations

A complete list of all samples specified with quantities of monomers, catalysts and solvents can be found in Appendix 1, table A.2.

4. 1. 1. Chemicals and materials

Chemicals

Sol-gel precursors 1,8-bis(triethoxysilyl)octane, bis[3-(triethoxysilyl)propyl]urea (60% in ethanol) and bis(triethoxysilylpropyl)amine (95% in ethanol) were obtained from Gelest Inc., Tetraethyl orthosilicate (TEOS, 98%) was obtained from Aldrich. Ethanol (anhydrous) and tetrahydrafuran (THF, anhydrous) were obtained from Aldrich Sigma. Hydrochloric acid (HCl (aq), 48-41%) was obtained from Alfa Æsar and ammonium hydroxide (NH_4OH, assay as NH_3 28-30%) was obtained from EM Science. Physical data for monomers can be found in Appendix A, Table A. 1.

Materials

Ceramic membranes (support: titania; membrane: ZrO_2-TiO_2) were obtained from Sterlitech ceramic membranes with 5 and 15 kilo Dalton, 47 mm diameter. An Inside disram™ membrane disc holder in stainless steel was supplied from Skutech. Micro slides (plain, selected, precleaned) in 25*75*1. 0 mm, were obtained from VWR.

4. 1. 2 . Polymerizations

Sol-gel polymerizations were conducted in anhydrous ethanol or THF. Ethanol and THF were filtered through a Teflon membrane (pore size 0.25 μm) and otherwise used as received. Appropriate amounts of monomers were dissolved in the desired solvent (~ 3mL) in 10 mL volumetric flaks. Aqueous catalyst (1N HCl, 1N NH_3 or 1N KOH) was dissolved in approximately 2 mL of solvent and mixed with the monomer. The

resulting mixture was diluted with solvent to a 10 mL total volume to give the desired concentration. The solution was mixed for about 10 seconds before poured into glass scintillation vials and tightly closed to prevent evaporation.

4,4'-Bis(4-(triethoxysilyl)styryl)biphenyl (Fluorescence monomer)

4,4'-Bis(4-(triethoxysilyl)styryl)biphenyl (Figure 4.1) was added to some of the solutions (see Appendix A, Table A.2) to monitor penetration and to observe the uniformity of the coating. The fluorescence monomer was prepared by a two fellow students [120] in the following procedure:

To a three neck 25 mL round bottom, triethoxy(4-vinylphenyl)silane (1.907 g, 7.2 mmol) was added. To this solution, a magnetic stir bar along with 4,4'-dibromophenyl (1. 176 g, 3.8 mmol) were added followed by anhydrous toluene (20 ml). To this solution, tri-o-tolylphosphine (0.085 g, $2.6x10^{-5}$ mol) along with palladium acetate (0.015 g, $4.45x10^{-5}$ mol) were added. To the solution, triethylamine (1.35 g, 1.33 mmol) was added. This solution was stirred and heated at 105° C. The solution was allowed to react for 24 h. The brown suspension was filtered through Celite® to remove palladium. The solvent was removed *in vacuo* and a crude yellow solid was obtained (1.909 g, 74 % in quantitative yield). The crude solid was purified by recrystallization from hexane/toluene (v/v = 3:1) to obtain a green solid and was obtained in 40-50% yield.

Mp = 156. 8 °C. ^{1}H-NMR (500 MHz, toluene-d8) δ = 7.86 (d, 4H) δ = 7.52 (d, 4H) δ = 7. 43 (d, 4H) δ = 7. 40 (d, 4H) δ = 7. 06 (d, 4H) δ = 3. 90 (s, 12H) δ = 1. 25 (s, 18H). ^{13}C-NMR (125 MHz, toluene-d8) δ = 140. 399, 139. 628, 136. 893, 135. 694, 131. 544, 129. 451, 129. 205, 127. 599, 127. 522, 126. 442, 59. 011, 18. 678. Anal. Calcd for $C_{40}H_{50}O_6Si_2$ (MALDI) Found: 682. 2251.

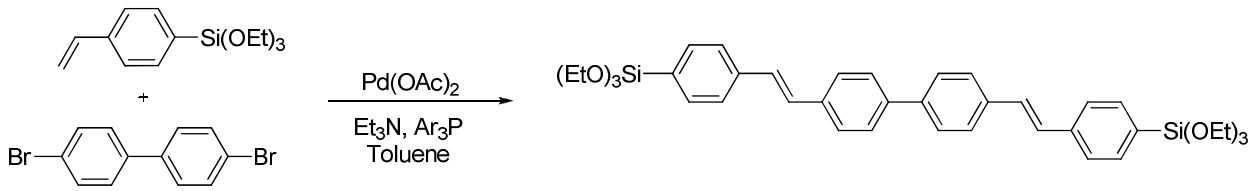

Figure 4. 1. Fluorescence monomer (*4,4'-bis(4-(triethoxysilyl)styryl)biphenyl)*

The fluorescence monomer (0.1 mol% of the precursor) was dissolved in approximately 2 mL of solvent and then the solution was sonicated until the monomer dissolved, just about 30 minutes. The solution was added to the volumetric flask (10 mL) and rest of procedure was done as described above. The sol-gels were further examined in a dynamic light scattering apparatus to determine the particle size growth over time

4. 2 Dynamic Light Scattering (DLS)

The sol-gel solutions were poured in to a cuvette (~ 1 mL) and placed inside a dynamic light scattering apparatus. Plastic cuvettes were used for solutions containing ethanol, and glass cuvettes were used for solutions containing THF. Preliminary light scattering measurements showed that it was best not to dilute the samples for light scattering, except in the case where fluorescence was involved. Sol-gels containing fluorescence monomers were diluted approximately 100 times in the desired solvent before measurements. A fixed scattering angle at 90 º was employed with a He-Ne laser (633 nm line). Dynamic light scattering measurements were done on a continuous basis until the solution gelled. Gelation was determined as the point at which the solution would no longer flow then the vial is tilted at a 90º angle.

4. 3. Coating

Three coating techniques were employed; dip coating, spin coating and a new method based on clogging the pores of the support.

Dip Coating

Dip coating was performed on square glass slides that were precleaned by soaking in HCl (12 M) for 45 minutes and then rinsed with water and ethanol and let dry for about one

hour. The glass slides were held in a pair of tweezers and then dipped in the scintillation vial until completely covered in solution and then quickly retrieved. They were then left on the bench to dry for one day before being studied in a microscope.

Spin Coating

Spin coating was preformed on both glass slides and ceramic supports. The glass slides were cleaned as described above, the ceramic supports were used as received. When the ceramic supports were reused, they were soaked in solution of HF (10 vol%) for about 10 minutes and then excessively rinsed with DI water.

The spin coating on glass slides was preformed in two ways;

(1) two drops of 100 μL of solutions was dropped on the support (motionless) and then the spinning was performed for 30 seconds at 1000 or 5000 rpm.

(2) two drops of 100 μL of solutions was dropped on the support while it already was moving at 1000 or 5000 rpm, and then left spinning for 30 seconds.

The spin coating on the ceramic supports were similarly spun in two ways:

(1) The sol-gel solutions were diluted 100 times in butanol and then the solutions were dropped on the support (motionless) until the entire surface was flooded and then the spinning was performed for 30 seconds at 5000 rpm.

(2) two drops of 100 two μL of solutions was dropped on the support while it already was moving at 2500 or 5000 rpm, and then left spinning for 30 seconds. The coated membranes were then taken to a microscope for further inspection.

Clogging

A closed system consisting of a vacuum pump and a metal disc holder was set-up. The clogging was employed on two different supports TiO_2 (5 and 15 kd) and Al_20_3 (5 kd) and used as received. The TiO_2 supports that were reused were cleaned in the matter described above. The vacuum was turned on and then the sol-gel solutions were applied with a pipette with drops of 2×100 μL with (1) no dilution and (2) 10 or 100 times dilution in ethanol or butanol. The vaccum was left on until there was no liquid left on top of support, about 30 minutes.

4. 4 Characterization

4. 4. 1 SEM

Specific details about the SEM execution (accelerating voltage, working distance etc). can be found in Appendix 3.

Preparation

Gels:

A drop of solution was deposited onto a silicon wafer and allowed to dry. The silicon wafer was then placed onto an SEM sample holder using a piece of sticky carbon tape. The sample was then sputter coated for 30 seconds with Pt at 5 milliamps

Silica wafer:

A silicon wafer was placed onto an SEM sample holder using a piece of sticky carbon tape. The sample was then sputter coated for 30 seconds with Pt at 5 milliamps, using the exact same preparation as for the gels.

4. 4. 2 Atomic Force Microscope (AFM)

Glass substrates were cleaned in HCl (12 M) for 45 minutes and rinsed with water and ethanol. The slides were let to dry for one hour and then two-three drops of diluted (~10 times) sol-gel solution was applied. The AFM imaging was done in tapping mode in air.

4. 5 Apparatus

Dynamic Light scattering

The dynamic light scattering measurements were carried out on a Malvern Zetasizer nano ZS90, which can measure particle size of a range from 0. 6 nm to 3 μm.

Field-Emission SEM

A Hitachi S-4800 Type II / ThermoNORAN NSS EDS (Figure 4.2.) was used from The University Spectroscopy and Imaging Facilities (USIF).

Figure 4. 2. SEM (Hitachi S-4800 Type II)

AFM

The samples were imaged using Dimension 3100 AFM instrument from Veeco instruments, Santa Barbara CA. A tapping cantilever made with silicon nitride, Si_3N_4(42N/M), also from Veeco Instrument was used.

Microscope

An Olympus BH2 microscope was employed for the characterization of the coatings.

5. 0 Results

In order to characterize the different effects of sol-gel parameters on the particle growth and final gel morphology, approximately 50 sol-gel solutions were prepared. Sol-gel solutions were prepared with different monomers (bis(triethoxysilyl)octane, bis[3-(triethoxysilyl)propyl]urea, bis(triethoxysilylpropyl)amine and tetraethoxysilane at different concentrations (0.05 M, 0.1 M, 0.2 M, 0.4 M, 0.6 M with different catalysts (HCl, NH_3, KOH,), different solvents (ethanol and tetrahydrafuran) and a different water to monomer ratios (6:1,1:1). Also, different coating techniques were used, including dip coating, slip-casting (clogging) and spin coating (1000 rpm, 2500 rpm and 5000 rpm). Higher quality micrographs can be retrieved in Appendix 0 (CD), "Micrographs," and all raw data from the DLS measurements can be obtained in Appendix 0, "Raw Data."

5. 1. Terminology

In this chapter, several abbreviations of the monomers will be made for simplicity sake: Bis(triEthoxySilyl)Octane will be referred to as BESO, bis[3-(triethoxysilyl)propyl]urea is simply referred to as Urea with capital U, bis(triethoxysilylpropyl)amine is similar abbreviated Amine with capital A, tetraethoxysilane will be referred to as TEOS, and last, 4,4'-bis(4-(triethoxysilyl)styryl)biphenyl will be referred to as fluorescence monomer or sometimes just as fluor. A summary of the abbreviations is given in Table 5.1, and their chemical structures are given in Figure 5.1.

Table 5. 1. Monomer abbreviations

Name	Abbreviation
Bis(triethoxysilyl)octane	BESO
Bis[3-(triethoxysilyl)propyl]urea	Urea
Bis(triethoxysilylpropyl)amine	Amine
Tetraethoxysilane	TEOS
4,4'-bis(4-(triethoxysilyl)styryl)biphenyl	Fluorescence monomer (fluor)

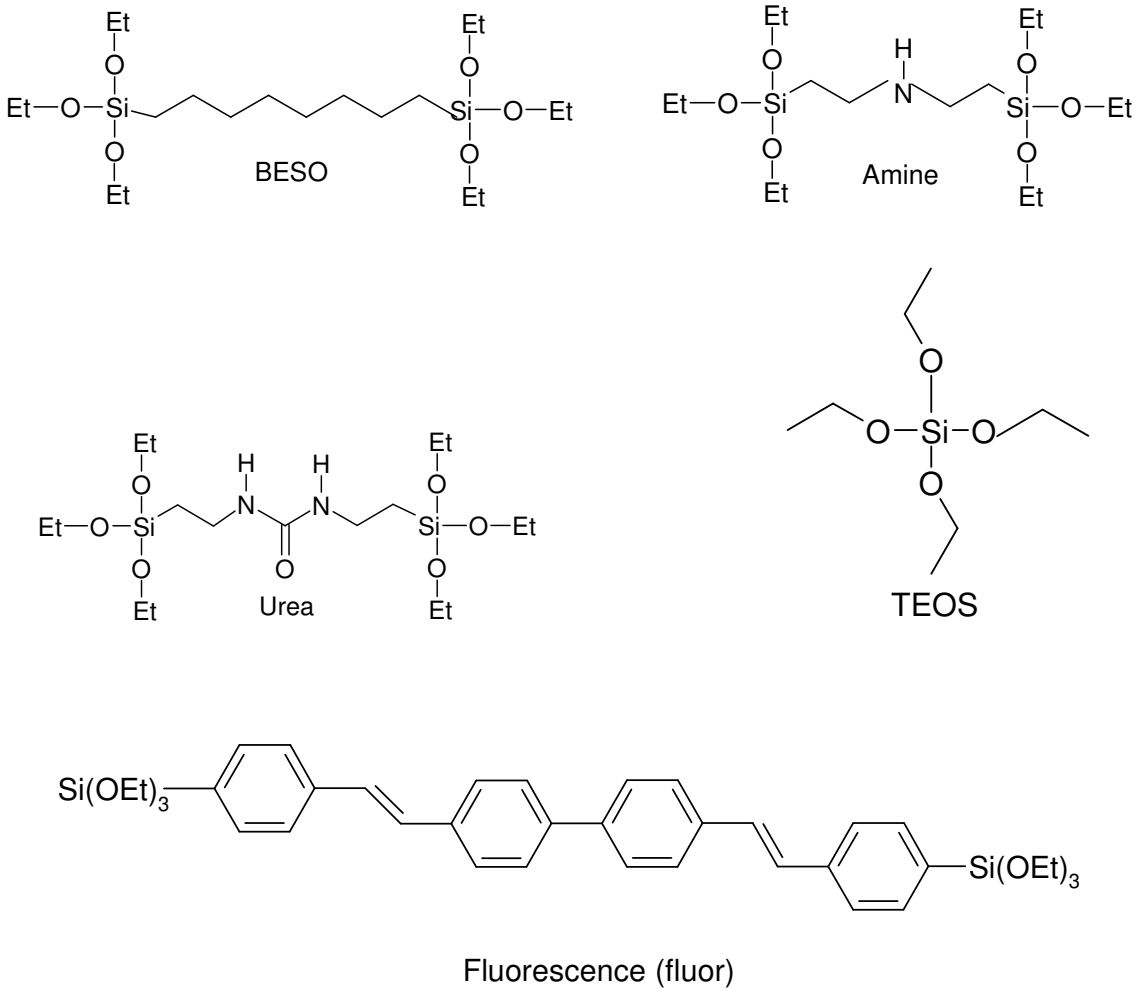

Figure 5.1. Chemical structure of BESO, Amine, Urea, TEOS and fluorescence.

5. 2 Effect of Parameters

Sol-gels were prepared at different conditions to determine how large the colloids would grow and to identify the best conditions for preparing colloids capable of coating a mesporous support. The effect of each parameter is given in the sections below. At the beginning of the project some *standard conditions* were chosen, and all other experiments are compared against these conditions. These standard conditions are:

1) HCl as the catalyst
2) Ethanol as the solvent
3) A water to monomer ratio 6:1

HCl was chosen to be the standard catalyst because dense membranes were desired. Ethanol was chosen to be the standard solvent because this is the parent alcohol, and a water to monomer ratio of 6:1 was chosen to make sure there was excess water. TEOS was prepared only for comparison as the particle growth of TEOS is well studied in literature [121-123] and could be used as a test to verify the other results obtained by DLS.

5. 2. 1 Effect of monomer concentration on particle size

Sol-gel solutions at various concentrations (0.05 M, 0.1 M, 0.2 M, 0.4 M, 0.5 M, 0.6 M, 1.0 M, 2.0 M) were prepared. As the purpose of the experiment was to see the effect of particle growth over time by dynamic light scattering, it was vital that the sol-gels did not gel immediately but were able to grow over for a period of time. Therefore, most sol-gels were first prepared at a concentration of 0.4 M and from this starting point it was decided, based on the time required for gelation, whether or not lower concentrations had to be prepared. It was determined that at least a growth period of one month was necessary to give the particles reasonable time to grow. If the sol-gels solutions gelled before this time, lower concentrations were prepared. The *gelation threshold* was determined to be the highest concentration that could be prepared without the sol-gel solution gelling before one month had passed. A presentation of the various monomers and their belonging gelation threshold are given in Table 5. 2.

Table 5. 2. Gelation Threshold

Name	Gelation threshold [M]
BESO	0. 2
Urea	0. 4
Amine	0. 05
TEOS	1. 0

As can be seen from Table 5.2, the amine bridged monomer has the lowest concentration threshold and TEOS has the highest at standard conditions. An overview of all the samples and their respectfully gelation time and size at gelation point can be retrieved in Appendix 4.

BESO

Firstly, the effect of concentration of BESO on colloids particle size will be discussed. The particle growth for BESO at a concentration of 0.4 M is given in Figure 5.2. The experiment was performed in duplicate (sample g [I] and g [II]) and show similar results with particles slowly increasing in size until gelation.

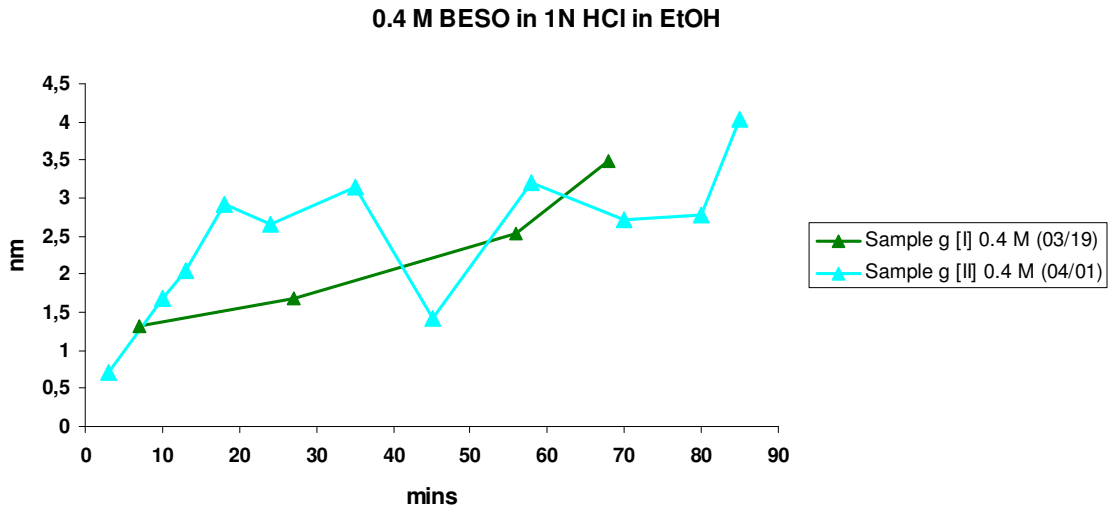

Figure 5.2. Particle growth vs. time for 0.4 M BESO at standard conditions

The solutions gel approximately after 70-90 minutes and reach a particle size up to 4 nanometers. Solutions at higher concentrations (0.6 M) were also prepared, however they gelled so rapidly (less then five minutes) that DLS measurements were not possible. The DLS results of sol-gels solutions prepared at lower concentrations, 0.2 M and 0.1 M respectively, are given in Figure 5.3.

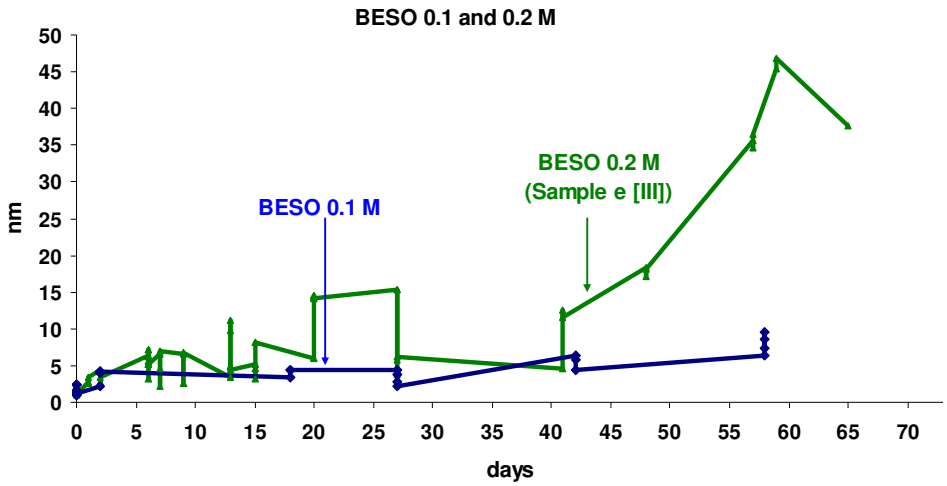

Figure 5.3. Particle growth vs. time for BESO 0.1 and 0.2 M at standard conditions

As mentioned in section 3. 3. 1, DLS measurements experience some noise due to the nature of experiments. Because the number average is calculated from the intensity distributions, an error here will results in an error to the 6^{th} power for the number distributions.

The concentration threshold for BESO is 0.2 M and the particles keep growing over time. This is the opposite of what is seen with silica, which quickly stabilizes after reaching a specific size. After about 2 months the gels prepared at 0.2 M gelled at a size of about 40 nanometers. This is considerably larger than the particles grown at 0.4 M, despite the lower concentration. When particles are grown at a lower concentrations than their threshold value they grow much slower, and they are smaller. After 2 months,

BESO at 0.1 M produces particles about 8 nanometer in diameter, which is much smaller then the 40 nanometer particles produced at 0.2 M. At BESO (0.1 M) the particles grow so slowly that it will be hardly practical for creating colloids larger than mesporous in a membrane support. Thus, from the DLS experiments it seems that particles grown at the threshold value produce the largest particles, and going higher or lower in concentration produce smaller ones.

Amine

The Amine was first prepared at a concentration of 0.4 M, but as it gelled after one day, subsequent polymerizations were conducted at 0.2 M Amine. At this concentration the sol-gel gelled after three days, when reaching a size of approximately 3-4 nanometers. Amines at 0.1 and 0.05 M were then prepared, and the particle growth over times for Amine at concentrations at 0.05 M and 0.1 M are given in Figure 5. 4.

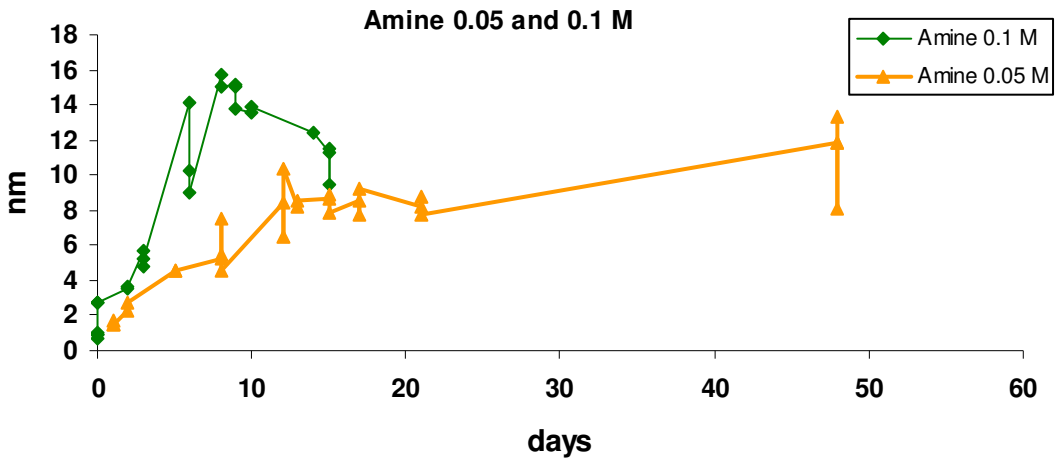

Figure 5.4. Particle growth vs. time for Amine 0.05 and 0.1 M at standard conditions

At 0.1 M, Amine gelled after 20 days and reached a size of about 10 nanometers. The polymerization with 0.05 M Amine is still slowly reacting after 48 days old and the

colloidal particles have reached 10 nm in diameter. It is expected that it will grow past the sizes produced by the 0. 1 M concentration, since the sol-gel is still a non-viscous solution, and thus there will be some time before it will gel. It is similar to the results that were seen with BESO, if the colloids are given time to grow (at least one month), the largest particles will be produced at its threshold value.

Urea

The particle growth over times for Urea at concentrations at 0.4 M and 0.2 M is given in Figure 5. 5.

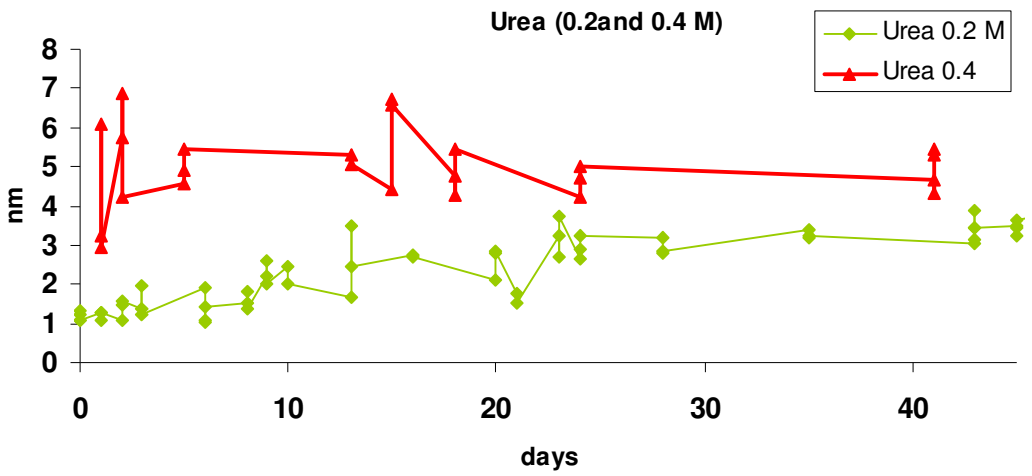

Figure 5.5. Particle growth vs. time for Urea 0.2 and 0.4 M at standard conditions

As for BESO, Urea grows the largest particles when it is prepared at its threshold value, 0.4 M respectfully. During this time, the Urea prepared at 0.4 M concentration contain larger particles than the one prepared at 0.2 M at all times.

It is therefore suggested that to produce large particles, the sol-gels need to be produced at their threshold value, meaning a concentration where they are allowed to grow for more than month. If the gels are prepared at higher values, the sol-gels gel more

rapidly, but they produce smaller particles. Large particles are desirable since supports with larger pores can be used, thus reducing the costs. Sol-gels produced at a higher concentrations value gel more rapidly and might be more desirable in industry, where time is an important factor.

5. 2. 2 Effect of catalyst

Three different catalysts were used in the sol-gel solutions, Hydrogen Chloride (HCl), ammonia (NH_3), and Potassium Hydroxide (KOH). As already mentioned in section 3.2.2, it is expected that basic catalysts results in small cluster formations and porous gels. An acid environment will produce long chains of particles and a compliant gel that eventually will collapse, and result in a dense gel. Since the purpose of this project was to prepare dense gas separation membranes, few experiments were performed with basic catalysts. The BESO was prepared with both HCl and NH_3 at 0.2 M, and the Urea was prepared with HCl and KOH at 0.2 M concentration.

BESO

Figure 5. 6 illustrates the effect of catalyst on the particle growth of 0.2 M BESO.

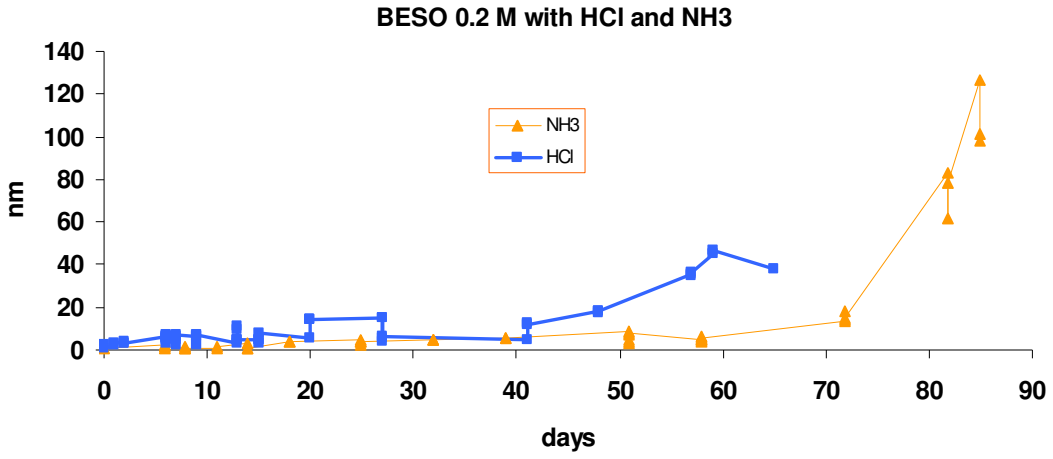

Figure 5.6. Particle growth vs. time for 0.2 M BESO with HCl and NH_3 as catalyst

From figure 5.6 it is clear that the sol-gel solution with NH_3 gels slower then the one with HCl, three months as opposed to two months, respectively. Another interesting observation is the different growth mechanisms the two catalysts seem to exhibit. The particle growth when acid is used seems to steadily increase over time. The base-catalyzed however, grows very slowly over time until right before the gelation point where the size increases rapidly. These findings agree with Norisuye and al. [124] who have proposed a growth mechanism for acid and base catalyzed gelation for tetramethoxysilane (TMOS). They have proposed that highly branched clusters are formed by basic catalysts while an acid leads to chainlike (or linear) molecules. For the basic catalyst, the small clusters grow independently and do not start to interconnect until they reach a significant size. At this point the interconnecting between the clusters is rapid and gelation occurs. From Figure 5.6 it can be seen that the basic catalyst produce cluster sizes of about 15 nanometers after 70 days, and 10 days later the growth has shoot up to 100 nanometer particles. One week later the solution had gelled. Therefore, at dilute concentrations the gelation point for base-catalyzed reactions will take longer because it takes longer time for the clusters to overlap. On the other hand, if the concentration is high enough, growing clusters easily overlap with each other and thus gelling can occur much sooner. Sol-gels prepared with HCl steadily increase their particle size over time that is what would be expected from a chainlike molecule growth. Figure 5. 7. represents the different growth mechanisms for acid (top) and base (bottom)

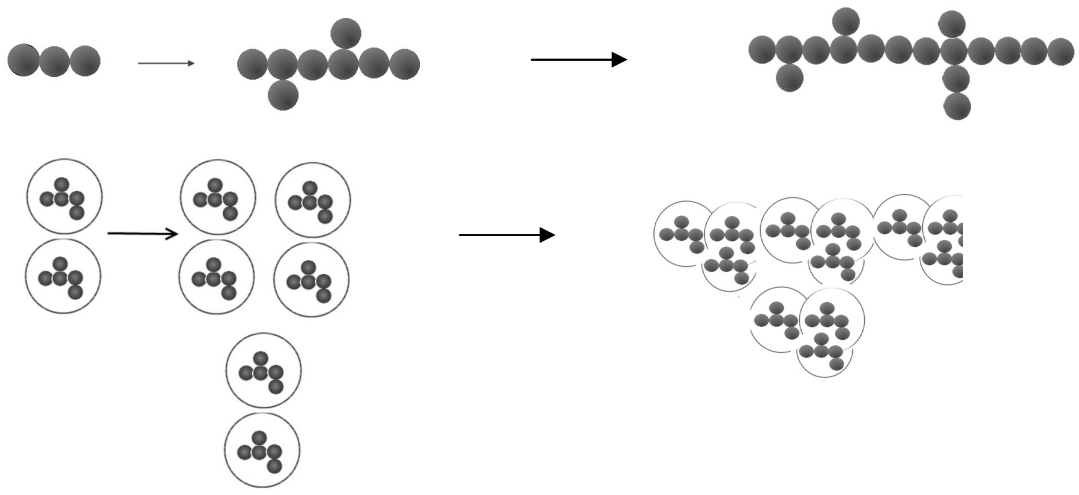

Figure 5.7. Cartoon of particle growth mechanism for acid (top) and base (bottom)

From the DLS experiments it is reasonable to conclude that the BESO exhibits similar acid/base growth mechanisms as TMOS [124].

However, it should be noted that another reason for the different growth mechanisms can simply be from he fact that ammonia escapes from the sol-gel solution, resulting in a drop in the pH. The lower pH will cause the particles to start aggregating, and thus gelation will occur not long after. To investigate the matter further a less volatile base should be used (NaOH, KOH).

Urea

As mentioned, Urea was prepared with both HCl and potassium hydroxide (KOH) as the catalyst. The results were very different, as the sample prepared with HCl gelled after 40 days and the one prepared with KOH after about 100 minutes. Besides from the gelation times, it seems that the two exhibits similar behavior; Both HCl (Figure 5.5) and KOH (Figure 5.8) produces particles about 8 nanometer before gelation. The final gels, however, exhibit widely different qualities, which will be further discussed in section 5.5. The basic catalyst was so much faster then the acidic catalyst, indicating that in this case a concentration of 0.4 M was high enough for the small clusters produced in the basic sol-gel, to overlap quickly and gel fast.

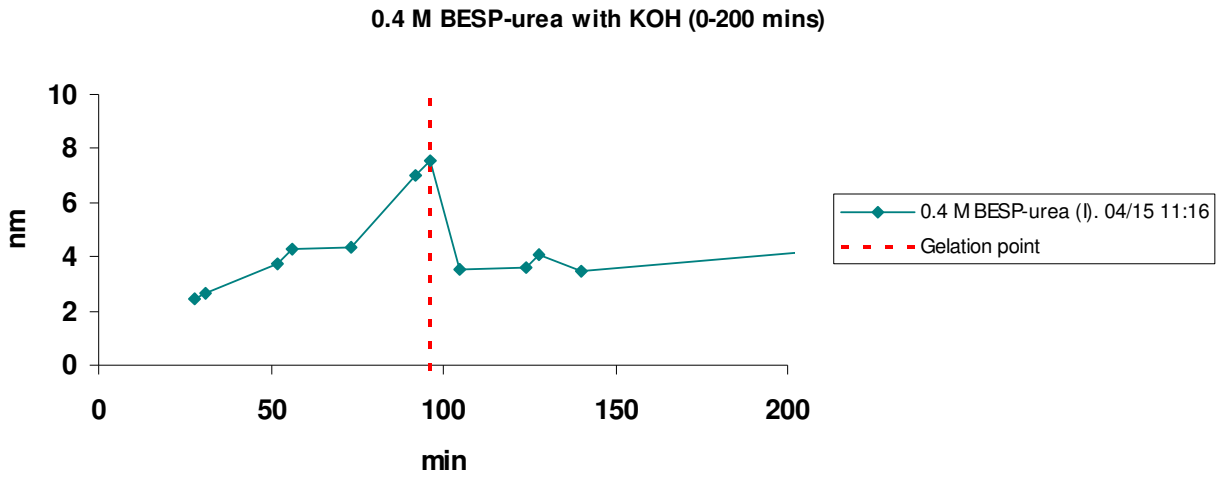

Figure 5.8. Particle growth vs. time for Urea (0.4 M) with KOH as catalyst

5. 2. 3 Effect of solvent

Sol-gels solutions were prepared with two different solvents, ethanol (EtOH) and tetrahydrafuran (THF). Because water and alkoxide are immiscible in all proportions, it is essential to add a solvent to make them miscible and facilitate hydrolysis.

BESO was prepared with EtOH and THF as the solvent at concentrations of 0.2, 0.4 and 0.6 M. The sol-gel solutions of BESO at 0.6 M gelled after five and seven minutes with THF and EtOH as solvents, respectively. The gelation time was so rapid that no DLS measurements were achieved, however the similar gelation times indicate that the particle growths were not affected by the solvent. The sol-gel solutions of BESO at 0.4 M gelled after 6 and 85 minutes with THF and EtOH as solvents, respectively. The particle size of the solution with THF was not measured as the gelation time was too short, however the particle size of the solution with EtOH was measured to be approximately 3.5 nanometer before gelation. At this concentration it seems that the particle growth was highly affected by the solvent as a sign of the different gelation times. At 0.2 M, the particle growth size seems to be unaffected by the type of solvent, as can be seen in Figure 5.9.

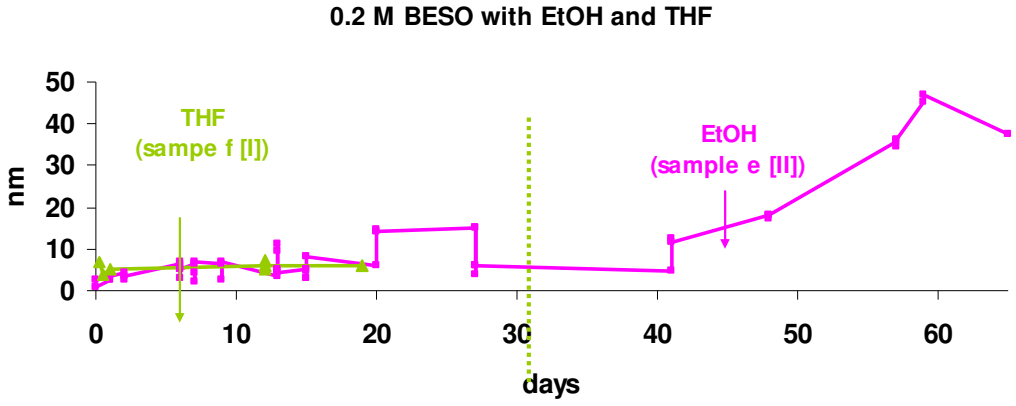

Figure 5.9. Particle growth over times for 0.2 M BESO with ethanol and THF.

The dotted, green line indicates the gelation time for the THF sample, approximately 5 weeks. Unfortunately, for THF the measurements were carried out only for 20 days due

to instrument problems. Anyway, it can be seen that for the first 20 days, the particle sizes are the same, but the difference lies in the gelation times. For BESO at 0.2 M the gelation time with ethanol as the solvent is approximately two times longer than with THF, 65 days and 35 days, respectively. The solvent does not seem to affect the particle size, however the growth rate is highly affected. Also, the two form completely different gels, as will be further discussed in section 5. 5.

5. 2. 4 Effect of water to monomer ratio

It is common to add at least three equivalents of water to the reaction as it is necessary for the onset of condensation reactions. However, by mistake some samples were prepared with deficit water amount, and the cases were investigated to see further what would happen. Figure 5.10 represents BESO 0. 2 M with one and six equivalents of water.

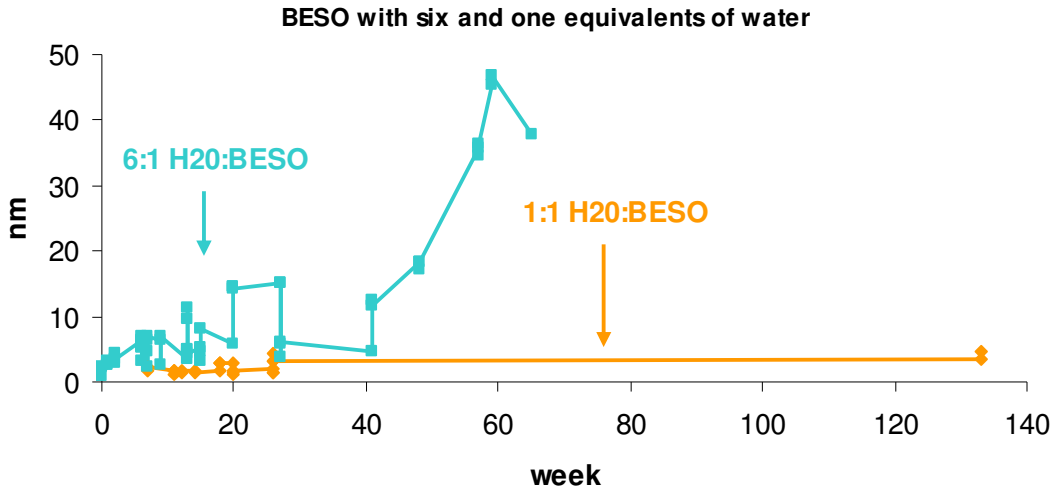

Figure 5.10. Particle size vs. time for 0.2 M BESO with one and six equivalents of water

The sample with deficit water did grow despite the lack of water, however at a much slower rate than the six equivalents of water sample. The samples continued to grow for about 20 days when it reached a size of about 3-4 nanometer, and after 5 months the particle sizes were unchanged.

5. 2. 5 Effect of fluorescence

A thin and uniform coating is critical in an asymmetric membrane, and in order to ensure that the membrane is located only on top of the support, the sol-gels were prepared with a small amount of a fluorescent co-monomer that will fluoresce under ultraviolet. Any material that penetrate into the support will show up under ultraviolet light. As little as 0.1 mol% of the monomer was added, and it was expected that such a small amount would not affect the size of the particles in the original sol-gel solution despite the much larger molecule size of the fluorescence.

Figure 5.11. shows a plot of particle sizes vs. time for Urea at 0.2 M concentration with and without fluorescence. From this figure it can be seen that the fluorescence monomer seem to be affecting the particle growth, as they show a larger particle size (~ 20 nanometer) compared to the standard Urea (~ 5 nanometer). Before drawing any conclusions, it is important to point out the DLS apparatus is sensitive to fluorescence, and it is possible that the sample might not be suitable for these measurements.

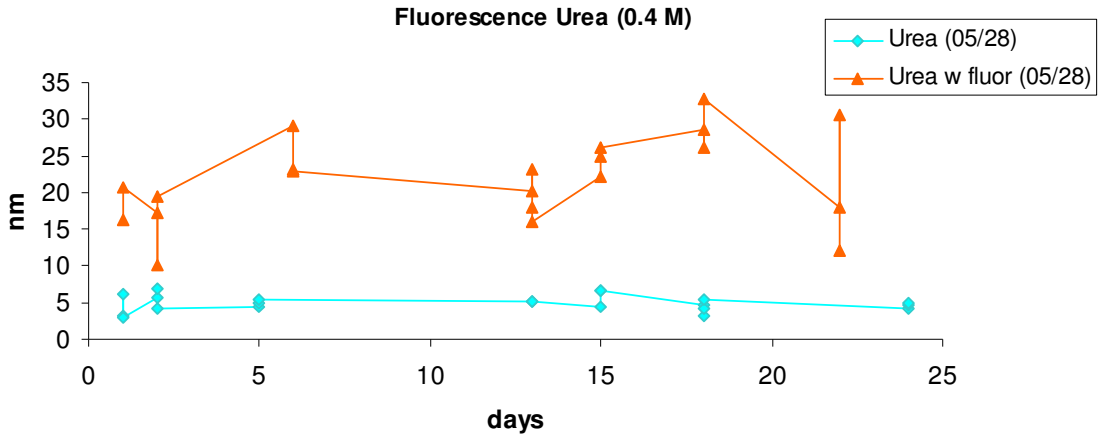

Figure 5.11. Particle growth over time for Urea 0.4M with and without fluorescence.

Fluorescence monomer was also added to the Urea at 0.2 M which shows similar behavior. Figure 5.12. presents the particle growth over time for Urea 0.2 M with and without fluorescence monomer. There appears to be large peaks of noise in the fluorescence samples, however, when the noise is disregarded it seems that the two samples overlap and produce the same particle sizes in the order of 4 nanometer.

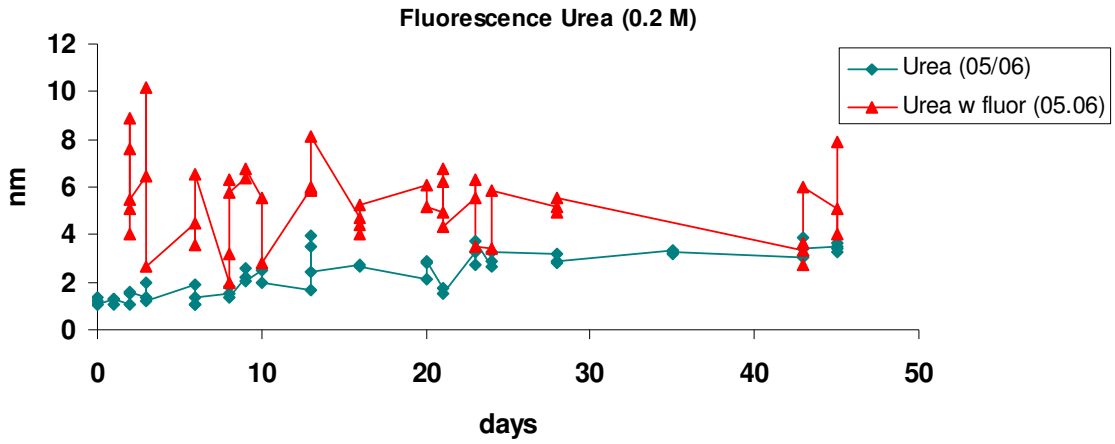

Figure 5.12. Particle growth over time for Urea 0.2 with and without fluorescence

Fluorescence monomer was also added to the BESO monomer and the Amine, the results are given in Table 5.13 and 5.14 respectively.

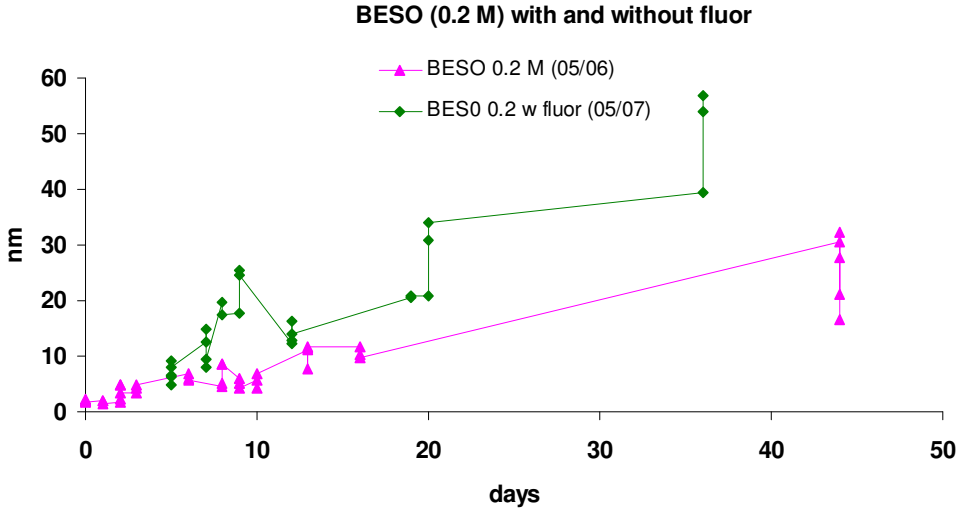

Figure 5.13. Particle size over time for BESO 0.2 M with and without fluorescent monomer

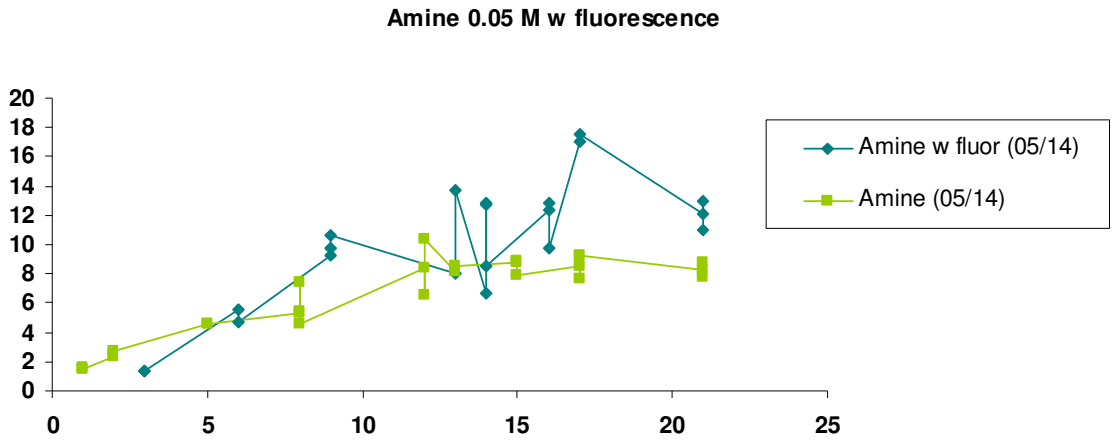

Figure 5.14. Particle size over time for Amine 0.05 M with and without fluorescent monomer

The samples with fluorescent monomer show a tendency to grow larger particles, however these samples also have larger noise peaks. Due to the apparatus' sensitivity to fluorescence it is possible that adding the monomer does not affect the particle size and that the larger particles that are observed are due to fluctuations and noise. For the Amine and Urea, it is likely that it is just noise that is causing the size difference. However, the BESO with fluorescence behaved differently than the one without fluorescence; the BESO prepared with fluorescence gelled faster, for example the BESO 0.2 M at standard conditions prepared without fluorescence gelled after approximately 2 months and the same one prepared with fluorescence gelled after about 43 days. This suggests that the fluorescent particles did in fact affect the particle growth of BESO. Also, the BESO prepared with fluorescence turned to a white gel, instead of a tinted blue which was the case for the other BESO gels. This indicates that the BESO particles prepared with fluorescence were in fact bigger, as larger particles scatter more light. The fluorescence monomer is a large molecule, and it is possible, that even at such small amounts, the size of the molecule makes the particles larger. Another possibility is that the monomer acts as some sort of catalyst. Amine and Urea have pendant bridging groups and might not have been affected by the fluorescence monomer due to steric hindrance. A similar observation has been done by Norisuye et al. who studied the DLS on the gelation process of another organic-inorganic polymer, tetramethoxysilane

(TMOS). They discovered that in the presence of an organic compound, such as poly(dimethylacrylamide) (poly-DMAA) or DMAA monomer, the gelation was accelerated [125]. The fluorescence monomer is a large molecule, and whether it is the size of the molecule that makes the particles larger, or if the monomer acts as some sort of facilitator in the process requires further investigations.

As mentioned earlier, TEOS was prepared as a comparison since its properties are well studies in literature. TEOS is known to grow to a stable particles size, and does not grow continuously until gelation [126].

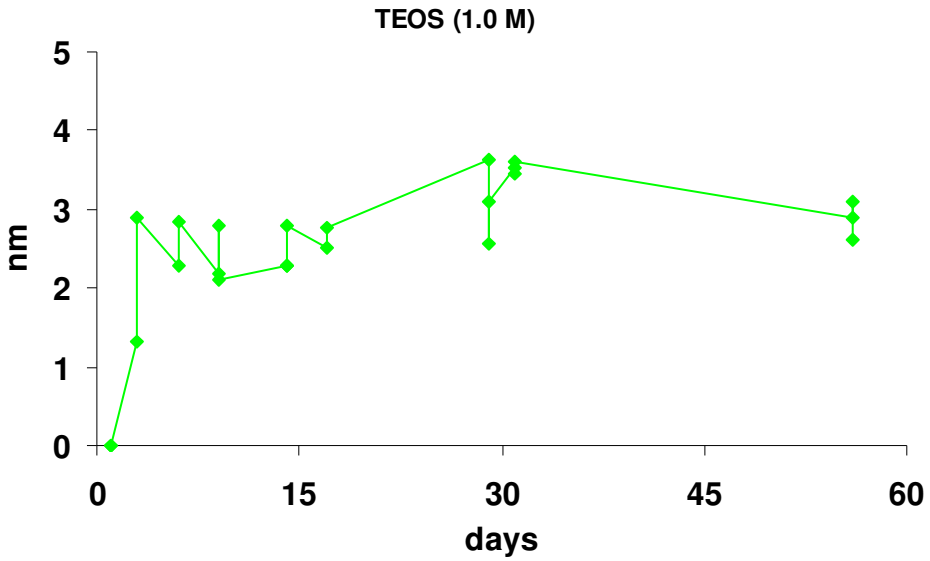

Figure 5.15. Particle growth vs. time for TEOS [1.0 M] at standard conditions

The results (Figure 5.15) were agreeable with those in literature, after reaching a size of about 3 nanometer, its size does not change over 60 days. This is the complete opposite of the BPs and is probably the most astonishing find of the DLS study; Bridged polysilsesquioxanes continue to grow larger over time, which is the complete reverse of silica which quickly reaches a stable size, and does not change over time.

5. 2. 6 Size distributions

Obtaining relatively monodisperse particles is important when preparing uniform coatings. Due to the structure of the monomer with six hydroxyl groups, it is reasonable to believe that the monomer will produce highly polydisperse solutions. However, from the DLS measurements the sol-gel solutions seem surprisingly monodisperse, at least in the beginning of the growth periods.

BESO

The sample distribution of BESO (0.2 M) is given in Figure 5.16.

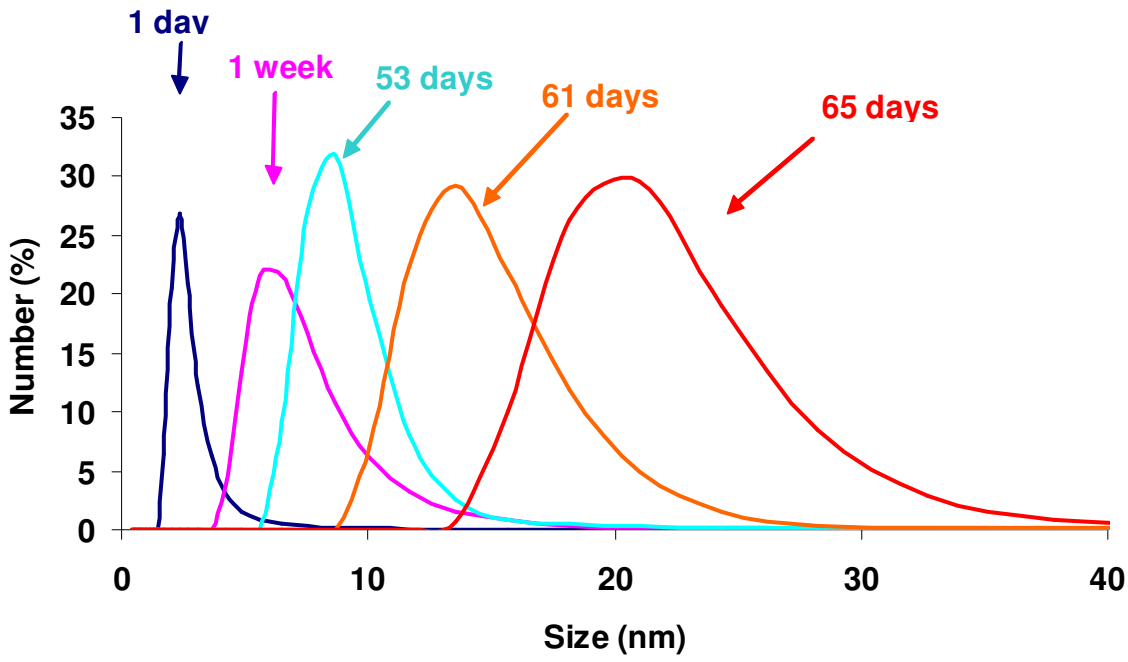

Figure 5.16. Size distribution of BESO (0.2M)

The size distribution of BESO (0.2 M) is relatively monodisperse at first, however after two months day the distribution is wide. This is expected since the monomer exhibits six hydroxyl groups which each can react at different rates. Right before the gelation point, large agglomerates are formed and therefore a wide distribution is seen. Even so, only one size peak was observed in the distributions, meaning all the particles were in the

same size range, which is promising in obtaining uniform membranes. A size distribution was also made for the BESO with fluorescence monomer (Figure 5.17).

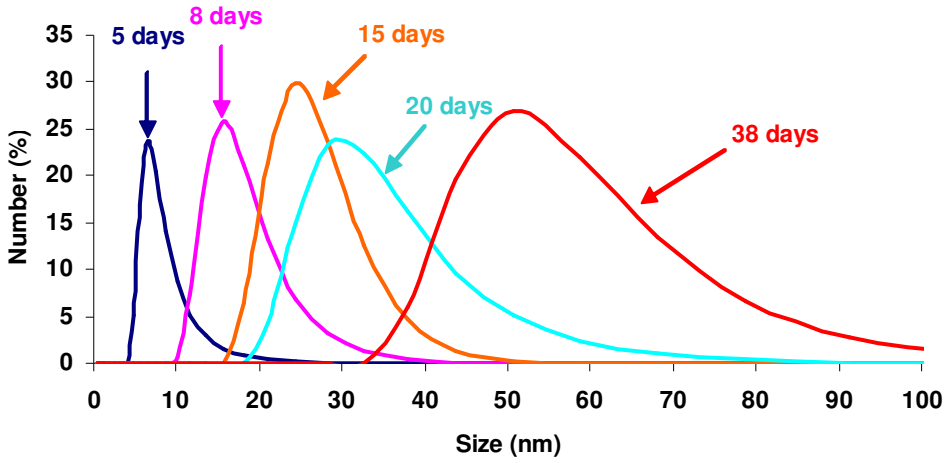

Figure 5.17. Size distribution of BESO (0.2M) w fluorescence

The same behavior is seen for the sol-gel with fluorescence. At the beginning the distribution is relatively monodisperse, and afterwards it becomes more and more polydisperse. A size distribution plot was also made for TEOS [1.0] for comparisons sake (Figure 5.18)

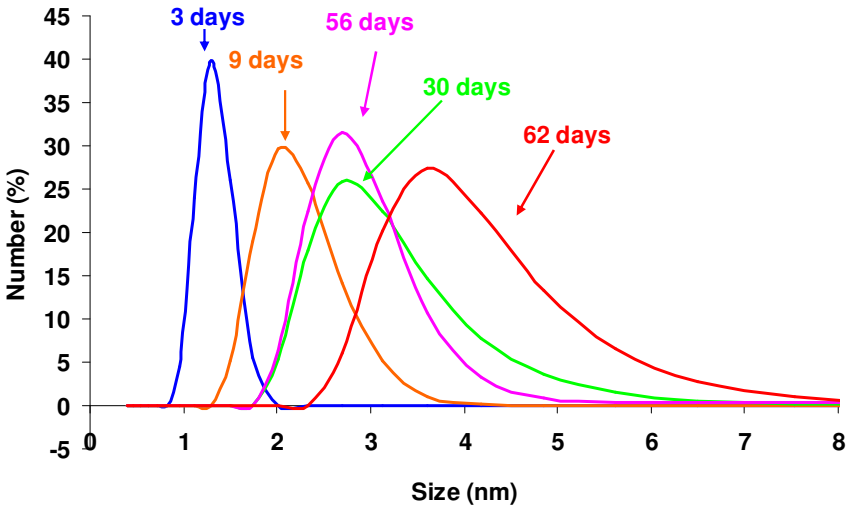

Figure 5.18. Size distribution plot by number for TEOS [1.0 M].

The size distributions for TEOS are relatively monodisperse, after 60 days the particle range is between 2-8 nanometer. Size distribution plots were also made for Amine, Urea, sample II (BESO with insufficient water), sample f (BESO in THF) and sample d (BESO with NH_3 as catalyst), (see appendix 5) which all exhibited the same behavior: Monodisperse distributions in the early growth period and more and more polydisperse over time. They also only exhibited one size peak. It might be desirable (in industry) to let the sol-gels only grow for a short period of time, as this will produce more uniform solutions. This will not only make the coating easier, as more uniform films will be produced, but also the membranes can be made in a shorter time. This of course will require supports with small pores, which are more cost extensive.

5. 3 SEM

As a back-up experiment for the dynamic light scattering measurements, SEM-images were taken of Urea (0.4 M) and Amine (0.1 M). The particle size of Amine (0.1 M) at standard conditions was measured approximately 10 nanometer with DLS the day before (15 days, April 30, see Appendix 0, Raw Data, "Amine"), and Figure 5.19 shows the results of SEM.

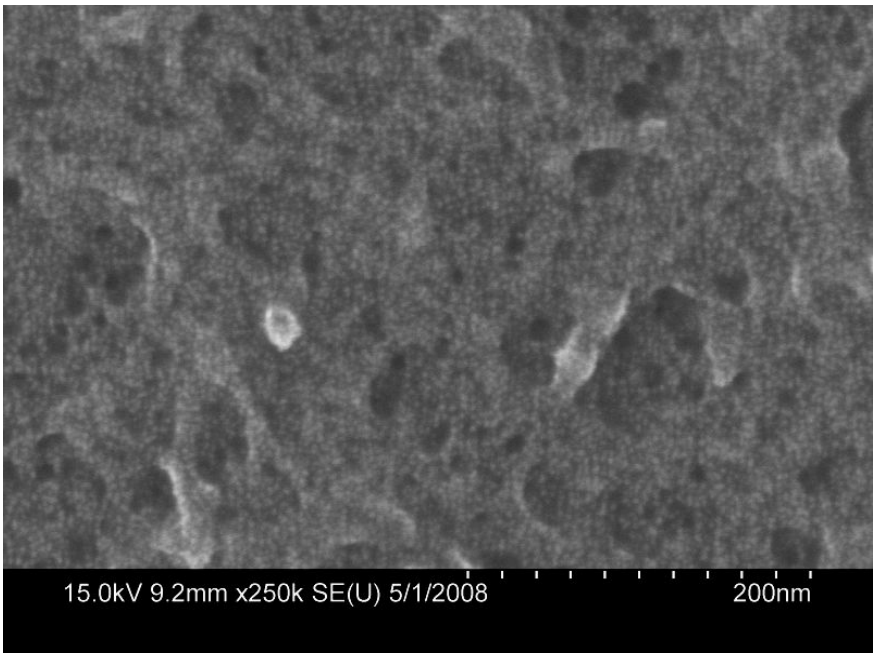

Figure 5.19. SEM image of Amine [0.1 M] (04/14)

Taking high quality SEM-images is difficult at such a small scale, however from the image it is possible to see tiny spherical spheres of a size close to 10 nanometer. As expected, the sizes seem to be somewhat smaller then 10 nanometer but all in all the two methods give similar results.

The particle size of Urea (0.4 M) at standard conditions was measured to be approximately 25 nanometer with DLS the day before (21 days, April 30, see Appendix 0, Raw data, "Urea"), and Figure 5.20 shows the results of SEM.

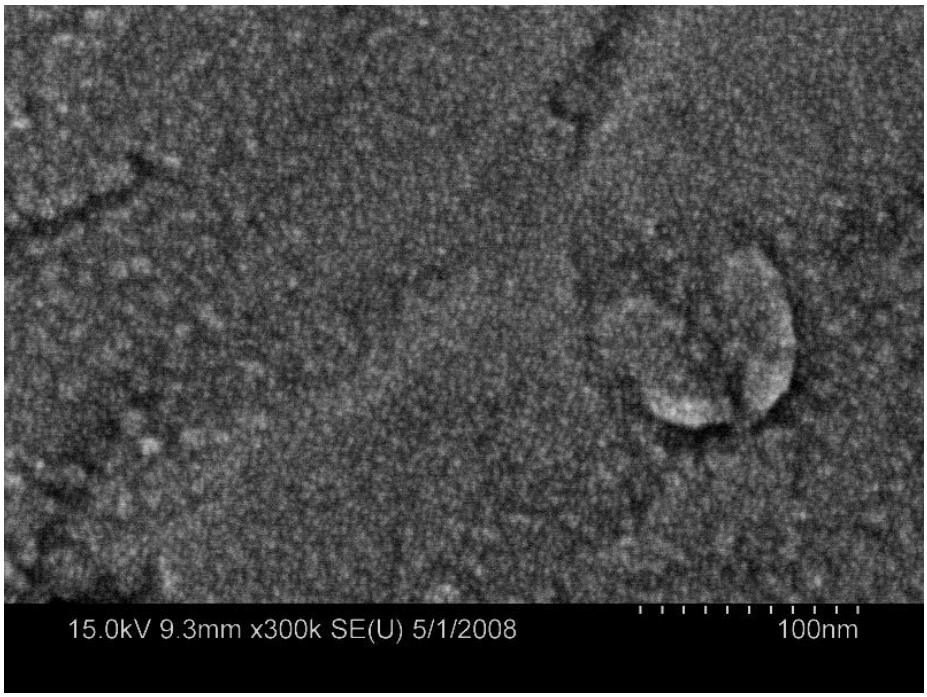

Figure 5.20. SEM image of Urea (0.4 M) (04/09)

From the SEM image, the Urea (0.4 M) particles seem to be even smaller than the Amine (0.1 M), approximately 3-4 nanometer. It was therefore suspected that there was something unusual with the Urea solution and new parallel was prepared. After 24 days the size was measured to be ~ 4 nanometer with DLS (see Appendix 0, Micrographs, fluorescence, "Urea (0.4) w comparison") which is in much better agreement with the SEM image. The SEM gives slightly smaller particle sizes then the DLS which is reasonable due to the fact that DLS measures the hydrodynamic diameter.

To make sure that in fact it was the sol-gel particles that were being observed in the SEM, a control image of a clean silica wafer was taken. The silica wafer was prepared in the same manner (cleaning, coating) as the sol-gels, and the image was taken with the same settings, Figure. 5.21.

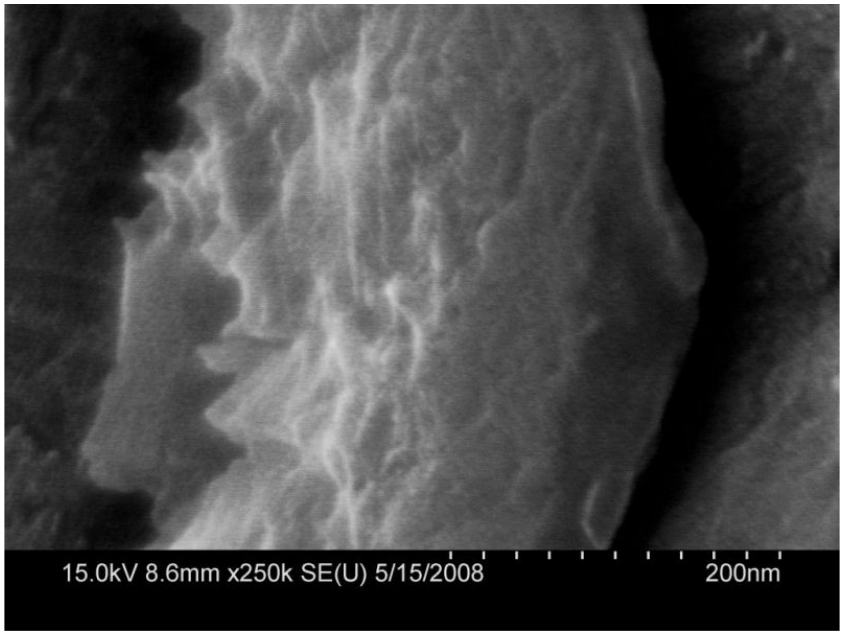

Figure 5.21. SEM image of silica wafer

No particles are observed in this image and it can be said with confidence that there are sol-gels particles being observed in Figures 5.19-20.

5. 4. Atomic Force Microscopy

Atomic force microscopy was used as a back-up of the DLS measurements for the BESO sample. The size of BESO (0.2 M) with fluorescence at standard conditions was measured to be ~30 nanometer at the day of the AFM preparation.

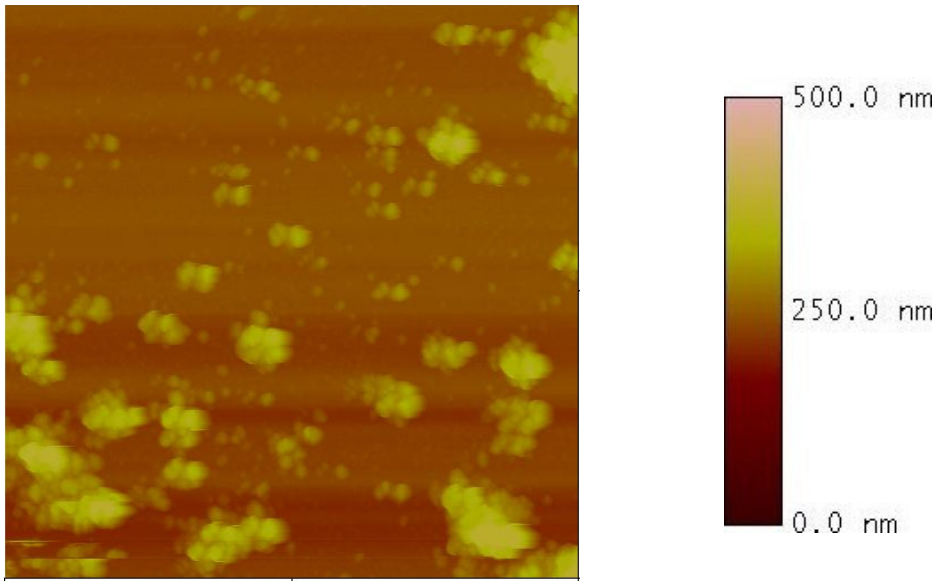

Figure 5.22. AFM image of BESO (0.2M) w fluor, height image 5 micrometer

The red color is the substrate and the bright yellow regions are the particles. It can be seen that some of the particles have formed aggregates as a results of the gelation that takes place when the solvent evaporates.

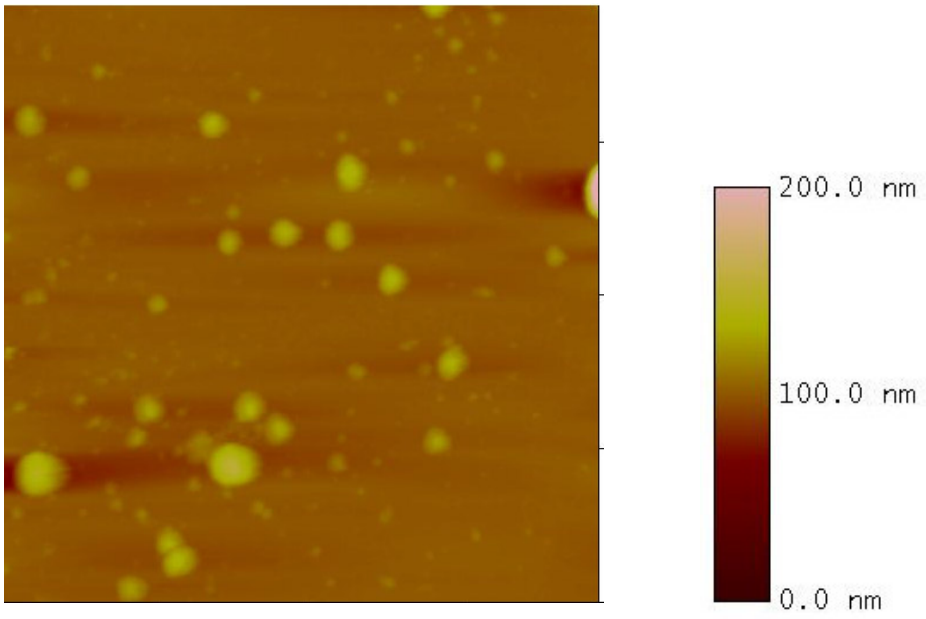

Figure 5.23. AFM image of BESO (0.2M) with fluor, height image 5 micrometer

The largest particles (aggregates) are about 79-205 micrometers, but much smaller particles are also observed. The smallest particles are in the range of 20-30 nanometers which are the same results as DLS. The sizes of the particles are determined using the section analysis of the horizontal distance (see Appendix 6).

5. 5 Gel morphology

Depending on the monomer, monomer concentration, type of solvents and catalysts, the gelation time was different as well as the final gel morphology. An overview is given in Appendix 4, table A.4. To test the gel properties after three and a half month, a small amount of stress (a plastic pipette was pressed down onto the gel) to study the strength of the gel. The gel strength is an important parameter when choosing a membrane, as it needs to handle high pressures in an industrial process.

BESO

The BESO (0.4 M) gels at standard conditions have a tinted blue color and experiences no cracking (Figure 5.24). Some syneresis is seen, but overall the gel is resistant to ageing processes.

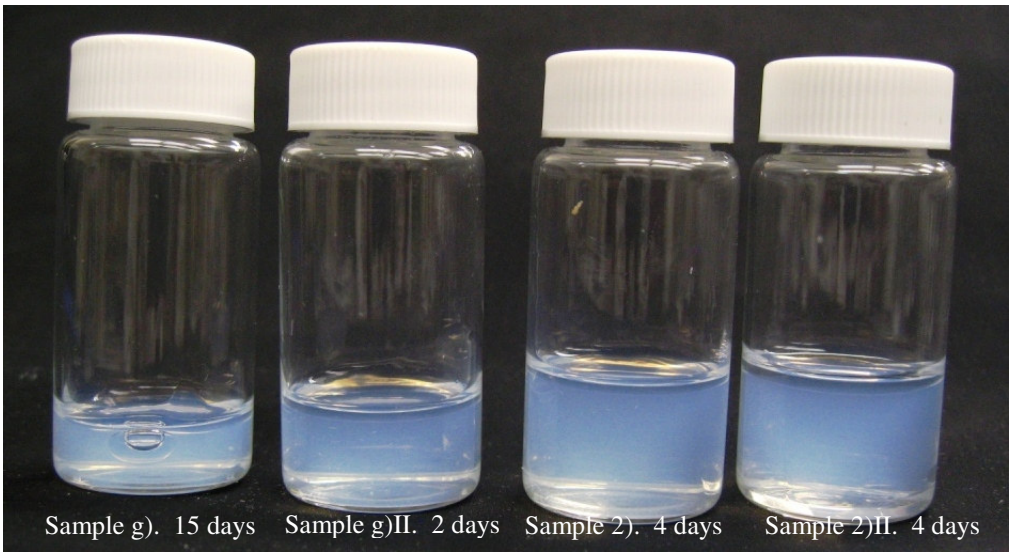

Figure 5.24. BESO (0.4 M) at standard conditions

After three and a half month there were still no cracks. However, when a small amount of stress was applied, the gel cracked into two large pieces, and when further stress was applied even more pieces. The BESO (0.4 M) prepared at standard conditions undergoes little syneresis, but is a brittle gel and cannot handle even small stresses.

When BESO is prepared at higher concentrations (0.6 M), this sample started cracking after 1 day and underwent severely more syneresis, see figure 5.25. The 0.4 M concentrations are to the left and the 0. 6M to the right.

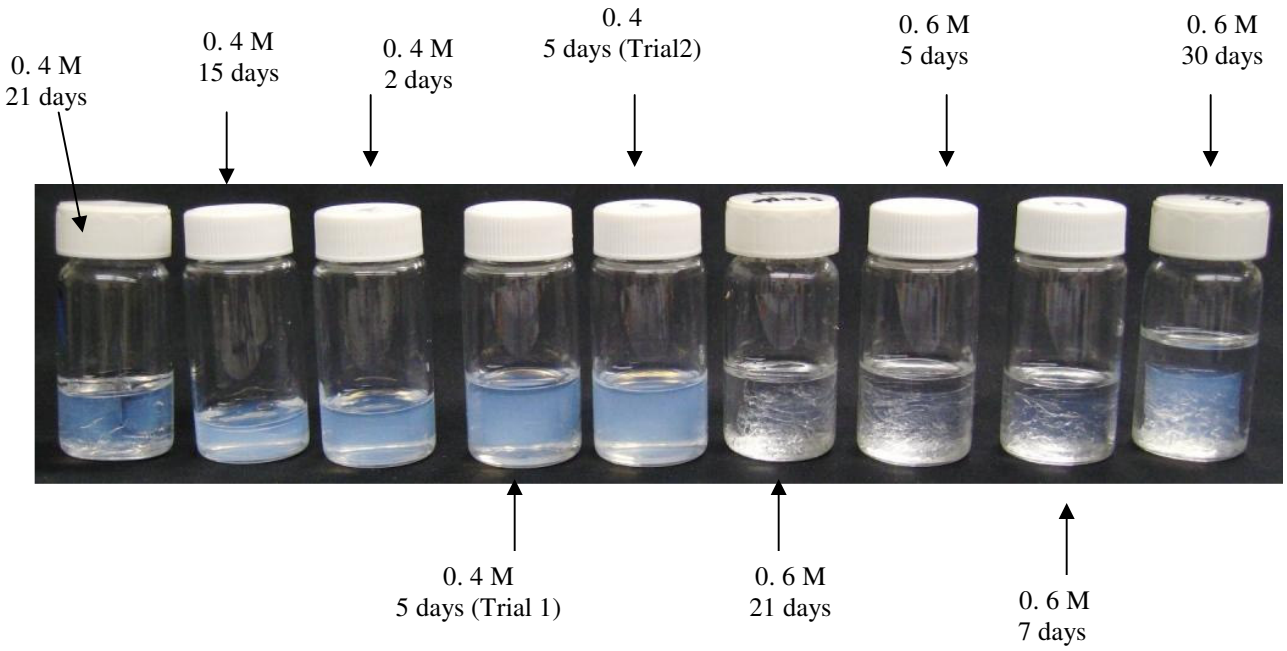

Figure 5.25. BESO in EtOH at 0. 4M and 0. 6M

An interesting observation can be made from the BESO (0.6 M), which started out as a clear gel, but after 30 days it turned light blue. This indicates the particles are still growing and interconnecting, as larger particles scatter more light then smaller ones. Also these results agree with the light scattering measurements, where it was found that the 0.4 M grows to a size of about 30 nanometer before gelation (and have a tinted blue

color at this point), but the 0.6 M only is about 3-4 nanometer (and have a clear color at this time).

Sol-gels prepared with THF are clear gels which suffer from syneresis and cracking. The clear color is in agreement with the DLS measurements which measured a particle size of about 5 nanometers before gelation.

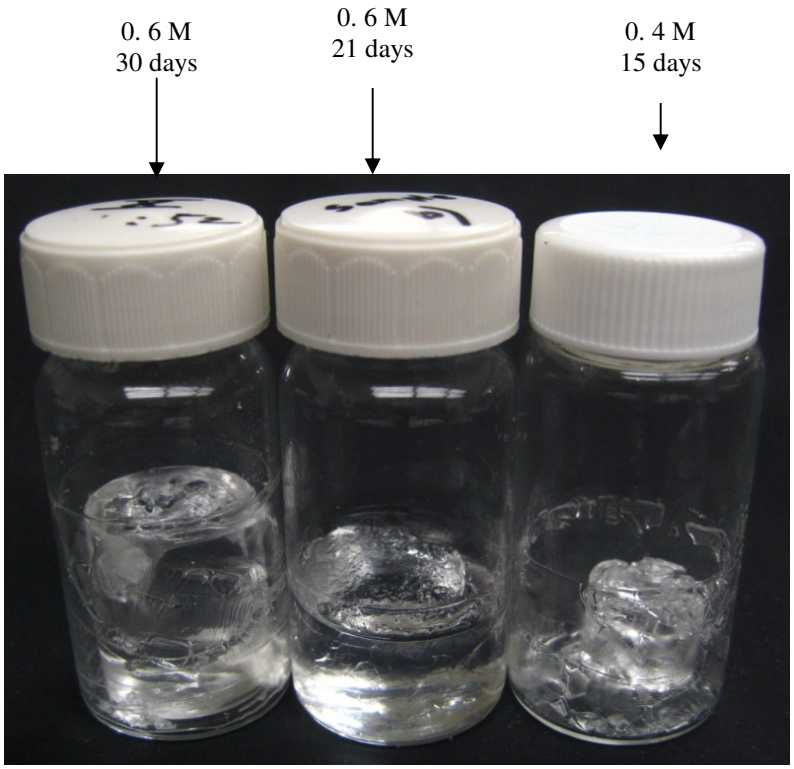

Figure 5.26. BESO (0.6, 0.4 M) with THF as solvent

The samples prepared with THF suffered from ageing processing at a much higher extent than the ones prepared with ethanol, see figure 5.27. The five samples to the left are prepared with ethanol and the one to the right with THF.

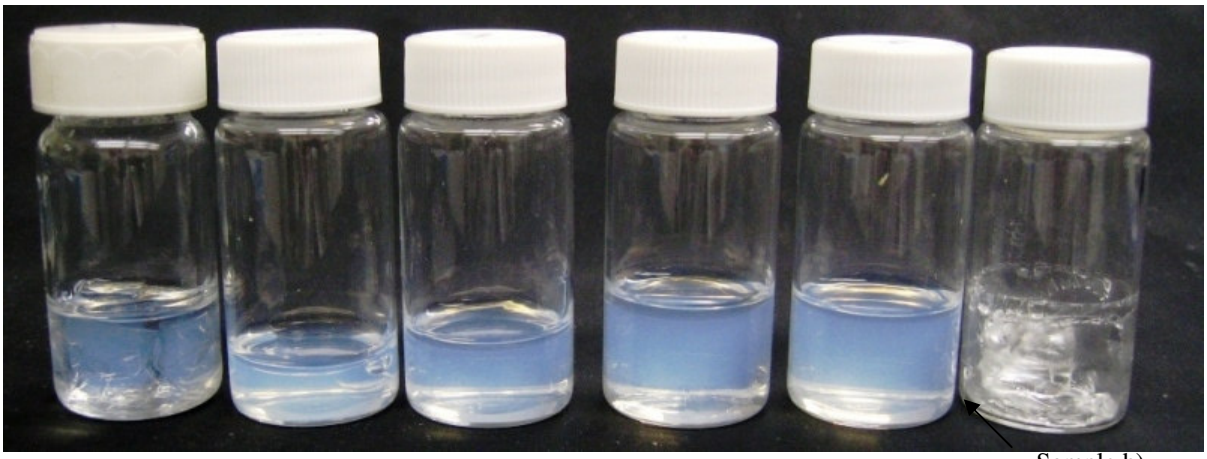

Figure 5.27. BESO (0.4 M) with Ethanol and THF

The samples are prepared at the same concentrations, and it is obvious that the sol-gel prepared with THF has undergone much more shrinkage and cracking after 15 days. Apparently the lid was not screwed on tightly enough, as the solvent has evaporated. As the gels prepared with THF have dried, it is reasonable that they also have undergone much more shrinkage and cracking, as the drying puts a great strain on the gel network. Even so, after three and a half month, the samples prepared with THF are much harder and stronger, and do not experience cracking when a small amount of stress is applied. The sol-gels prepared with THF undergo a lot of shrinkage and cracking the first days, but after this process they are very strong,

When the sol-gels were prepared at a concentration of 0.6 M, the differences were more subtle. Figure 5.28 show the sol-gels prepared at 0.6 M, the second to the left being the one prepared with THF.

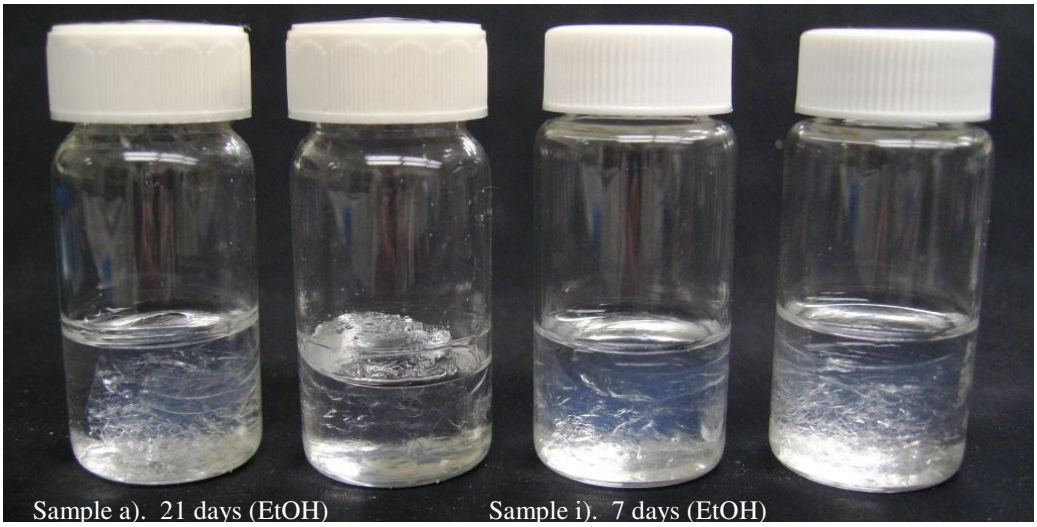

Figure 5.28. BESO (0. 6 M) prepared with ethanol and THF.

It seems that at a concentration of 0.6 M the one prepared with THF is more resistant to cracking then the ones prepared with ethanol. The samples prepared with ethanol are very brittle, and with a small amount of stress they collapsed in small pieces, similar to glass. The one prepared with THF is hard and did not collapse under a small amount of stress. It is even more obvious when prepared at 0.8 M, Figure 5.29

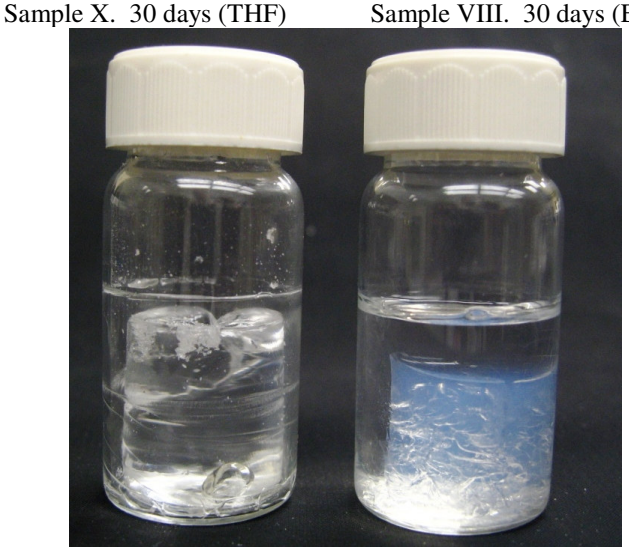

Figure 5.29. BESO (0. 8 M) with THF (left) and Ethanol (right) after 30 days

At a concentration of 0.8 M the gel prepared with THF is a strong, monolithic gel that does not crack under stress, even three and a half month after preparation. The one prepared with ethanol, however, is brittle, and under a small amount of stress it underwent serious cracking.

Amine

The Amine was prepared at 0.1 and 0.2 M and gelled after 20 and 3 days, respectively. The Amine (0.1 M) has undergone both ageing and drying, due to the cork not being screwed on tightly, and thus this, it has shrunk extensively (Figure 5.30).

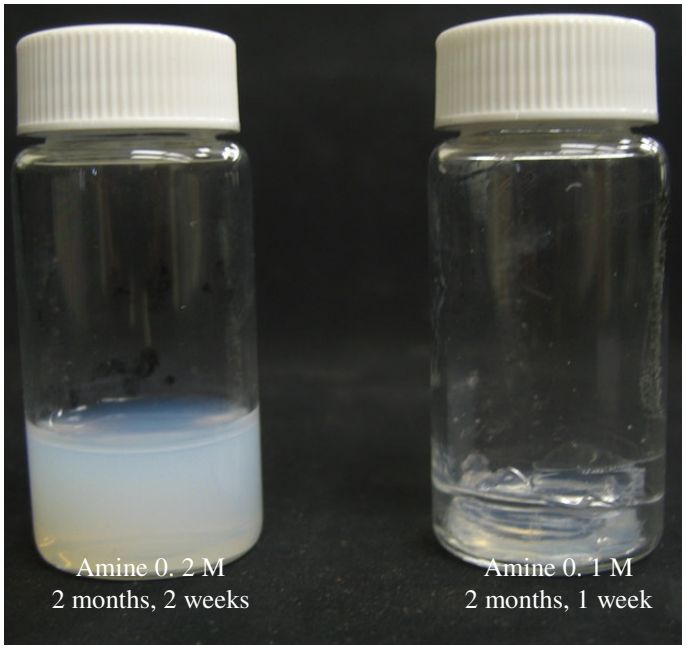

Figure 5.30. Amine w 0. 2 M (left) and 0. 1 M (right)

Therefore, the amine with the higher concentration has no cracks and has undergone very little syneresis. Even so, the Amine prepared at 0. 1 M is a much harder gel, as opposed to the one prepared at 0.2 M which is soft and compliant. A mechanical strong membrane is important in gas processing where high pressures might be applied, and in terms of durability a hard, strong membrane is desirable.

Urea

The Urea prepared at standard conditions generally does not behave too well under ageing, as can be seen in Figure 5. 31.

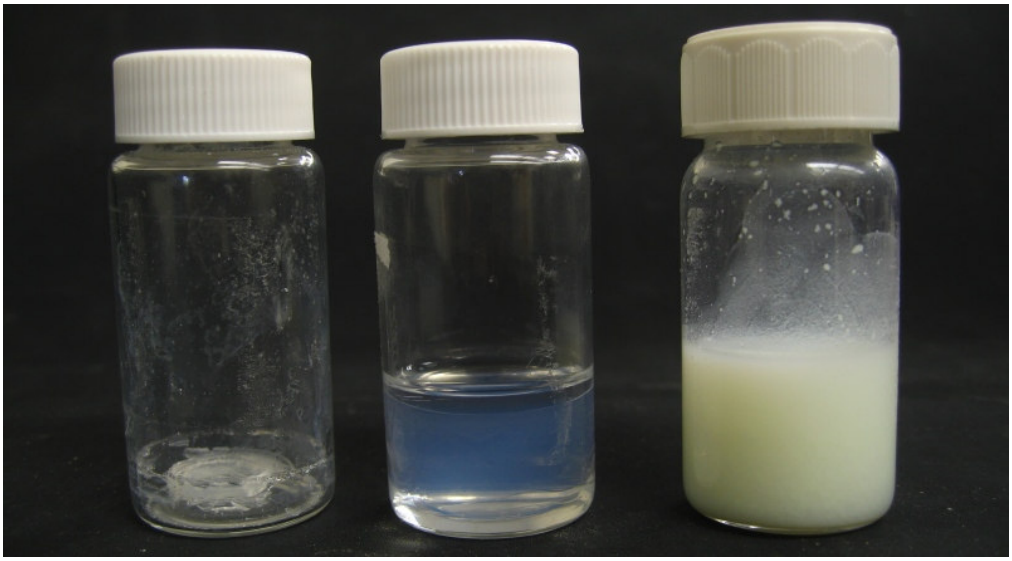

Urea (0. 4M) 2.5 months | Urea (0. 4M) KOH 63 days | Urea (0. 6M) w fluor 3 weeks

Figure 5.31. Urea at standard conditions, with KOH as catalyst, and with 0.6M w fluorescent monomer

After 2.5 months the gel has shrunk severely, and not much of the gel is left. However, it should be noted that the volume was not too large in the first place, as can be seen from the ring marks around the vial. The gel seems to be tackling ageing much better when prepared with KOH, after 63 days the gel has hardly changed, and no cracks can be observed. It should be noted that this gel has not been dried, as opposed to the Urea (0.4 M) where all the solvent has evaporated. However, when a small amount of stress was applied to the gel, it cracked severely. The one prepared with HCl is a dense, hard gel which shows no signs of cracking when applied the same amount of stress. The fact that the gel prepared with HCl is much stronger can resist cracking better than the one prepared with KOH, is due to widely different structures of these gels. BPs prepared with

base have a porous structure which is soft and compliant. The structure prepared with HCl collapses during ageing, and the result is dense, strong structure. Also, Urea prepared at 0.6 M shows no signs of either cracking or syneresis, and has a light yellow color, due to the presence of fluorescent monomer. However, this is a very soft and compliant gel, and most likely not suitable for industrial use.

From visual inspections of the gel, and by applying a small amount of stress to the gels, it can be concluded that to obtain a hard, strong gel, the gels must be prepared at low concentrations (not higher then 0.2 M or preferably, at a lower concentration than their threshold value) and an acidic catalyst should be used. THF is desirable as the solvent since it produces strong and hard gels.

The fluorescence monomer incorporated well into the sol-gel system as can be seen when the sol-gels were put under fluorescence lighting (Figure 5.32)

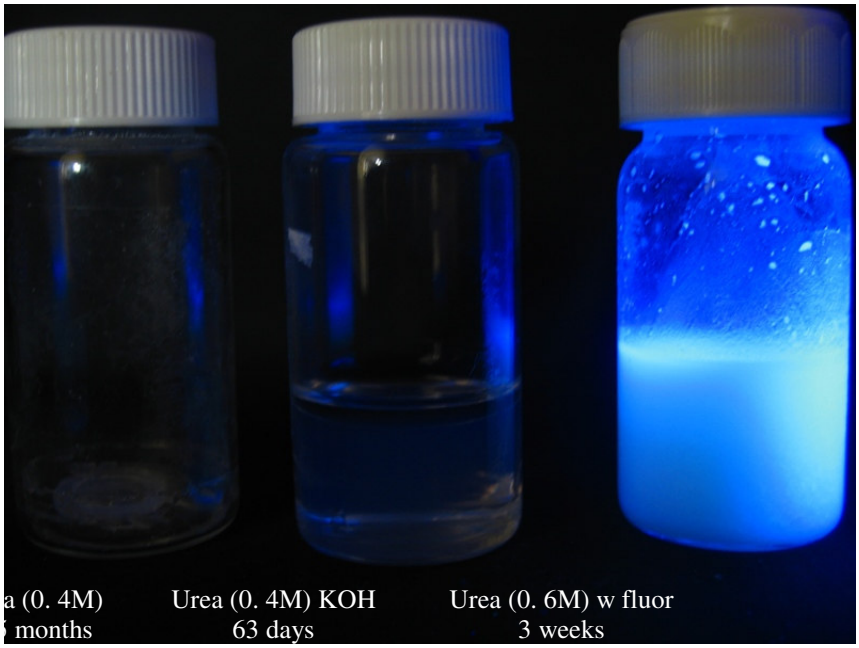

Figure 5.32. Effect of fluorescence monomer (to the right)

This photograph illustrates how bright the gel becomes with fluorescence monomer and therefore if the coating was to go through the support, it would easily be spotted with the bare eye, under fluorescence lighting.

5. 6. Coating

Three different coating techniques were employed, dip coating, spin coating and by allowing the sol to seal the pores from a solution on top of the membrane (similar to clogging a glass frit filter) with vacuum. The three different monomers (BESO, Urea, Amine) behave differently depending on the coating technique. Amine show the greatest resistance when it comes to cracking and BESO the least.

Before coating the TiO_2 and Al_2O_3 supports, practice was preformed on glass slides. All micrographs are denoted with the support used. It should be noted that preparing coatings on glass slides is much simpler than porous supports since the dense glass allows for more uniform films. Also, different magnifications were used and are denoted 10x or 20x, indicating 10 times or 20 times magnification Micrographs of plain supports (uncoated) can be retrieved in Appendix 0, Micrographs, "TiO_2 support (plain)," for comparisons sake.

5. 6. 1 Dip coating

Dip coating was the least successful coating technique as the films prepared in this manner resulted in a too thick film and the BESO suffered from serious cracking (Figure 5.33, 5.34) and the Urea from phase separation (Figure 5.35a-b).

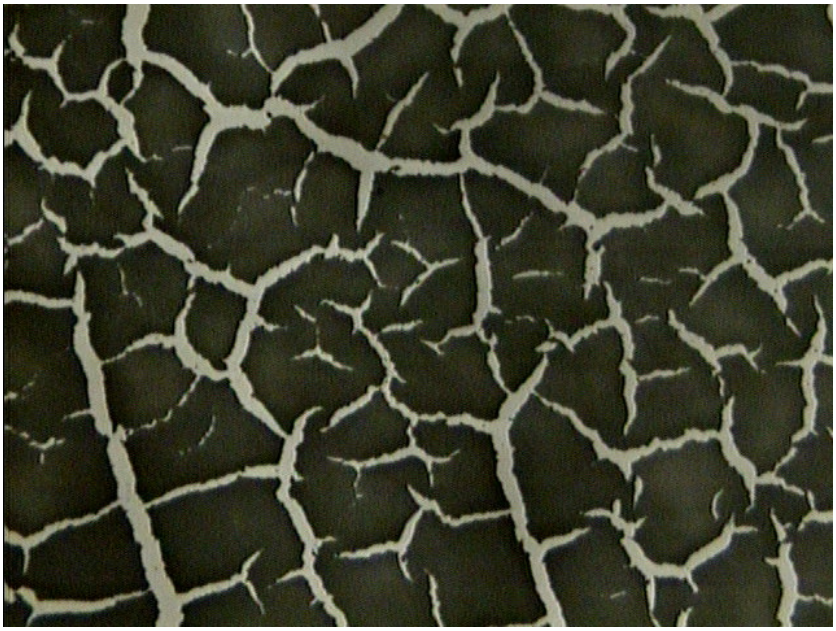

Figure 5.33. Dip coating micrograph of BESO 0.2 M (Sample eIII), 10x (glass slide).

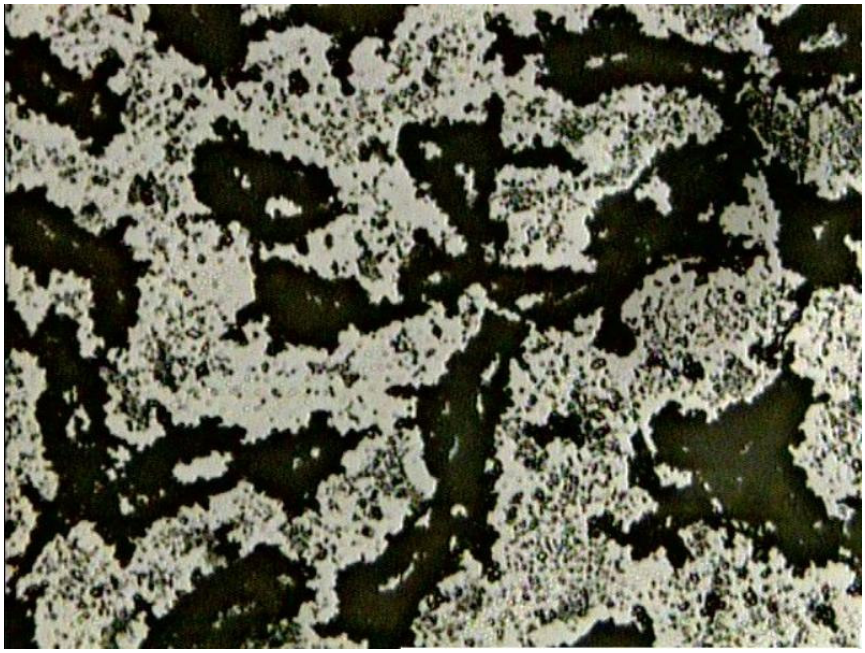

Figure 5.34. Dip coating micrograph of BESO 0.2 M w fluorescence, 10x (glass slide).

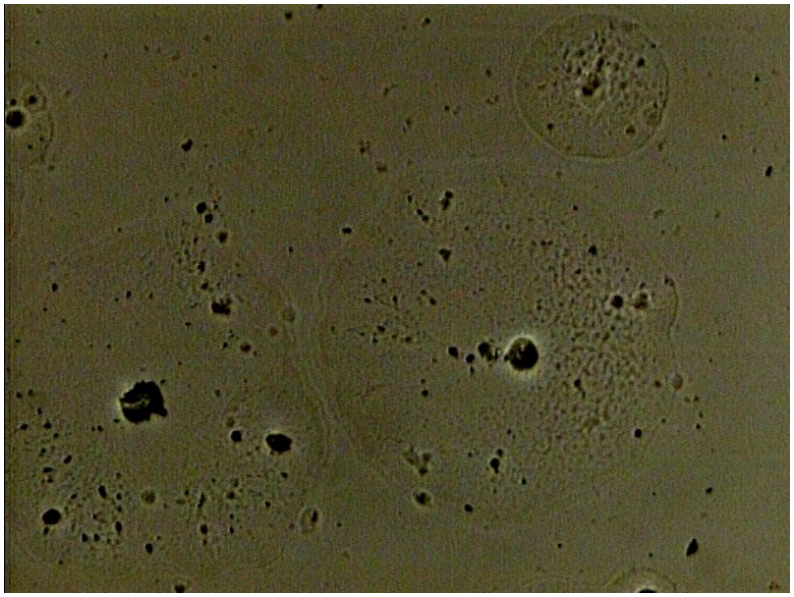

Figure 5.35a). Dip coating micrograph of Urea 0.4 M, 10x (glass slide)

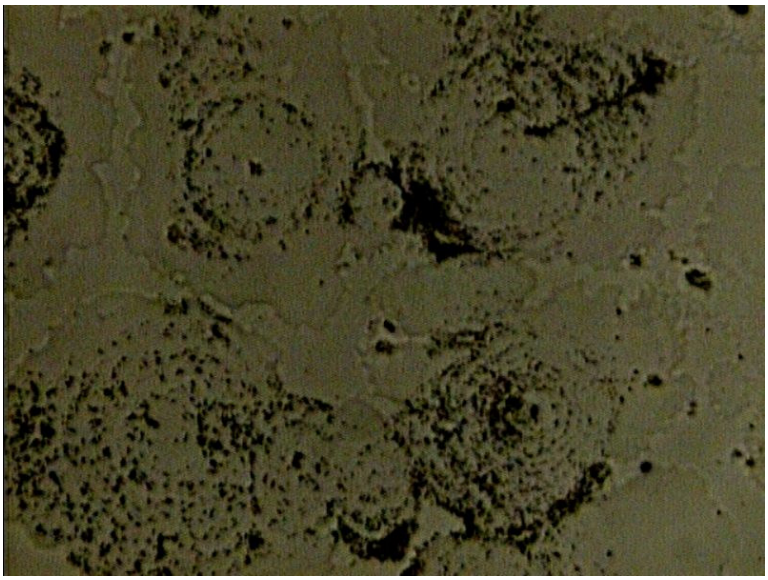

Figure 5.35b) Dip coating micrograph of Urea 0.4 M w fluorescence at 10x (glass slide)

As most of the sol-gel solutions are quite viscous it is difficult to make thin films with dip coating.

5. 6. 2. Spin coating

Spin coating was employed as it is a known technique to produce very thin films.

Spin rates

The sol-gel solutions were spun at different spin rates, 1000, 2500 and 5000 rpm. Figures 5.36-5.37 show the effect of the different spin rates for Urea (0.2 M) with fluorescence.

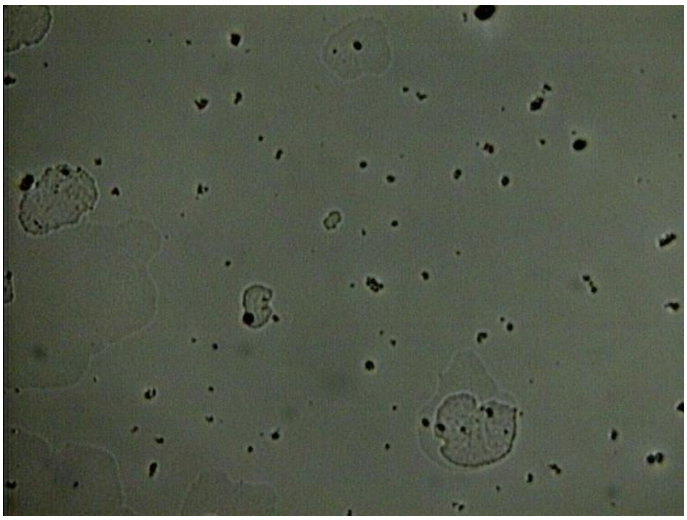

Figure 5.36. Micrograph image of Urea 0.2 M w fluorescence spun coat at *1000 rpm* (glass slide)

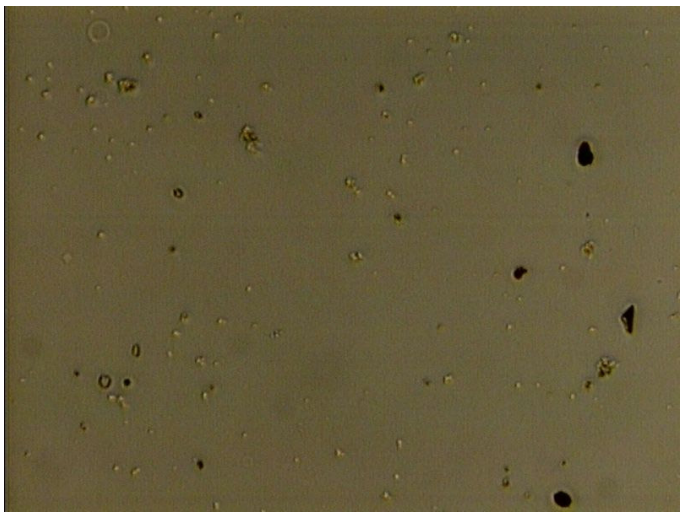

Figure 5.37. Micrograph image of Urea 0.2 M w fluorescence spun coat at *5000 rpm* (glass slide)

For Urea, the film spun at 5000 rpm is more uniform and does not have areas with phase separation as the one spun at 1000 rpm. For BESO, spinning at higher spin rates is vital as it avoids cracking, see Figures 5.38-39.

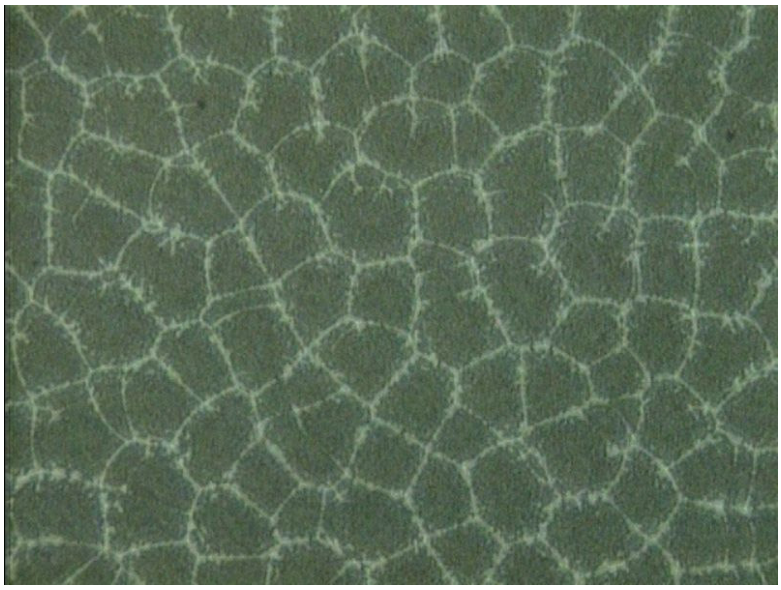

Figure 5.38. Micrograph of BESO 0.2 M (sample eIII) spun at *1000 rpm*

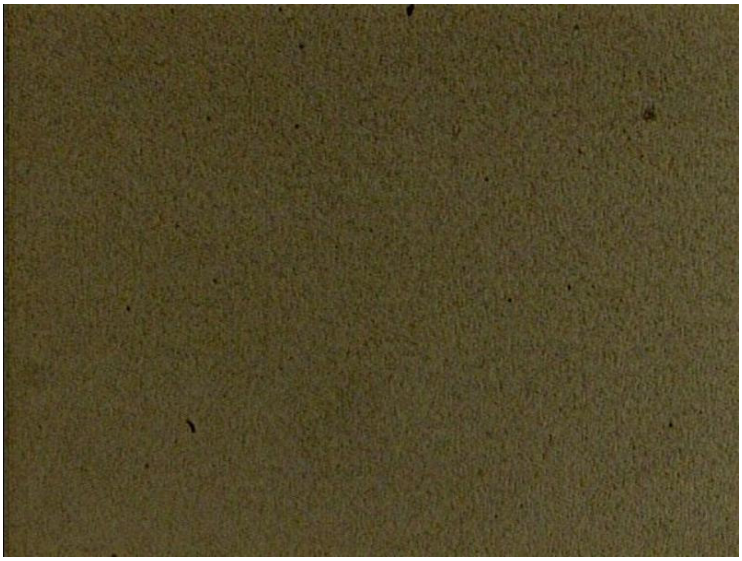

Figure 5.39. Micrograph of BESO 0.2 M (sample eIII) spun at *5000 rpm*

It seems that BESO is a mechanically weaker monomer compared to the amine and urea, as it undergoes cracking at more conditions. When the spin rate is too slow it cracks, since a slower spin rate results in a thicker film and therefore more stress is applied to the gel when the solvent evaporates.

Moving or motionless chuck?

When executing spin coating, there are two choices; applying the solution before the chucks starts rotating, of after it has started moving. It seemed that when the chuck was motionless before applying the coating there were problems with cracking, however when the chuck was already moving when the coating was applied there were problems with a "star pattern" (Figure 5.40).

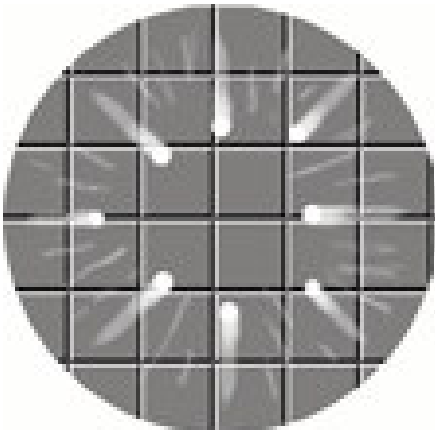

Figure 5.40. Cartoon of "star pattern"

The star pattern can be explained by the motion of the chuck as it is going around and around the solutions is thrown is spiral movements. When the solution is applied before the spinning rotation, it is allowed to wet the whole surface before it starts spinning, thus eliminating the spiral pattern. However, this also causes the film to be very thick and as mentioned earlier a thick film causes high tensions to the gel network and therefore cracking. Figures 5.41 and 5.42 represent Urea 0.2 M with fluorescence at motionless and moving chuck, respectively.

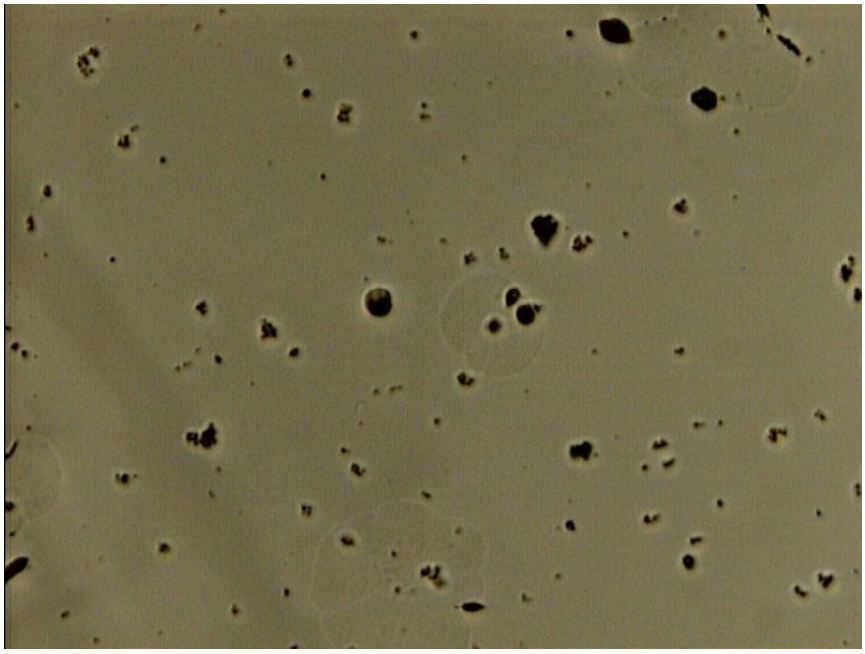

Figure 5.41. Micrograph of Urea 0.4 M w fluorescence spun with motionless chuck at 5000 rpm (glass slide)

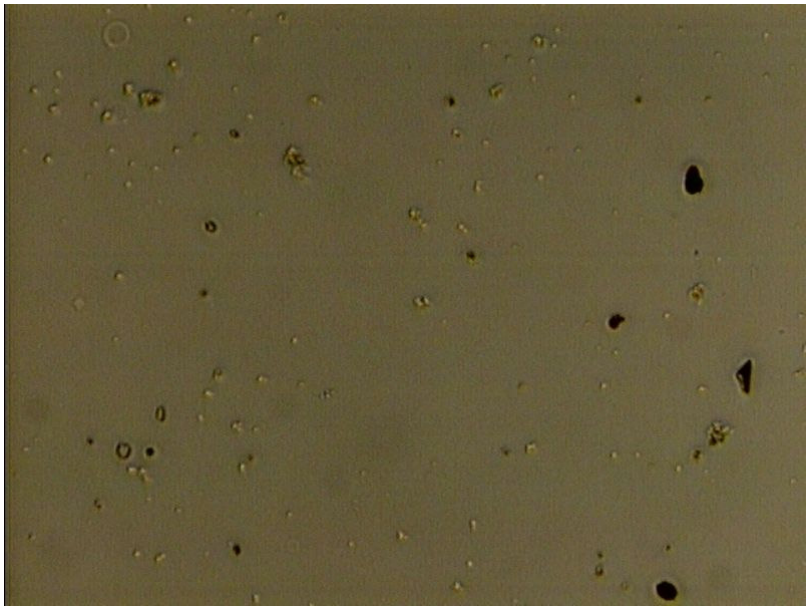

Figure 5.42. Micrograph of Urea 0.4 M w fluorescence spun with moving chuck at 5000 rpm (glass slide)

For Urea, the difference is rather subtle, however it can be seen that liquid areas (phase separation) can be found when the chuck is motionless at coating application. The star pattern is obvious when the membrane is inspected under fluorescent lighting.

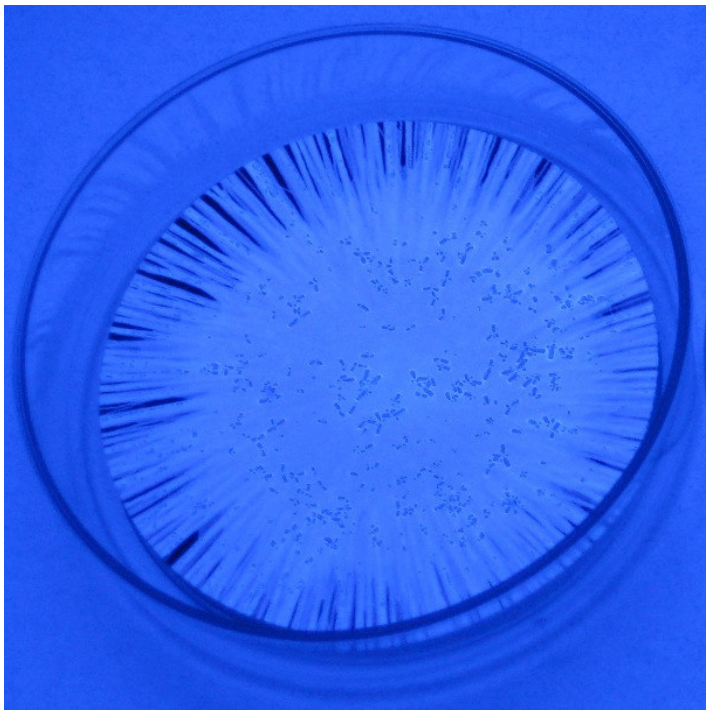

Figure 5.43. Photograph taken with a digital camera under fluorescence lighting, Urea 0.2 M with fluorescence monomer

Also, there seems to be large particles deposited in the center, most likely aggregates.

The same experiments were carried of for BESO (0.2 M) with fluorescence but on a TiO_2 support, (Figure 5.44a,b and 5.45). The TiO_2 support is porous and has an uneven surface and thus it is harder to obtain a uniform film. Regardless of the support, it can be seen that by spinning with a motionless chuck (Figure 5.44a) cracking occurs, but this is avoided when the chuck is moving at the application of coating (Figure 5.45). However, the start pattern is also observed in this case (Figure 5.46), but not seen in the motionless case (Figure 5.44b), where the edge of the support is studied.

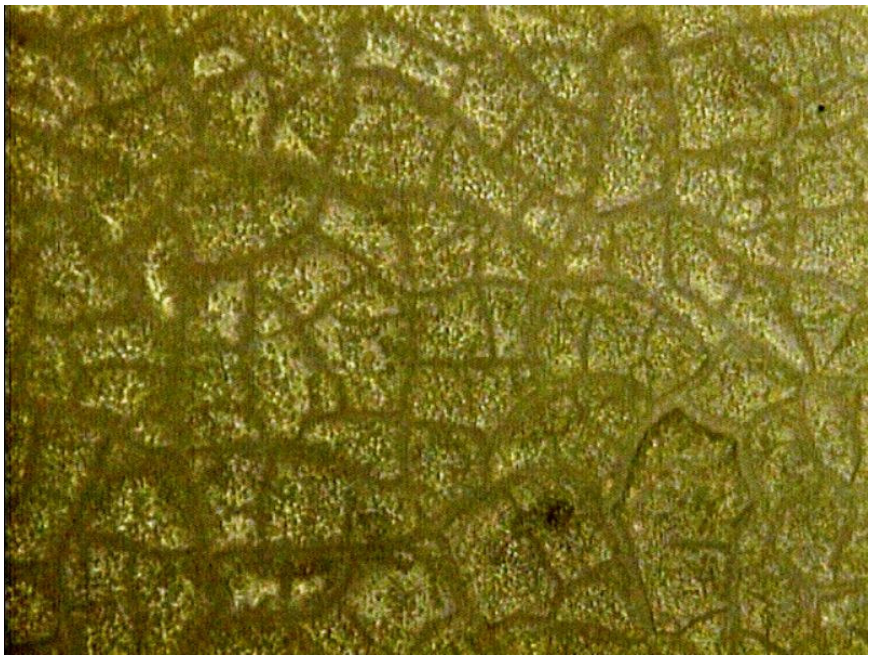

Figure 5.44a. Micrograph of BESO 0.2 M, flooded then spun at 5000 rpm, 20x (TiO_2)

Figure 5.44b. Micrograph of BESO 0.2 M, flooded then spun at 5000 rpm (edge), 10x (TiO_2)

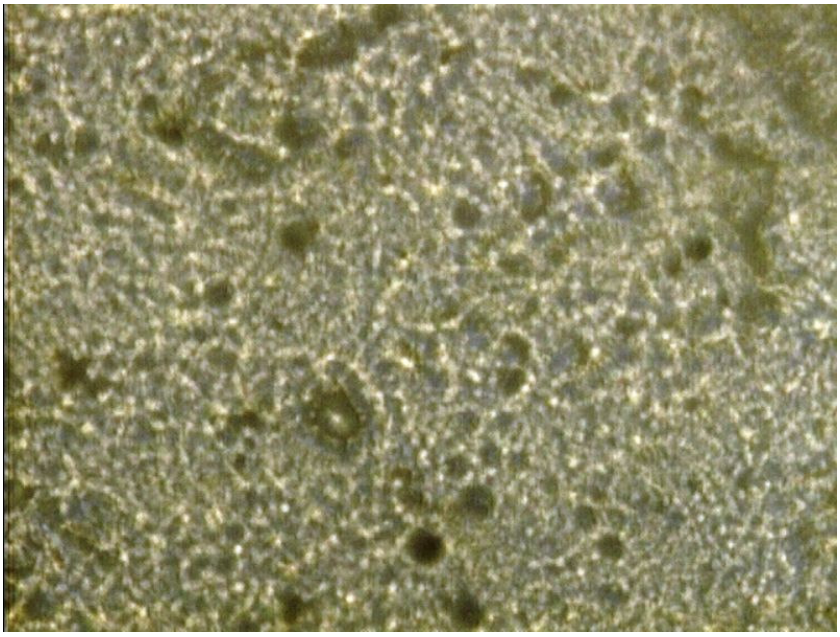

Figure 5.45. Micrograph of BESO 0.2M with fluorescence spun with moving chuck at 5000 rpm, 10x (TiO_2)

It can therefore be concluded that a moving chuck before solution application is vital to reduce the chance of cracking, however it is also important that enough amount of solutions applied to cover the whole support.

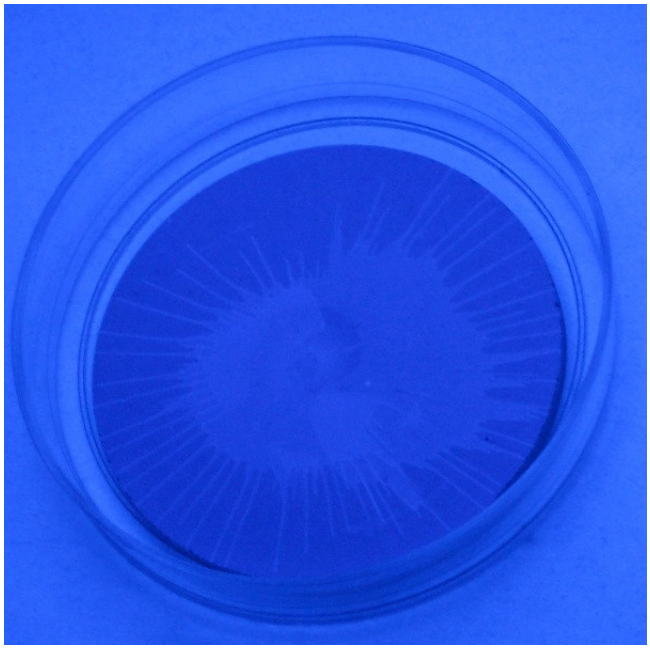

Figure 5.46. Photograph taken with a digital camera under fluorescence lighting, BESO 0.2 M with fluorescence monomer

Change of solvent/dilution

As ethanol is a very volatile solvent, it was investigated what would happen if the sol-gels were diluted with butanol and afterwards spun. The sol-gel solutions were diluted with ethanol and butanol at 1:10 and 1:100 ratios, respectively. All of the solutions diluted with butanol were spun at 5000 rpm with a moving chuck.

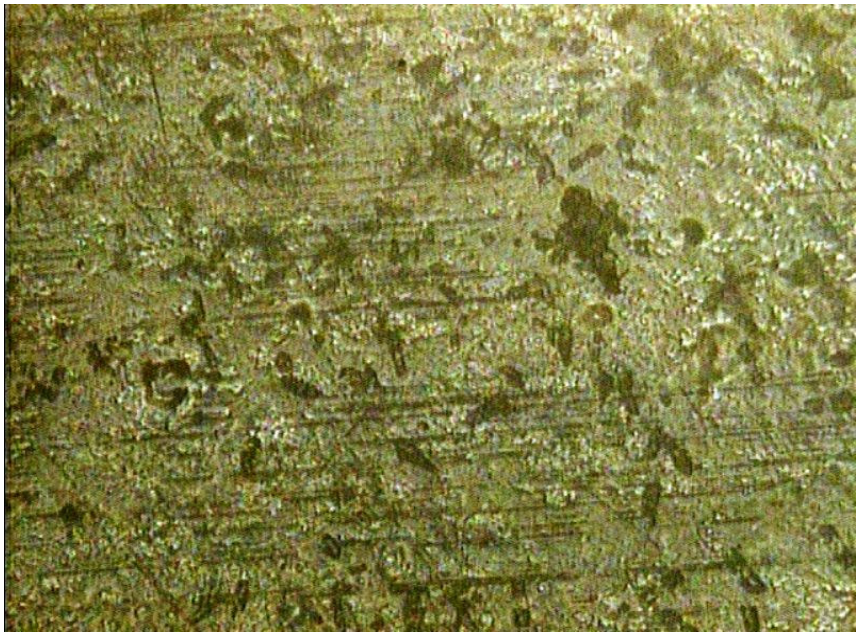

Figure 5.47. Micrograph of BESO 0.2 M w fluorescence spun diluted 10x in *butanol*, 10x (TiO_2).

From Figure 5.47 there seems to be large aggregates of monomer (oligomers). Apparently the monomer forms oligmers instead of a polymer network when the solvent evaporates slowly.

Figure 5.48. Micrograph of Urea (0.4M) with fluorescence, diluted 100x in *butanol*, 10x (TiO_2).

Urea (Figure 5.48), was diluted in butanol 100 times which had an unfortunate effect as the network underwent cracking. It therefore seems that too much dilution will also cause too much stress on the gel when it is drying, due to the fact the large amount of liquid that is trying to escape.

The amine (Figure 5.49) seemed to be unaffected by the dilution and change of solvent, and has been determined to be the toughest monomer since it exhibits the biggest resistance to cracking.

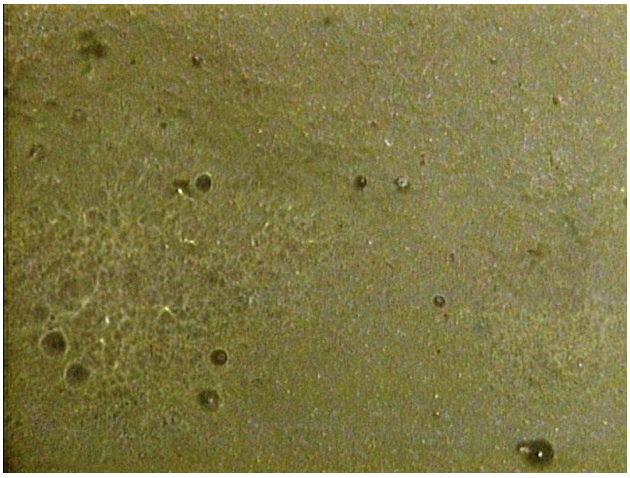

Figure 5. 49. Micrograph of Amine(0.05 M) with fluorescence, diluted 100 times in *butanol*, 10x (TiO_2).

Unfortunately, changing the solvent to a less volatile solvent did not improve the film properties, for BESO large clusters of oligomers formed in the center, and the Urea experienced cracking.

Fluorescence

An interesting phenomenon has been detected when it comes to the role of the fluorescence monomer in the coatings. Sol-gels prepared with fluorescence show less compliance to undergo cracking and in most cases avoid it completely. Not only is fluorescence extremely helpful when preparing coating since the final results can be seen at an instant (instead of going to a microscope), but it also seems to be helping the mechanical properties of the film. Figures 5.50-51 show BESO with and without fluorescence respectively, and figures 5.52-53 are micrographs of urea with and without fluorescence. Amine did not crack under any of the circumstances (Figure 5. 54-55)

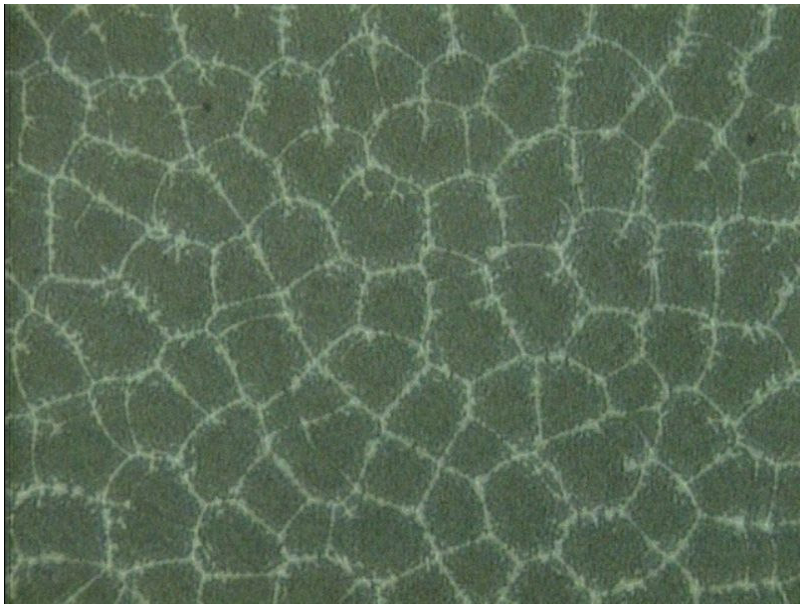

Figure 5.50. Micrograph of BESO 0.2M *(no fluorescence)* spun at 1000 rpm, 10x (glass slide)

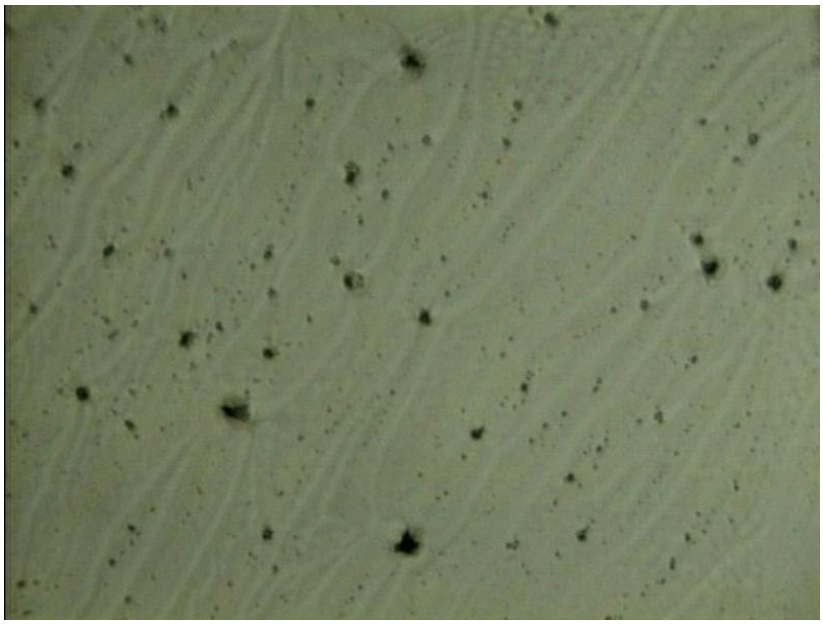

Figure 5.51. Micrograph of BESO (0.2 M) *with fluorescence* spun at 1000 rpm, 10x (glass slide)

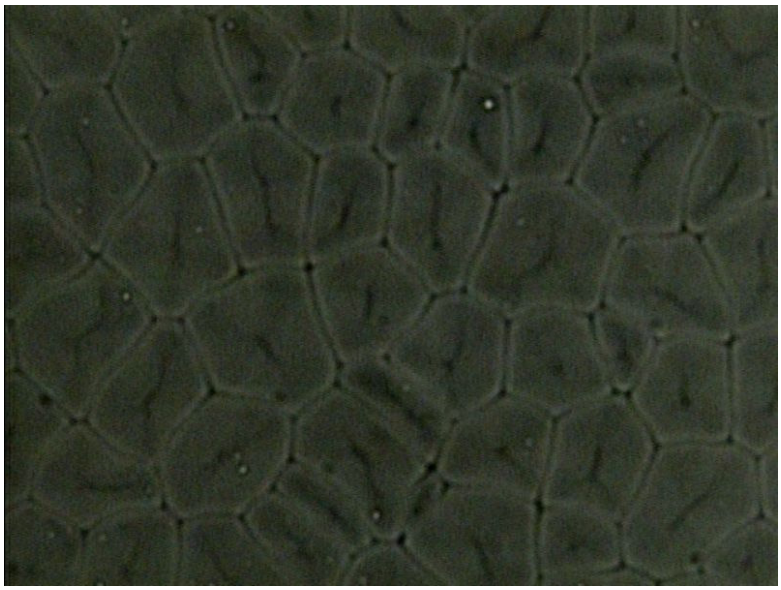

Figure 5.52. Micrograph of Urea 0.4 M *(no fluorescence)* spun at 1000 rpm, 10x (glass slide)

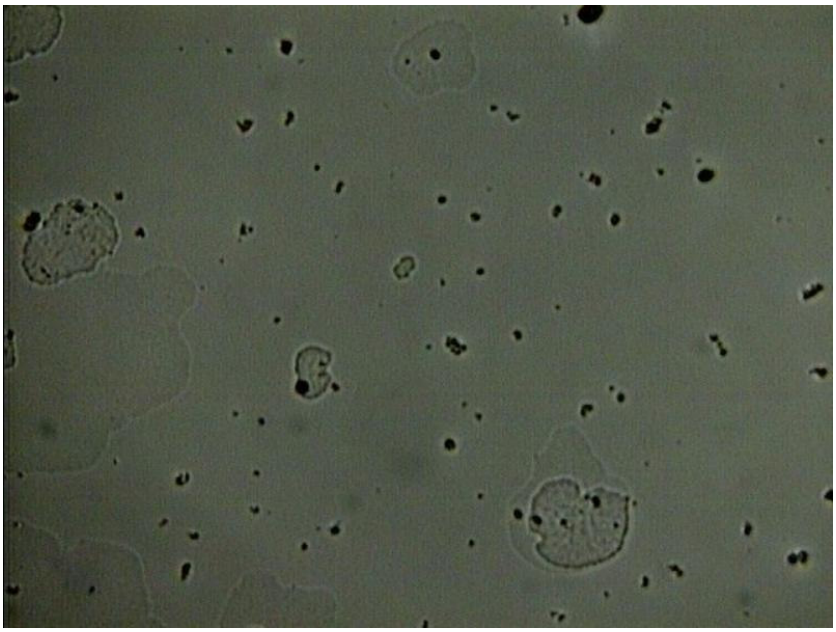

Figure 5.53. Micrograph of Urea 0.4 M *with fluorescence* spun at 1000 rpm, 10x (glass slide)

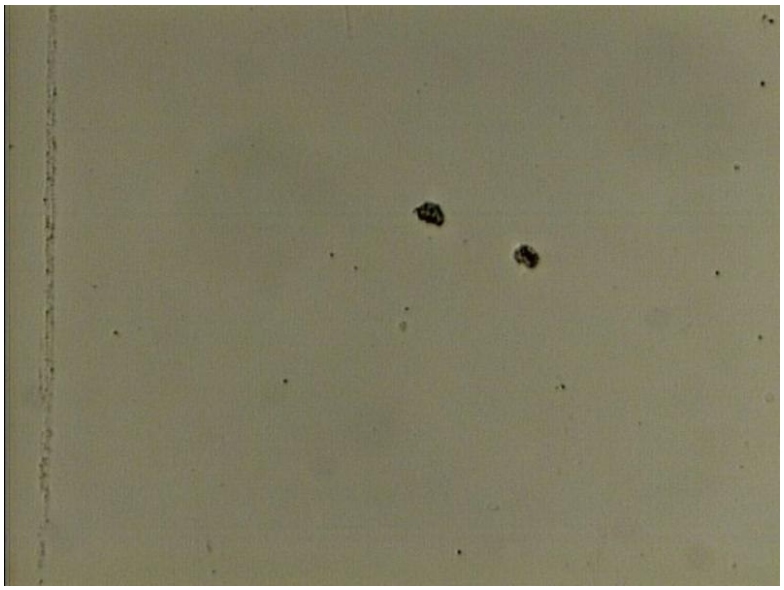

Figure 5.54. Micrograph of Amine 0.05 M (*no fluorescence)* spun at 5000 rpm, 10x (glass slide)

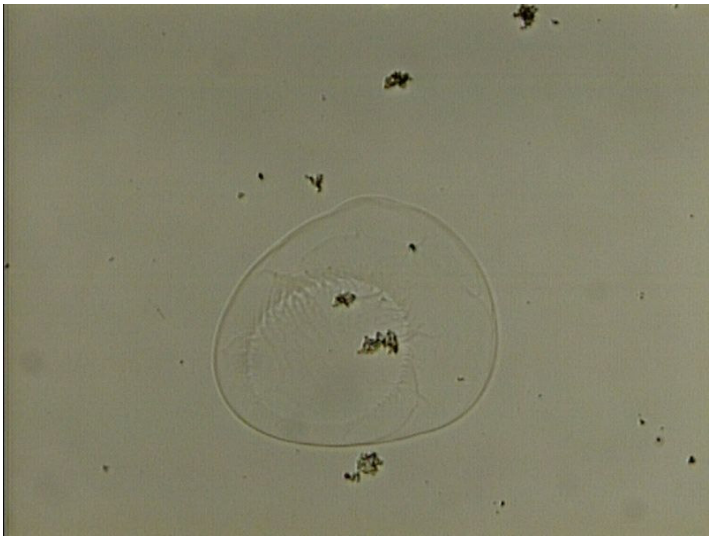

Figure 5.55. Micrograph of Amine 0.05 M (*no fluorescence)* spun at 5000 rpm, 10x (glass slide)

The fluorescence monomer consists of four aromatic groups which make it tough and rigid. Even though only 0.1 mol% was added to the solution it was enough to make a considerably stronger sol-gel network.

Clogging

It is common that filters will clog when performing some sort of filtration. This idea was the background for the last coating technique which will be referred to as clogging.

The idea of clogging is that the smallest particles in the sol-gel solution will pass through the support during filtration and the largest particles stay on the surface, the result being a uniform layer of the largest particles which will gel and form an even film. The vacuum should make sure that the pressure is equally distributed through out the film so that a uniform film is produced. However, there were detected some problems with producing uniform films, most likely due to the vacuum not being able to distribute an equal pressure. A lot of solution needs to be added in order to cover the whole membrane and make sure that the liquid is equally distributed through out the support, resulting in a thick layer. As mentioned earlier, thick layers are undesirable as they result in high stresses on the films, and it can be seen in Figure 5.56 as the film underwent cracking.

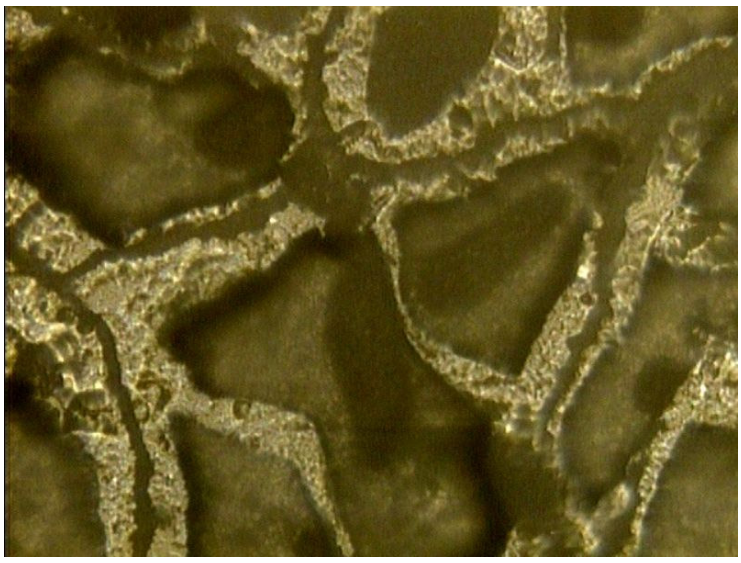

Figure 5.56. BESO 0.2 M with fluorescence, 0.*2ml* on a 15kd support, 10x

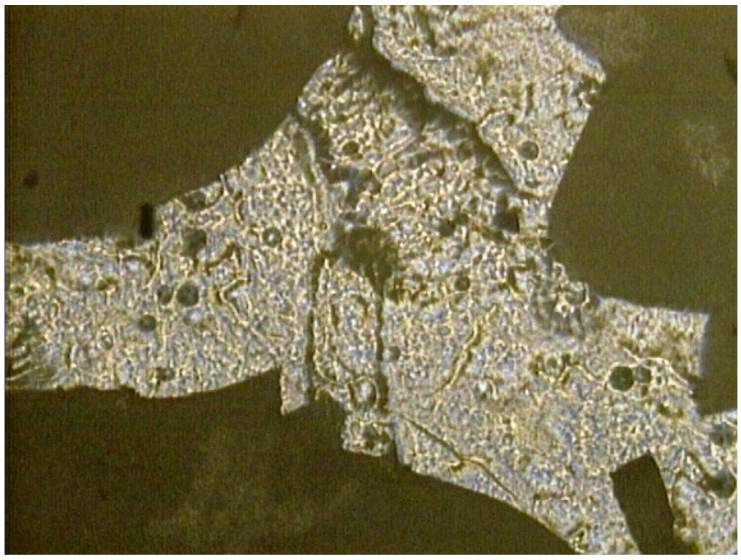

Figure 5.57. BESO 0. 2 M with fluorescence, *2ml* on a 15kd support, 10x

This first attempt was done with BESO without dilution and by adding 0.2 mL of the solution (figure 5.56), this resulted in the film curling and detaching from the support. Secondly, it was attempted to add more solvent, ten times more specifically (2.0 mL), however there was still a problem with curling, detaching and cracking (Figure 5.57)

Further testing was therefore done with amine as it is the monomer least prone to cracking. The amine did not curl up and detach from the support, however serious cracking is detected (Figure 5.58). When the sample was diluted 10 times the situation was improved, however uniformity of the film is not obtained (Figure 5.59).

Figure 5. 58. Amine (0.05M) with fluorescence clogged on 5kd support, 10x (TiO_2)

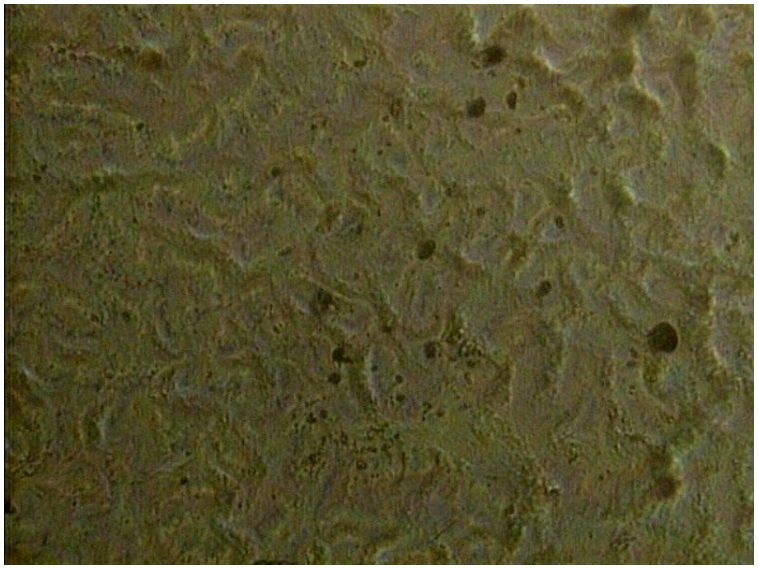

Figure 5.59. Amine (0.05M) with fluorescence, clogged on a 15kd support, *diluted*, 10x

The coating is bumpy and not evenly distributed on the support, in fact there were large areas where no coating at all. Due to the fact that the evaporation of the solvent is more rapid than the penetration of the smallest particles, the idea is hard to realize. Several attempts were done to overcome the obstacles, diluting 10 and 100 times, changing the solvent and adding different quantities of solutions. However, the results are thick, uneven film with huge clusters of films unevenly distributed through out the support. Further investigations are being completed at this moment.

6. Discussion

Further investigations should include obtaining monodisperse solutions, as monodisperse solutions form smoother coatings. It is suggested to (1) only let the sol-gels grow for a short amount of time as relatively monodisperse solutions are formed in the beginning (usually less then a week), or (2) grow the particles at Stöber conditions [127], as this process is widely used in producing monodisperse spherical silica particles. The first requires supports with small pores which are expensive and therefore method (2) is more attractive for industrial realization.

Another area in need of further investigations is the effect of solvent. The few samples that were prepared with THF seem to exhibit strong and hard gels, which is attractive in a gas separation unit where high pressures can be applied. It is suggested that mechanical testing is preformed for both gels prepared with and without THF, preferably applying high pressures to the gels.

Coating the membranes was challenging and not successful. Dip coating is not suitable due to the high viscosity of the BPs, however spin coating brought on some issue with uneven films, or more specifically a "star pattern." The star pattern was a problem when the chuck was rotating at application, but if it was not moving there were issues with cracking. In order to obtain even films and reduce the start pattern, it is suggested that a compromise between the two is made: Firstly, a small amount of sol-gel can be applied on a motionless chuck, and then spinning should be executed for a specific amount of time, then apply more solution while the chuck is moving. The optimal conditions in this case will most likely require many trial and error experiments, however spinning is a more of an art than science and this procedures is required for any new solvent that is being spun. The dispense rate, spin speed and the acceleration setting are all parameters that can be optimized, as well as it is important that the solution do not sit on the substrate too long prior to the spinning starts. At last it is crucial that the fluid is being dispensed at the center of the substrate surface.

Using clogging as the coating technique was not successful, however it is expected that this method will be the superior once the worst obstacles are overcome:

Due to the fact that the smallest particles go through the support and only the largest are left to form the membrane, the result should be a uniform film. Further investigations should be preformed with pressure on top, instead of vacuum, additional dilution, different solvents, and experiments with supports with larger pores should be preformed. A big problem was the fact that the solvent evaporated before the smallest particles had penetrated, causing an uneven film. Another option is to look into spray coating which was not tried in this project.

Now as control of the particle size has been obtained, next in line is gas testing in order to verify the reproducibility of the membranes. Also, the gas testing experiments should be completed over a certain amount of time, to determine the durability of the membrane.

At last it is important to address some challenges that are still left in order for industry use: Growing sol-gels particles at reasonable sizes is time-consuming and not practical for industry, improvements to the process includes

(1) Using THF as the solvent since sol-gels prepared with THF gelled at a much faster rate than the ones prepared in their parent alcohol. It can also be worth looking into other solvents that might facilitate the sol-gel rate even more
(2) Use higher concentrations (though this causes the gels to be more brittle and it grows smaller particles)
(3) Using a higher concentration of catalyst, or using excess catalyst.

Even though the effect of many of the parameters in the sol-gel process of BPs has been characterized, an optimization of the process is still needed for industry use.

7. Conclusions

Membrane technology was decided to be the most promising technology for CO_2 capture of flue gases. The different parameters effect on the sol-gel growth rate and size were studied: It was discovered that the particles of bridged polysilsesquioxanes grow until they gel, and do not follow the same behavior as silica, which quickly reaches a steady size. It was concluded that by allowing the sol-gels to grow for more than one month (threshold value), the largest particles were produced. The growth mechanism of acidic and basic catalyst has been discovered to be widely different; an acid catalyst leads to chainlike (or linear) molecules, while highly branched clusters are formed by a basic catalyst. The gelation time for a basic catalyst is highly dependent on the concentration of the sol-gel, since the concentration needs to be high enough for the small clusters to overlap. Changing the solvent from the parent alcohol (ethanol) to THF did not seem to affect the particles size, but the growth rate was highly accelerated. Adding fluorescent monomer did not seem to affect the particle sizes of Urea and Amine, however when fluorescence was supplied to the BESO, the results was shorter gelation times and larger particles, indicated by both the fact that the gel was white compared (fluorescence) to translucent blue (no fluorescence), and also by the DLS measurements. It is believed that the fluorescent monomer act as some sort of facilitator in the particle growth of BESO. Monodisperse solutions were only obtained in the beginning of the growth period, and polydisperse solutions were produced afterwards (usually more than a week). SEM and AFM were used as back-up tests for the DLS, and the results were in agreements; SEM showed slightly smaller particles than the DLS which is reasonable due to the nature of experiment as DLS measures the hydrodynamic radius.

From visual inspections of the gel, and by applying a small amount of stress to the gels, it can be concluded that to obtain a hard, strong gel, the gels must be prepared at low concentrations (not higher then 0.2 M or at their threshold value) and an acidic catalyst should be used. Also, THF should be used as the solvent to obtain hard gels. The fluorescent monomer incorporated well into the structure of the gel, which can be seen under fluorescent lighting.

Amine shows the greatest resistant to cracking and BESO the least. Dip-coating was not successful due to the high viscosity of the sol-gels which results in thick films and severely cracking, spin coating avoided the cracking, however there was an issue with "star patterns." Applying the coating with a motionless chuck avoided the spiral pattern but induced cracking.

Changing the solvent to a less volatile solvent did not improve the film properties, as large clusters of oligomers formed in the center of the sample prepared with BESO, and the Urea sample underwent cracking.

The fluorescent monomer had additional benefits; Firstly, the uniformity of the membrane could be determined at an instant under fluorescent lighting, and no extra characterization was needed, (i.e. a microscope). Also, the coatings prepared with fluorescence were more resistant to cracking, even though a little as 0.1% molar was added to the sol-gel solution.

Clogging was not a successful coating technique as the final film was uneven, and was deposited as lumps over the support. However, huge potential is expected with this method as it is only in the start-up face.

1. IPCC, *"Climate Change 2007." IPCC Fourth Assessment Report (AR4)*. 2007.
2. Audus, H., Freund, P. and Smith, A., *Global warming damage and the benefits of mitigation*. 1995, IEA Greenhouse gas R&D programme.
3. United Nations Framework Convention on Climate Change, *Kyoto Protocol*. [cited 2008 May 29]; Available from: http://unfccc.int/kyoto_protocol/items/2830.php.
4. Bank, W., *World Development Indicators 2007* 2007: Green Press Initiative
5. Klara, S.M., Srivastava, R.D., and McIlvried, H.G., *Integrated collaborative technology development program for CO2 sequestration in geologic formations--United States Department of Energy R&D.* Energy Conversion and Management, 2003. **44**(17): p. 2699-2712.
6. Lindeberg, E. and Bergmo, P. *The Long-Term Fate of CO2 Injected into an Aquifer*. in *Greenhouse Gas Control Technologies - 6th International Conference*. 2002. Kyoto, Japan.
7. Kaarstad, O., *Emission-free fossil energy from Norway* Energy Convers. Mgmt 1992. **33**(5-8): p. 781-786.
8. Torp, T.A., Brown, K.R., Rubin, E.S., Keith, D.W., et al., *CO2 underground storage costs as experienced at Sleipner and Weyburn*, in *Greenhouse Gas Control Technologies 7*. 2005, Elsevier Science Ltd: Oxford. p. 531-538.
9. Hsu, C.-F., Koinis, R.L., and Fox, C.E., *Technology, experience speed CO2 flood design.* Oil & Gas, 1995. **93**(43).
10. Figueroa, J.D., Fout, T., Plasynski, S., McIlvried, H., et al., *Advances in CO2 capture technology--The U.S. Department of Energy's Carbon Sequestration Program.* International Journal of Greenhouse Gas Control, 2008. **2**(1): p. 9-20.
11. Dillon, D.J., Panesar, R.S., Wall, R.A., Allam, R.J., et al., *Oxy-combustion processes for CO2 capture from advanced supercritical PF and NGCC power plant*, in *Greenhouse Gas Control Technologies 7*. 2005, Elsevier Science Ltd: Oxford. p. 211-220.
12. Buhre, B.J.P., Elliott, L.K., Sheng, C.D., Gupta, R.P., et al., *Oxy-fuel combustion technology for coal-fired power generation.* Progress in Energy and Combustion Science, 2005. **31**(4): p. 283-307.
13. Aaron, D. and Tsouris, C., *Separation of CO_2 from Flue Gas: A Review.* Separation Science and Technology, 2005. **40**(1): p. 321-348.
14. Gottlicher, G. and Pruschek, R., *Comparison of CO_2 removal systems for fossil-fuel power plant processes.* Energy Convers. Manage, 1996. **38**: p. 38.
15. Condorelli, P., Smelser, S. C. and McCleary, G. J. , *Engineering and Economic Evaluation of CO_2 Removal from Fossil-Fuel-Fired Power Plants, Volume 2: Coal Gasification Combined-Cycle Power Plants*. 1991, Electric Power Research Institute: Palo Alto, CA.
16. Bolland, O., *Natural gas fired powered plant (in Norwegian).* Energy in Norway, 2000.
17. Teng, F. and Tondeur, D., *Efficiency of Carbon storage with leakage: Physical and economical approaches.* Energy, 2007. **32**(4): p. 540-548.
18. Chapel, D., Ernest, J., and Mariz, C, *Recovery of CO2 from flue gases: commercial trends*, in *Canadian Society of Chemical Engineers Annual Meeting*. 1999: Saskatchewan,Canada.

19. Gottlicher, G., and Pruschek, R. , *Comparison of CO2 removal systems for fossil-fuel power plant processes.* Energy Convers. Manage, 1996. **38**.
20. Elwell, L.C., *Special Reports: Technology options for capturing CO_2.* Power, 2006. **150**(8).
21. Sander, M.T. and Mariz, C.L., *The Fluor Daniel® econamine FG process: Past experience and present day focus.* Energy Conversion and Management, 1992. **33**(5-8): p. 341-348.
22. Yagi, Y., Mimura, T., Iijima, M., Ishida, K., et al., *Improvements of carbon dioxide capture technology from flue gas*, in *Greenhouse Gas Control Technologies 7*. 2005, Elsevier Science Ltd: Oxford. p. 1139-1145.
23. Hakka, L., *Integrated Regenerable SO_2 and CO_2 Capture*, in *International Post-Combustion CO2 Capture Network (Presentation from Cansolv Tech.)*. 2007: Lyon, France.
24. Riemer, P.W.F., Webster, I.C., Omerod, W.G., and Audus, H. , *Results and full fuel cycle study plans from the IEA greenhouse gas research and development programme.* Fuel, 1994. **73**(7): p. 1151–1158.
25. Audus, H., *Greenhouse gas mitigation technology: an overview of the CO2 capture and sequestration studies and further activities of the IEA greenhouse gas R&D programme.* Energy, 1997. **22**.
26. Li, X., Hagaman, E., Tsouris, C., and Lee, J.W. , *Removal of carbon dioxide from flue gas by ammonia carbonation in the gas phase.* Energy Fuels, 2003. **17**(1): p. 69–74.
27. Chaffee, A.L., Knowles, G.P., Liang, Z., Zhang, J., et al., *CO_2 capture by adsorption: Materials and process development.* International Journal of Greenhouse Gas Control, 2007. **1**(1): p. 11-18.
28. Plaza, M.G., Pevida, C., Arenillas, A., Rubiera, F., et al., *CO2 capture by adsorption with nitrogen enriched carbons.* Fuel, 2007. **86**(14): p. 2204-2212.
29. Satyapal, S., Filburn, T., Trela, J. and Strange, J. , *Performance and properties of a solid amine sorbent for carbon dioxide removal in space life support applications.* Energy Fuels, 2001. **15**(2): p. 250–255.
30. Baltus, R., and DePaoli, D. , *Separation of CO2 using room temperature ionic liquids*, in *Oak Ridge National Laboratory Environmental Sciences Division Carbon Management Seminar Series*. 2002: Oak Ridge, TN.
31. Stern, S.A., *Polymers for Gas Separations: The Next Decade.* Journal of Membrane Science, 1994. **94**: p. 1-65.
32. Mulder, M., *Basic Principles of Membrane Technology*. 1996, Dordrecht: Kluwer Academic Publishers.
33. Cassidy, P.E., *Thermally stable polymers*. Marcel Dekker. 1980, New York.
34. Baker, R.W., Ind. Eng. Chem. Res, 2002. **41**.
35. Shea, K.J. and Loy, D.A., *Bridged Polysilsesquioxanes. Molecular-Engineered Hybrid Organic-Inorganic Materials.* Chem. Mater., 2001. **13**: p. 3306-3319.
36. Figueroa, J.D., Fout,T., Plasynski,S., McIlvried, H. and Srivastava, R.D., *Advances in CO2 capture technology—The U.S. Department of Energy's Carbon Sequestration Program.* International Journal of Greenhouse Gas Control, 2008. **2**: p. 9-20.

37. Federation of Electric Power Companies, J. 2001 [cited; Available from: http://www.fepc.or.jp/english/info/energyandenv/35.html.
38. Meratla, Z., *Combining cryogenic flue gas emission remediation with a CO2/O2 combustion cycle.* Energy Convers. Manage, 1997. **38**: p. S147–S152
39. Pruscheck, R., Oeljeklaus, G., Haupt, G., Zimmermann, G., Jansen, D., and Ribberink, J.S., *The role of IGCC in CO2 abatement*. Energy. Convers. Manage, 1997
40. ATLAS Research and Technology Development http://europa.eu.int/comm/energy_transport/atlas/htmlu/ccpgigcc.html (accessed Oct 2007)
41. Cullinane, J.T. and Rochelle, G.T., *Carbon dioxide absorption with aqueous potassium carbonate promoted by piperazine.* Chemical Engineering Science, 2004. **59**(17): p. 3619-3630.
42. Rochelle, G., Chen, E., Dugas, R., Oyenakan, B., and Seibert, F. *Solvent and process enhancements for CO2 absorption/stripping*. in *Annual Conference on Capture and Sequestration*. 2005. Alexandria, VA.
43. Bai, H. and Yeh, A.C., *Removal of CO2 Greenhouse Gas by Ammonia Scrubbing.* Ind. Eng. Chem. Res. , 1997. **36**: p. 2490-2493.
44. Yang, Q.Y., Zhong, C.L., and Chen, J.F., *Computational study of CO2 storage in metal-organic frameworks.* Journal of Physical Chemistry C, 2008. **112**(5): p. 1562-1569.
45. Willis, R.R., Benin, A.I., Low, J.J., Bedard, R., and Lesch, D., *Annual Report, Project DE-FG26-04NT42121*. 2006, National Energy Technology Laboratory.
46. Bao, L. and Trachtenberg, M.C., *Facilitated transport of CO2 across a liquid membrane: Comparing enzyme, amine, and alkaline.* Journal of Membrane Science, 2006. **280**(1-2): p. 330-334.
47. Kanel, J.S., *Overview: industrial application of ionic liquids for liquid extraction*, in *Chemical Industry Vision 2020 Technology Partnership Workshop. .* 2003: New York.
48. Keskin, S., Kayrak-Talay, D., Akman, U., and Hortaçsu, Ö., *A review of ionic liquids towards supercritical fluid applications.* The Journal of Supercritical Fluids, 2007. **43**(1): p. 150-180.
49. Aaron, D., and Tsouris, C., *Separation of CO2 from Flue Gas: A Review.* Separation Science and Technology, 2005. **40**.
50. Falk-Pederson, O., Dannström, H., Gronvold, M., Stuksrud, D., and Ronning, O.,, *Gas treating using membrane gas/liquid contactors*, in *Fifth International Conference on Greenhouse Gas Control Technologies*. 2000: Cairns, Australia.
51. Mulder, M., *Basic Principles of Membrane Technology*. 2003, Enschede: Kluwer Academic Publishers.
52. Zhu, Z., *Permeance should be used to characterize the productivity of a polymeric gas separation membrane (Letter to the Editor).* Journal of Membrane Science, 2006. **281**: p. 754–756.
53. Javaid , A., *Membranes for solubility-based gas separation applications* Chemical Engineering Journal, 2005. **112**: p. 219–226.
54. Koros, W.J. and Fleming, G.K., *Membrane-based gas separation.* Journal of Membrane Science, 1993. **83**.

55. Karger, J. and Ruthven, D.M., *Diffusion in zeolites and other microporous solids*, ed. J.W.S. Inc. 1992, New York.
56. Fain, D.E., *Membrane gas separation principles.* MRS Bull, 1994. **40**.
57. Sotirchos, S.V. and Burganos, V.N., *Transport of gases in porous membranes.* MRS Bull, 1999. **41**.
58. Uhlhorn, R.J.R., Keizer, K. and Burggraaf, A.J. , *Gas transport and separation with ceramic membranes. Part I. Multilayer diffusion and capillary condensation.* Journal of Membrane Science, 1992. **66**.
59. Kesting, R.E. and Fritzsche, A.K., *Polymeric gas separation membranes*, ed. J.W.S. Inc. 1993, New York.
60. Kim, T.-J., Li, B. and Hägg, M.-B., *Novel Fixed-Site-Carrier Polyvinlamine Membrane for Carbon Dioxide Capture.* Journal of Polymer Science, 2004. **42**.
61. Robeson, L.M., *Correlation of separation factor versus permeability for polymeric membranes.* Journal of Membrane Science, 1991. **62**: p. 165-185.
62. Mahajan, R., Vu, D.Q., and Koros, W.J., *Mixed Matrix Membrane Materials: An Answer to the Challenges Faced by Membane Based Gas Separations today?* J. Chin. Inst. Chem. Engrs., 2002. **33**(1): p. 77-86.
63. Hillock, A.M.W., Miller, S.J., and Koros, W.J., *Crosslinked mixed matrix membranes for the purification of natural gas: Effects of sieve surface modification.* Journal of Membrane Science, 2008. **314**(1-2): p. 193-199.
64. Pandey, P. and Chauhan, R.S., *Membranes for gas separation.* Prog. Polym. Sci., 2001. **26**: p. 853-893.
65. Bai, C.S., Jia, M.D., Falconer, J.L., and Noble, R.D., *Preparation and Separation Properties of Silicalite Composite Membranes.* Journal of Membrane Science, 1995. **105**(1-2): p. 79-87.
66. Fan, J., Hu, X.Y., Ohya, H., Ueda, Y., et al., *Preparation of palladium-silica conjugated membrane for selective hydrogen permeation.* Chinese Journal of Chemical Engineering, 2002. **10**(5): p. 580-586.
67. Brurggraaf, A.J. and Keizer, K., *Inorganic Membranes (Chapter 2. Synthesis of Inorganic Membranes)*, ed. R.R. Bhave. 1991, New York.
68. Govind, R. and Atnoor, D., *Development of a composite palladium membrane for selective hydrogen separation at high temperature*
Ind. Eng. Chem. Res., 1991. **30**(3): p. 591-594.
69. Itoh, N., *Membrane reactor using Palladium.* AiChE J., 1987. **33**(9): p. 1576-1578.
70. Gobina, E. and Hughes, R., *Ethane dehydrogenation using a high-temperature catalytic membrane reactor.* Journal of Membrane Science, 1994. **90**(1-2): p. 11-19.
71. Ziaka, Z.D., Minet, R.G. and Tsotsis, T.T. , *A high temperature catalytic membrane reactor for propane dehydrogenation.* Journal of Membrane Science, 1993. **77**: p. 221-232.
72. Buxbauma, R.E. and Markerb, T.L., *Hydrogen transport through non-porous membranes of palladium-coated niobium, tantalum and vanadium.* Journal of Membrane Science, 1993. **85**(1): p. 29-38.

73. Merkel, T.C., Freeman, B.D., Spontak, R.J. , He, Z. and Pinnau,I. , *Ultrapermeable, reverse-selective nanocomposite membranes.* Science, 2002. **296**: p. 519-522.
74. Sridhar, S., Smitha, B., and Aminabhavi, T.M., *Separation of Carbon Dioxide from Natural Gas Mixtures through Polymeric Membranes - A review.* Separation & Purification Reviews, 2007. **36**: p. 113-174.
75. Hench, L.L. and West, J.K., *The Sol-Gel Process.* Chem. Rev., 1990. **90**: p. 33-72.
76. Guizard, C., *Fundamentals of Inorganic Membrane Science and Technology (chapter 7).* , ed. A.J. Burggraaf and L.Cot. 1996: Elsevier Science.
77. Brinker, C.J., Sehgal, R., Hietala, S, L., Deshpande, R., Smith, D.M., Loy, D. and Ashley, C.S., *Sol-gel strategies for controlled porosity inorganic materials.* Journal of Membrane Science, 1994. **94**: p. 85-102.
78. Mørk, P.C., *Surface and Colloid Chemistry (in Norwegian).* 2004, Trondheim: Tapir
79. Hench, L.L., Wang, S.H., and Nogues J.L., *Gel-Silica Optics.* Multifunctional Materials edited by (SPIE, Bellingham, WA, 1988), 1988. **878**: p. 76-85.
80. Hench, L.L., Wilson, M. J. R., Balaban, C.,Nogues, J. L. *Sol-Gel Processing of Large Silica Optics*. in *Proceedings of 4th International Conference on Ultrastructure Processing of Ceramics, Glasses and Composites*. 1989. Tucson, AZ.
81. Vysotskii, Z.Z. and Strazhesko, D.N., *Adsorption and Absorbents*, ed. Wiley. Vol. 1. 1973, New York.
82. West, J.K., Nikles, R. and LaTorre, G. , *Better Ceramics Through Chemistry*, ed. M.R. Society. Vol. 121. 1988, Pittsburgh.
83. Brinker, C.J. and Scfierer, G.W., *Sol-Gel Science*, in *Academic Press*. 1989: New York.
84. Sherwood, T.K., *The Drying of Solids—I.* Ind. Eng. Chem., 1929. **21**: p. 12-16.
85. Sherwood, T.K., *The Drying of solids—II.* Ind. Eng. Chem., 1929. **21**: p. 976-980.
86. Sherwood, T.K., *The Drying of Solids—III Mechanism of the Drying of Pulp and Paper.* Ind. Eng. Chem., 1930. **22**: p. 132-136.
87. Nogami, M. and Moriya, Y., *Glass formation through hydrolysis of Si(OC2H5)4 with NH4OH and HCl solution.* Journal of Non-Crystalline Solids, 1980. **37**(2): p. 191-201.
88. Dabrowski, A. and Barczak, M., *Bridged Polysilsesquioxanes as a Promising Class of Adsorbents. A Concise Review.* Croatica Chemica Acta, 2007. **80**(3-4): p. 367-380.
89. Dow Corning: Barry, A.J., Depree, L. and Hook, D.E., *Production of organohalosilanes (Br. patent).* 1950: Great Britain
90. Kohjiya, S. and Ikeda, Y., *Reinforcement of general-purpose grade rubbers by silica generated in situ.* Rubber Chemistry and Technology, 2000. **73**(3): p. 534-550.
91. Boldebuck, E.N., *Esters of ethynyl siliconic acid (U.S. Patent).* 1951: USA.
92. Shea, K.J., Loy, D.A. and Webster, O., *Arylsilsesquioxane Gels and Related Materials. New Hybrids of Organic and Inorganic Networks.* Am. Chem. Soc, 1992. **114**: p. 6700-6710.

93. Sharp, K.J. and Michalczyk, M.J., *Star Gels: New Hybrid Network Materials from Polyfunctional Single Component Precursors.* J. Sol-Gel Sci. Technol., 1997. **8**(1-3): p. 541-546.
94. Wright, J.D. and Sommerdijk, N.A.J.M., *Sol-gel materials, Chemistry and Applications*. 2000, Washington D.C.: Taylor & Francis Ltd.
95. Loy, D.A., Carpenter, J.P., Myers, S.A., Assink, R.A., Small, J.H., Greaves, J. and Shea, K.J., *Intramolecular Condensation Reactions of Bis(triethoxysilyl)alkanes. Formation of Cyclic Disilsesquioxanes.* Am. Chem. Soc, 1996. **118**(35): p. 8501 - 8502.
96. Loy, D.A., Carpenter, J.P., Yamanaka, S.A., McClain, M.D., Greaves, J., Hobson, S. and Shea K.J., *Polymerization of Bis(triethoxysilyl)ethenes. Impact of Substitution Geometry on the Formation of Ethenylene- and Vinylidene-Bridged Polysilsesquioxanes.* Chem. Mater., 1998. **10**(12): p. 4129 - 4140.
97. Cerveau, G., Corriu, R.J. P., Framery, E., Ghosh, S. and Mutin, H.P. , *Hybrid materials and silica: drastic control of surfaces and porosity of xerogels via ageing temperature, and influence of drying step on polycondensation at silicon.* J. Mater. Chem., 2002. **12**: p. 3021 - 3026.
98. Douglas, D.A., Jamisona, G.M., Baughera, B.M., Russicka, E.M., Assinka, R.A., Prabakara, S., and Shea K.J., *Alkylene-bridged polysilsesquioxane aerogels: highly porous hybrid organic-inorganic materials.* J. Non-Cryst. Solids, 1995. **186**: p. 44-53.
99. Oviatt, H.J., Shea, K.J. and Small, J.H., *Alkylene-bridged silsesquioxane sol-gel synthesis and xerogel characterization. Molecular requirements for porosity.* Chem. Mater., 1993. **5**(7): p. 943-950.
100. Cerveau, G., Corriu, R.J.P. and Lepeytre, C., *Organic–inorganic hybrid silica: chemical reactivity as a tool for studying the solid arrangement as a function of molecular structure.* J. Mater. Chem., 1995. **5**: p. 793 - 795.
101. Lee, T.M., Ma, C.C.M., Hsu, C.W., and Wu, H.L., *Effect of molecular structures and mobility on the thermal and dynamical mechanical properties of thermally cured epoxy-bridged polyorganosiloxanes.* Polymer, 2005. **46**(19): p. 8286-8296.
102. Li, C., Glass, T. and Wilkes, G.L., *NMR Studies of Sol-Gel Derived Hybrid Materials Based on Triethoxysilylated Diethylenetriamine and Tetramethoxysilane.* Journal of Inorganic and Organometallic Polymers, 1999. **9**(2): p. 79-106.
103. Vlasova, N.N., Pestunovich, A., Pozhidaev, Y.N., Kirillov, A.I. and Voronkov, M.G., Izv. Sib. Otd. Akad. Nauk SSSR, Ser. Khim. Nauk, 1989. **2**.
104. Choi, K.M. and Shea, K.J., *Hybrid Materials for Electrical and Optical Application, Sol-Gel Synthesis of Bridged Polysilsesquioxanes*, in *Photonic Polymer Synthesis*, G. Wise, Wnik, G., Trantolo, M., Graham, B., Dekker, M., Editor. 1998: New York.
105. Burleigh, M.C., Markowitz, M.A, Spector, M.S and Gaber, B.P, *Porous polysilsesquioxanes for the adsorption of phenols.* Environmental science & technology, 2002. **36** (11): p. 2515-2518
106. Loy, D.A. 1991, University of California, CA: Irvine.

107. Dabrowski, A., Barczak, M., Robens, E., Stolyarchuk, N. V., Yurchenko, G. R., Matkovskii, O. K. and Zub, Y. L., *Ethylene and phenylene bridged polysilsesquioxanes functionalized by amine and thiol groups as adsorbents of volatile organic compounds.* Applied surface science, 2007. **253**(13): p. 5747-5751.
108. Honma, I.N., H., Nishikawa, O., Sugimoto, T. and Nomurab, S., *Amphiphilic Organic/Inorganic Nanohybrid Macromolecules for Intermediate-Temperature Proton Conducting Electrolyte Membranes.* J. Electrochem. Soc., 2002. **149**(10): p. A1389-A1392.
109. Lu, Y., Fan, H., Doke, N., Loy, D.A., Assink, R.A., LaVan, D.A. Brinker, C.J., *Evaporation-Induced Self-Assembly of Hybrid Bridged Silsesquioxane Film and Particulate Mesophases with Integral Organic Functionality.* J. Am. Chem. Soc, 2000. **122**: p. 5258-5261.
110. Chisem, I.C., Rafelt, J., Shieh, M.T., Chisem, J. , Clark, J.H., Jachuck, R., Macquarrie, D., Ramshawb, C. and Scottb, K., *Catalytic oxidation of alkyl aromatics using a novel silica supported Schiff base complex.* Chem. Comm. , 1998: p. 1949-1950.
111. Kirillov, A.I., Panezhda, E.V., Pozhidaev, Y.N., Belousova, L.Y., Vlasova, N.N. and Voronkov, M.G., *Silver(I) sorption with organosilicon polymer poly[N-(3-silsesquioxanylpropyl)thioacetamide].* Russian Journal of Applied Chemistry, 2000. **73**(3): p. 554-555.
112. Vlasova, N.N., Kirillov, A.I., Pozhidaev, Y.N., Panezhda, E.V., et al., *Organosilicon complexing sorbents of rare-earth elements.* Doklady Akademii Nauk, 1999. **364**(4): p. 492-494.
113. Vlasova, N.N., Pozhidaev, Y.N., Raspopina, O.Y., Belousova, L.I., et al., *Polyorganylsilsesquioxanes containing carbofunctional groups (NH)(2)C(SO2). Synthesis and sorption properties.* Russian Journal of General Chemistry, 1999. **69**(9): p. 1391-1394.
114. Gavalas, G.R., Megiris, C.E. and Nam, S.W., *Deposition of H-2-Permselective SiO_2-films.* Chemical engineering science, 1989. **44**(9): p. 1829-1835.
115. Gryaznov, V.M., Serebryannikova, O.S., Serov, Y.M., Ermilova, M.M., Karavanov, A.N., Mischenko, A.P. and Orekhova, N.V., *Preparation and catalysis over palladium composite membranes.* Applied Catalysis A, 1993. **96**(1): p. 15-23.
116. Li, Z.Y., Maeda, H., Kusakabe, K., Morooka, S., Anzai, H. and Akiyama, S., *Preparation of palladium-silver alloy membranes for hydrogen separation by the spray pyrolysis method.* Journal of Membrane Science, 1993. **78**(3): p. 247-254.
117. Schubert, D.W. and Dunkel, T., *Spin coating from a molecular point of view: its concentration regimes, influence of molar mass and distribution.* Mat. Res. Innovat., 2003|. **7**: p. 314-321.
118. Dunkel, T., *Diploma thesis*, in *GKSS Forschungszentrum & FH*. 2000: Aachen.
119. Schubert, D.W., *Spin coating as a method for polymer molecular weight determination.* Polymer Bulletin, 1997. **28**(2): p. 177-184.
120. Wertz, J. and Boday, D., *4,4'-bis(4-(triethoxysilyl)styryl)biphenyl* Prepared at the University of Arizona, Editor. 2008: Tucson.

121. Okubo, T., Miyamoto, T., Umemura, K., and Kobayashi, K., *Seed polymerization of tetraethyl orthosilicate in the presence of colloidal silica spheres.* Colloid Polym. Sci., 2001. **279**: p. 1236-1240.
122. Arroyo, R., Rodriguez, R., and Salinas, P., *Master behavior for gelation in a sol-gel process under different temperature and pH conditions.* Journal of Non-Crystalline Solids, 1993. **163**: p. 90-96.
123. Sadasivan, S., Rasmussen, D.H., Chen, F.P., and Kannabiran, R.K., *Preparation and characterization of ultrafine silica.* Colloids and Surfaces, 1998. **132**: p. 45-52.
124. Norisuye, T. and Shibayama, M., *Time-Resolved Dynamic Light Scattering Study on the Dynamics of Silica Gels during Gelation Process.* Macromolecules, 2000. **33**: p. 900-905.
125. Norisuye, T. and Shibayama, M., *Time-Resolved Dynaamic Light Scattering Studies on Gelation Process of Organic-Inorganic Polymer Hydbrids.* Macromolecules, 1999. **12**: p. 1528-1533.
126. Okubo, T., Okada, S., and Tsuchida, A., *Kinetic Study on the Colloidal Crystalliization of Silica Spheres in the Highly Diluted and Exhaustively Deionized Suspensions as Studied by Light-Scattering and Reflection Spectroscopy.* Journal of Colloid and interface science, 1997. **189**: p. 337-347.
127. Stober, W., Fink, A., and Bohn, E., *Controlled Growth of Monodisperse Silica Spheres in the Micron Size Range* J. Colloid Interface Sci., 1968. **26**: p. 62-69.

A.0. Appendices

In this chapter a full project description can be found (appendix 1), a complete list of all samples specified with quantizes of monomers, catalysts and solvents (appendix 2), SEM execution details (appendix 3), gelation data (appendix 4), size distributions (appendix 5) and atomic force microscopy size determination (appendix 6).

List of Tables

List of Figures

Appendix 1. Project description

A full project description is given below.

Engineering Membrane Selectivity for CO_2 Separation

Professor Douglas Loy, Department of Material Science and Engineering
Professor Glenn Schrader, Department of Chemical and Environmental Engineering
University of Arizona
Tucson, Arizona 85721

Suggested Research Topic for Ms. Hanne Skogestad

For Masters Degree in Chemical Engineering from the Norwegian University of Science and Technology (NTNU), Trondheim, Norway

With increasing energy costs associated with purifying gases and the need to sequester carbon dioxide from industrial processes to mitigate global warming, new, thermally robust membrane materials with improved selectivity for carbon dioxide are needed. This research focuses on preparing hybrid organic-inorganic films bearing amine, amide or urea functionalities in organic bridging groups as carbon dioxide selective membranes [1]. This project will investigate bridged polysilsesquioxanes [2] because their intimate mixing of organic and inorganic phases at the molecular level permit fundamental studies in structure property relationships to be performed. This project will focus on the development of sol-gel polymerization chemistry of amine, urea and hydrocarbon bridged polysilsesquioxanes (Scheme 1) to allow the formation of asymmetric coatings on porous ceramic supports and the development of fluorescent co-monomers to permit imaging of the thin film membranes.

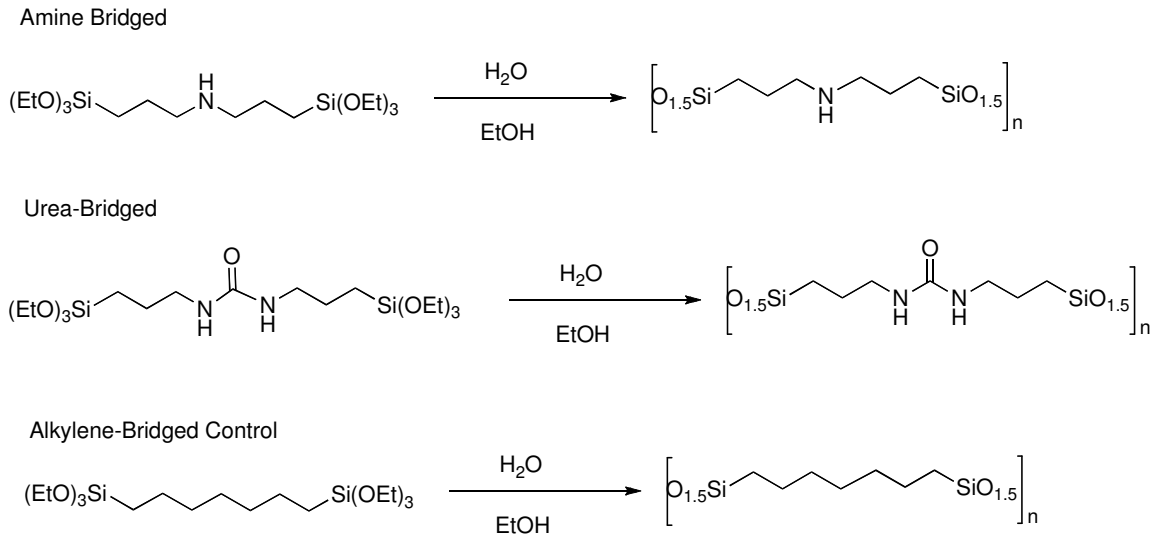

Scheme 1. Sol-gel polymerization of bridged monomers to afford, non-porous, thin film membranes for carbon dioxide selective separation.

Because the bridged polysilsesquioxanes are highly cross-linked materials, their membranes are too brittle without some support material. Therefore, the bridged polysilsesquioxanes will be prepared on porous zirconia or alumina membranes. Deposition of sol-gel processed silica films on inorganic supports has been reported before allowing ultra-thin films to be prepared [3]. In order to calculate the permeability of gases, it is important to know the thickness of the membranes on the support. Inspection of cross sections will reveal the thickness of the layer on the top of the support, but doesn't insure that the membrane material hasn't penetrated into the support. Silica membranes on alumina supports were made by growing the colloidal silica in the sol to diameters greater than the pore diameters in the support then casting or dip coating the sol onto the support [4]. This project will represent the first application of this colloidal size exclusion approach to bridged polysilsesquioxane membranes. The size of the bridged colloids as a function of polymerization pH, monomer concentration and monomer type will be monitored over time with dynamic light scattering. The size and size dispersity of the colloids in the sol will be determined.

Membranes will be prepared by growing the bridged polysilsesquioxane colloids to a size larger than that of the pores in the surface of the mesoporous support then

casting the sol onto the support to create a thin, inorganic supported, hybrid membrane. This approach allows membranes of controlled thickness to be prepared because all of the hybrid will be on the surface of the support and not extending into the microporous structure. This approach also permits membranes to be prepared by applying the sol to the support membrane and allowing the membrane to be sealed by the colloid particles. In this manner any leaks in the membrane will be sealed as the sol is drawn towards the defect or gap in the coating by the flow of solvent. In order to ensure that the membrane is located only on top of the support, the hybrid colloid will be prepared with a small amount of a fluorescent co-monomer (Scheme 2) that will fluoresce under ultraviolet. Any material that has penetrated into the support will show up under ultraviolet light. Microscopic inspection of the cross-sections can also provide destructive characterization.

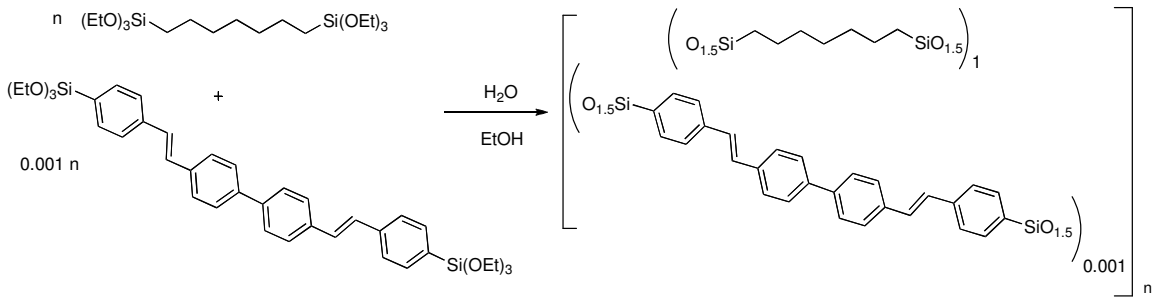

Scheme 2. Sol-gel polymerization of colloid with blue fluorescent dye bridged monomer to image hybrid thin film in asymmetric membranes.

This work will provide a new, efficient route to preparing bridged polysilsesquioxane membranes for gas separations. It will provide the first study of the colloidal species formed by the sol-gel polymerizations of bridged monomers using light scattering. It will also represent the first time hybrid colloids of controlled size are used to prepare membranes using size exclusion and fouling to create ultra thin membranes on porous ceramic supports. Lastly, it will be the first time that a fluorescent monomer has been used to image the thin film, working layer of an asymmetric membrane. This work will

provide the foundations for significant new developments in sol-gel based membranes and for gas separation membranes in general.

[1] Cong, H.; Radosz, M.; Towler, B. F.; Shen, Y. *Separ. Purific. Techn.* **2007**, *55*, 281.
[2] Shea, K.J.; Loy, D. A., *Chem. Mater.* **2001**, *13*, 3306.
[3] Morooka, S.; Kusakabe, K. *MRS Bull.* **1999**, *24*, 25.
[4] Cao, Guozhong; Lu, Yunfeng; Delattre, Laurent; Brinker, C. Jeffrey; Lopez, Gabriel P. *Adv. Mater.* **1996**, *8*, 588.

Appendix 2. Experimental Data sheet

Some physical data of the monomers are given in Table A.1, and a complete list of all samples specified with quantities of monomers, catalysts and solvents can be found in Table A.2.

Table A. 1 Physical Data of Monomers

Name	Molecular weight [g/mol]	Density [g/mL]
BESO	438,75	0,98
Amine	425,71	Unknown
Urea	440,66	Unknown
TEOS	208,33	0,94

Table A. 2 Experimental Data Sheet

Sample name		**Monomer**			**Catalyst**				**Eqv. of H20**	**EtOH**	**Tot. vol.**	**Conc.**	**Solvent**	**Date of preparation**
	name	[g]	[mol]	mL	type	mL	g	mol		mL	mL	mol/L	type	
Amine (0.05 M) w fluor	Amine	0,2129	0,0005	-	H_20	0,0541	0,0541	0,0030	6,3	-	10	0,05	EtOH	May 13
Amine (0.05 M) [I]	Amine	0,2088	0,0005	-	H_20	0,0546	0,0546	0,0030	6,5	-	10	0,05	EtOH	May 14
Amine 0.1	Amine	0,4441	0,001	-	H_20	0,1096	0,1096	0,0061	5,8	-	10	0,10	EtOH	Apr 15
Amine 0.2	Amine	0,8962	0,002	-	H_20	0,2134	0,2134	0,0118	5,9	-	10	0,20	EtOH	Apr 10
Amine 0.4	Amine	1,7919	0,004	-	H_20	0,4333	0,4333	0,0240	6,0	-	10	0,40	EtOH	Apr 9
a)	BESO	2,6314	0,006	2,6851	HCl	0,648	0,6480	0,0360	6,0	6,7	10,03	0,60	EtOH	Mar 13
b)	BESO	2,6321	0,006	2,6859	HCl	0,6468	0,6468	0,0359	6,0	6,7	10,03	0,60	THF	Mar 13
BESO 0.1 [I]	BESO	0,4374	0,001	0,4463	HCl	0,1022	0,1022	0,0057	5,7	9,451	10	0,10	EtOH	Apr 22

Table A.2. continues…

Sample name	Monomer				Catalyst				Eqv. of H20	EtOH	Tot. volume	Conc.	Solvent	Date of preparation
	name	[g]	[mol]	mL	type	mL	g	mol		mL	mL	mol/L	type	
BESO (0.2 M) w fluor [I]	BESO	0,8789	0,002	0,8969	HCl	0,2214	0,2214	0,0123	6,1	8,882	10	0,20	EtOH	May 1
BESO (0.2 M) w fluor[II]	BESO	0,8806	0,002	0,8986	HCl	0,2173	0,2173	0,0121	6,0	8,884	10	0,20	EtOH	May 6
c)	BESO	1,7525	0,004	1,7883	HCl	0,4495	0,4495	0,0249	6,2	7,8	10,04	0,40	EtOH	Mar 13
d)	BESO	1,7552	0,004	1,7911	NH_3	0,434	0,4340	0,0241	6,0	7,8	10,03	0,40	EtOH	Mar 13
e)	BESO	0,8778	0,002	0,8957	HCl	0,2218	0,2218	0,0123	6,2	8,9	10	0,20	EtOH	Mar 19
e) [2]	BESO	0,8773	0,002	0,8952	HCl	0,2167	0,2167	0,0120	6,0	8,9	10	0,20	EtOH	Apr 1
e) [3]	BESO	0,8780	0,002	0,8959	HCl	0,2175	0,2175	0,0121	6,0	8,9	10	0,20	EtOH	Apr 1
e) [4]	BESO	0,8775	0,002	0,8954	HCl	0,2171	0,2171	0,0120	6,0	8,9	10	0,20	EtOH	Apr 1
e) [5]	BESO	0,8771	0,002	0,8950	HCl	0,2172	0,2172	0,0121	6,0	8,888	10	0,20	EtOH	May 6
f)	BESO	0,8786	0,002	0,8965	HCl	0,2169	0,2169	0,0120	6,0	8,9	10	0,20	THF	Mar 19
g) [I]	BESO	1,7552	0,004	1,7911	HCl	0,4331	0,4331	0,0240	6,0	7,8	10	0,40	EtOH	Mar 19
g) [II]	BESO	1,7550	0,004	1,7908	HCl	0,4388	0,4388	0,0244	6,1	7,8	10	0,40	EtOH	Apr 1
h)	BESO	1,7550	0,004	1,7908	HCl	0,432	0,4320	0,0240	6,0	7,8	10	0,40	THF	Mar 19
i)	BESO	2,6325	0,006	2,6863	HCl	0,6474	0,6474	0,0359	6,0	6,7	10	0,60	EtOH	Mar 27
TEOS 0.2 [I]	TEOS	0,4178	0,002	0,4468	HCl	0,1456	0,1456	0,0081	4,0	9,408	10	0,20	EtOH	Apr 22
TEOS 2.0 [I]	TEOS	4,1683	0,020	4,4581	HCl	2,1743	2,1743	0,1207	6,0	3,368	10	2,00	EtOH	Apr 28
TEOS 1.0 [I]	TEOS	2,0801	0,010	2,2247	HCl	0,7257	0,7257	0,0403	4,0	7,05	10	1,00	EtOH	May 13
Urea (0.2 M) w fluor	Urea	1,4682	0,002	-	HCl	0,2175	0,2175	0,0121	6,0	-	10	0,20	EtOH	May 6
Urea (0.2 M) [I]	Urea	1,4680	0,002	-	HCl	0,2161	0,2161	0,0120	6,0	-	10	0,20	EtOH	May 6
Urea 0.4 [I]	Urea	2,7113	0,004	-	HCl	0,4334	0,4334	0,0241	6,5	-	10	0,37	EtOH	Apr 9
Urea (0.4 M) w fluor	Urea	2,9385	0,004	-	HCl	0,4295	0,4295	0,0238	6,0	-	10	0,40	EtOH	May 28
Urea (0.4 M) [II]	Urea	2,9361	0,004	-	HCl	0,4318	0,4318	0,0240	6,0	-	10	0,40	EtOH	May 28
Urea 0.4 KOH [I]	Urea	2,9373	0,004	-	HCl	0,4333	0,4333	0,0240	6,0	-	10	0,37	EtOH	Apr16
Urea 0.6 [I]	Urea	4,4060	0,006	-	HCl	0,6487	0,6487	0,0360	6,0	-	10	0,60	EtOH	May 28
Urea 0.6 w fluor [I]	Urea	4,4070	0,006	-	HCl	0,649	0,6490	0,0360	6,0	-	10		EtOH	May 28

Table A.2. continues…

Sample name		Monomer			Catalyst				Eqv. of H20	EtOH	Tot. volume	Conc.	Solvent	Date of preparation
	name	[g]	[mol]	mL	type	mL	g	mol		mL	mL	mol/L	type	
I	BESO	1,7542	0,004	1,7900	HCl	0,043	0,0430	0,0024	0,6	10	11,83	0,34	EtOH	Feb 14
II	BESO	0,8782	0,002	0,8782	HCl	0,043	0,0430	0,0024	1,2	10	10,92	0,18	EtOH	Feb 14
III	BESO	1,7550	0,004	1,7908	HCl	0,043	0,0430	0,0024	0,6	10	11,83	0,34	EtOH	Feb 14
IV	BESO	0,8771	0,002	0,8950	NH_3	0,043	0,0430	0,0024	1,2	10	10,94	0,22	EtOH	Feb 26
V	BESO	0,8775	0,002	0,8954	HCl	0,043	0,0430	0,0024	1,2	10	10,94	0,18	THF	Feb 26
VI	BESO	0,8779	0,002	0,8958	HCl	0,043	0,0430	0,0024	1,2	10	10,94	0,18	EtOH	Feb 26
VII	BESO	1,7548	0,004	1,7906	NH_3	0,043	0,0430	0,0024	0,6	10	11,83	0,20	THF	Feb 26
VIII	BESO	3,5082	0,008	3,5799	HCl	0,173	0,1730	0,0096	1,2	10	13,75	0,58	EtOH	Mar 4
IX	BESO	3,5083	0,008	3,5800	NH_3	0,173	0,1730	0,0096	1,2	10	13,75	0,58	EtOH	Mar 4
X	BESO	3,5085	0,008	3,5802	HCl	0,173	0,1730	0,0096	1,2	10	13,75	0,58	THF	Mar 4
XI	BESO	3,5000	0,008	3,5715	NH_3	0,173	0,1730	0,0096	1,2	10	13,74	0,58	THF	Mar 4

Appendix 3. SEM details

Details of the SEM execution is given in Table A.3.

Table A.3. SEM execution details

Name	*Amine [0.1M] (04/15).*	*Urea [0.4] (04/09)*
InstructName	S-4800	S-4800
SerialNumber	HI-9137-0001	HI-9137-0001
SampleName	Amine2	Urea
Format	tif	tif
ImageName	Amine_2_q28.tif	Urea_2_q30.tif
Date	05.01.2008	05.01.2008
Time	10:30:37	11:02:11
Media	RE[ ]	RE[ ]
DataSize	2560x1920	2560x1920
PixelSize	0.1984375	0.1653646
SignalName	SE(U)	SE(U)
AcceleratingVoltage	15000 Volt	15000 Volt
DecelerationVoltage	0 Volt	0 Volt
Magnification	250000	300000
WorkingDistance	9200 um	9300 um
EmissionCurrent	8200 nA	9800 nA
LensMode	High	High
PhotoSize	1000	1000
MicronMarker	200	100
SubMagnification	0	0
SpecimenBias	0	0
Condencer1	14000	Co14000
ScanSpeed	Slow4	Slow3
CalibrationScanSpeed	25	25
ColorMode	Grayscale	Grayscale
ScreenMode	Small Screen	Small Screen
Condition	Vacc=15kV	Vacc=15kV
Mag	x250k	x300k
WD	9.2mm	9.3mm
DataDisplayCombine	1	1
StageType	5	5
StagePosition X	40542000	37727000
StagePosition Y	54810000	49597000
StagePosition R	0	0
StagePosition Z	8000000	8000000
StagePosition T	0	0

Appendix 4. Geleation Data

The following table represents the various gelation times of the different samples, and also a description of their appearances two weeks later is presented. Some of the gelation times are not known because these gels were not continuously monitored, and an exact time could not be given.

Table A. 4. Geleation Data

Sample	Date prepared	Monomer conc. (mo/L)	Catalyst	Solvent	Equiv. of H2O	Gelation time	Size before geleation (nm)	Color	Ageing
Amine 0.1	15.apr	0,01	None	EtOH	5,98	~ 20 days	11	tinted blue	shrinkage, some cracks
Amine 0.2	10.apr	0,21	None	EtOH	5,92	~ 3 days	~3-4	white trans	some liquid, no cracks
Amine 0.4	09.apr	0,4	None	EtOH	6,01	~ 1 day	Unknown	white trans	some liquid, some cracks
Sample a)	13.mar	0,60	HCl	EtOH	6,00	5 mins	unknown	clear	some liquid, many cracks
Sample b)	13.mar	0,60	HCl	THF	5,98	6 mins	4.629 (geled)	clear	some liquid, some cracks
BESO (0.2M) w spheres	May 7	0,20	HCl	EtOH	6,00	~ 43 days	~50 nm	white (trans)	some liquid, no cracks
c)	13.mar	0,40	HCl	EtOH	6,25	60 mins	2.332 (10 mins)	tinted blue	some liquid some craks
d)	March 13	0,40	NH_3	EtOH	6,02	<3 months	~ 200 nm	white	gelation not uniform
e [III]	10.apr	0,20	HCl	EtOH	6,03	~2 months	35	tinted blue	some liquid, no cracks
f [I]	March 19	0,20	HCl	THF	6,00	~ 3 weeks	unknown	clear	no cracks or liquid
g) [I]	19.mar	0,48	HCl	EtOH	6,01	85 mins	3.479 (68 mins)	tinted blue	no cracks, some liquid
g) [II]	01.apr	0,44	HCl	EtOH	6,09	92 min	3.133 (58 mins)	tinted blue	no cracks, some liquid
h)	19.mar	0,44	HCl	THF	8,77	6 mins	unknown	clear	no liquid, some cracks
i)	27.mar	0,60	HCl	EtOH	5,99	7 mins	3.356 (geled)	clear	liquid, no cracks
KOH	04.apr	0,40	KOH	MeOH	6,02	45 mins	35	white	some liquid, no cracks
NaOH	04.apr	0,40	NaOH	MeOH	6,04	38 mins	37	white (trans)	no liquid, some cracks
TEOS 2.0	28.apr	2,00	HCl	EtOH	6,00	7 days	unknown	clear	shrinkage, some cracks
Urea 0.6 w fluor	May 28	0,60	HCl	EtOH	6,00	<1 day	unknown	Light yellow	little liquid, no cracks
Urea 0.4 KOH	15.apr	0,4	KOH	EtOH	5,96	~ 3 hours	4 nm	clear	some liquid, some cracks
VIII	04.mar	0,58	HCl	EtOH	1,20	~1200	unknown	tinted blue	lots of liquid and cracks
X	04.mar	0,58	HCl	THF	1,20	45 mins	unknown	clear	no liquid, little cracks

Appendix 5. Size distributions

To keep track of the size distributions in the sol-gels, size distributions plots were made for Amine (0.05 M) with and without fluorescence (Figure A.1-2), Urea (0.2 M) with and without fluorescence (Figure A.3-4), Sample II (Figure A.5) and the plots for Urea (0.4 M) with and without fluorescence (Figure A.6-7), sample d (Figure A.8), sample f (Figure A.9) and Urea (0.4 M) KOH (Figure A.10) were directly copied from the software provided by Malvern. All plots are based on a number distribution (see Chapter 3.5.5)

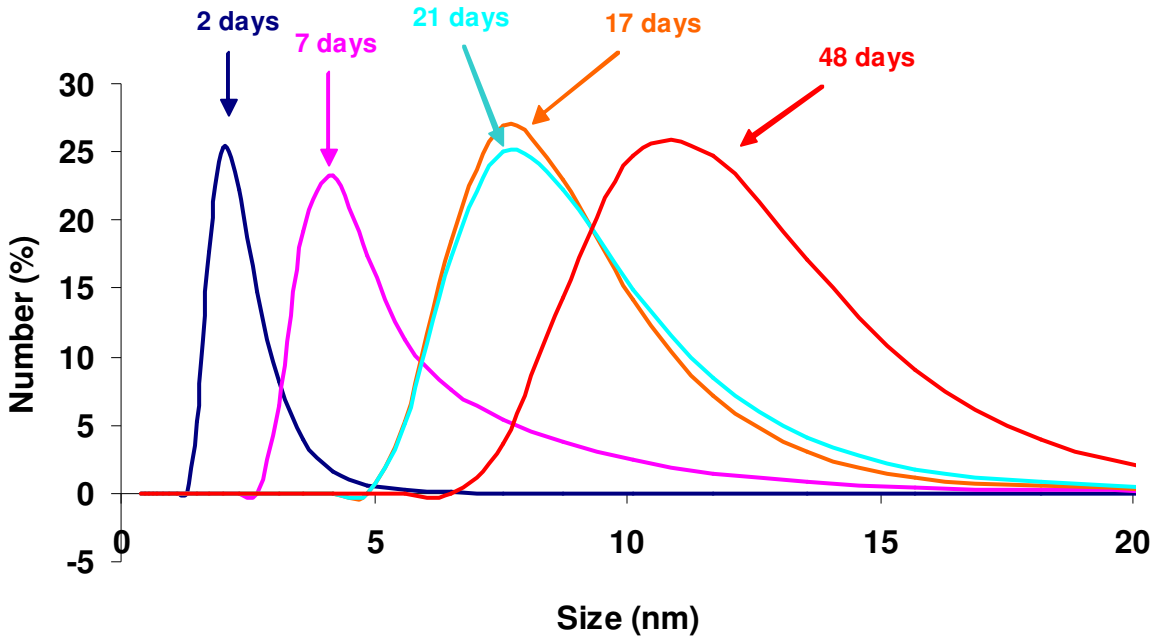

Figure A. 1. Size distriubution plot for Amine 0.05 M

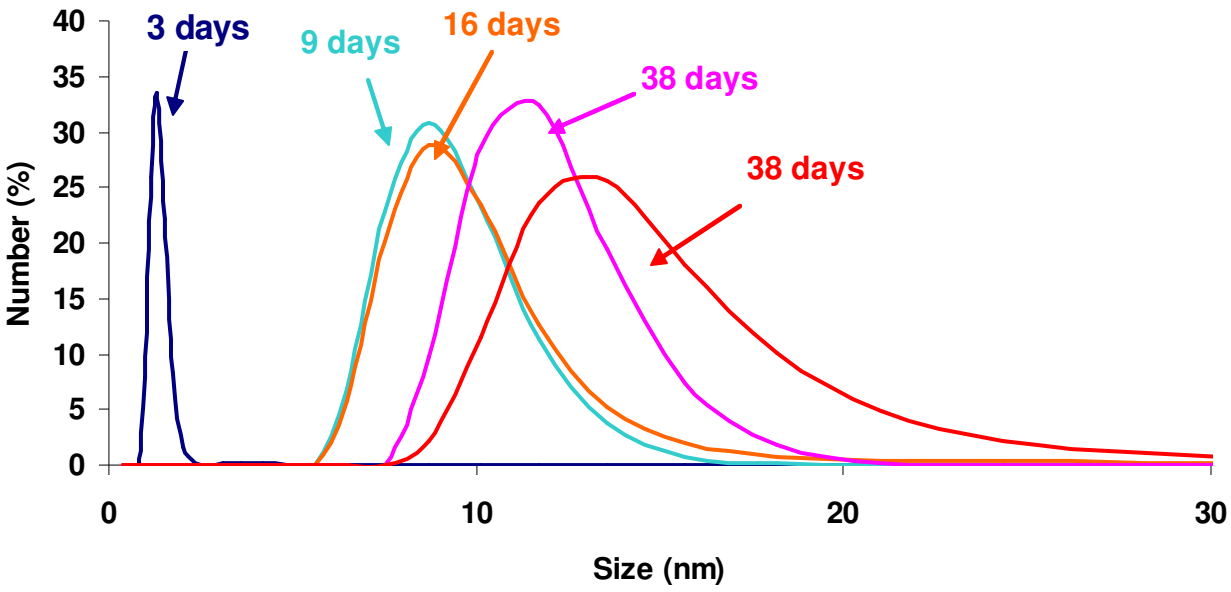

Figure A. 2. Size distriubution plot for Amine 0.05 M with fluorescence

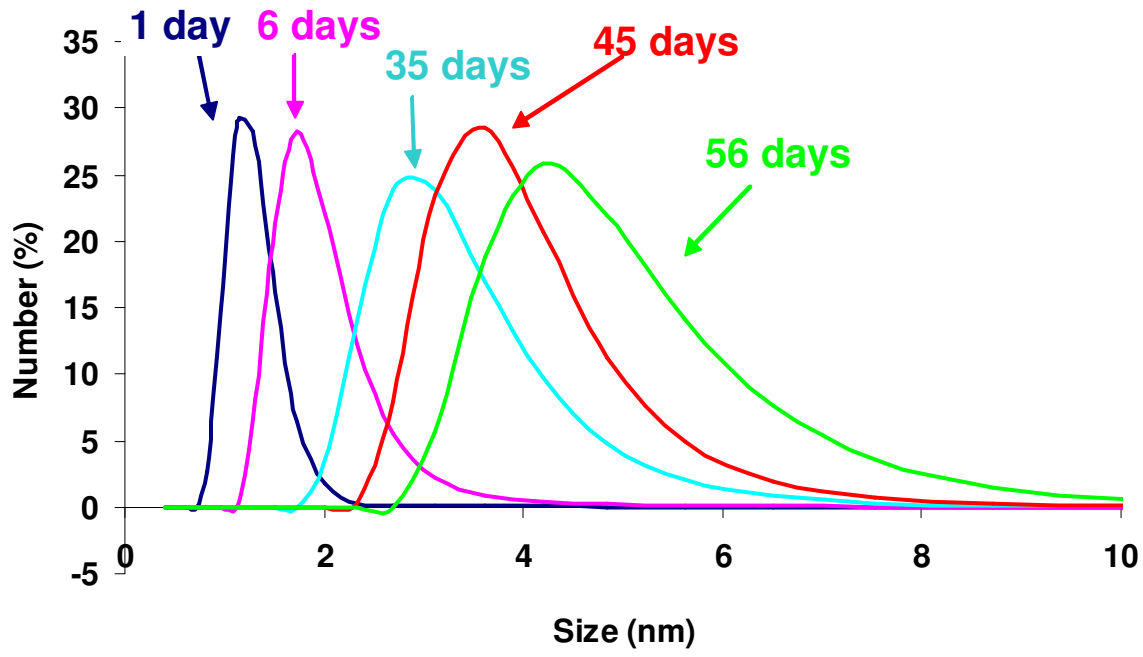

Figure A. 3. Size distriubution plot for Urea (0.2M)

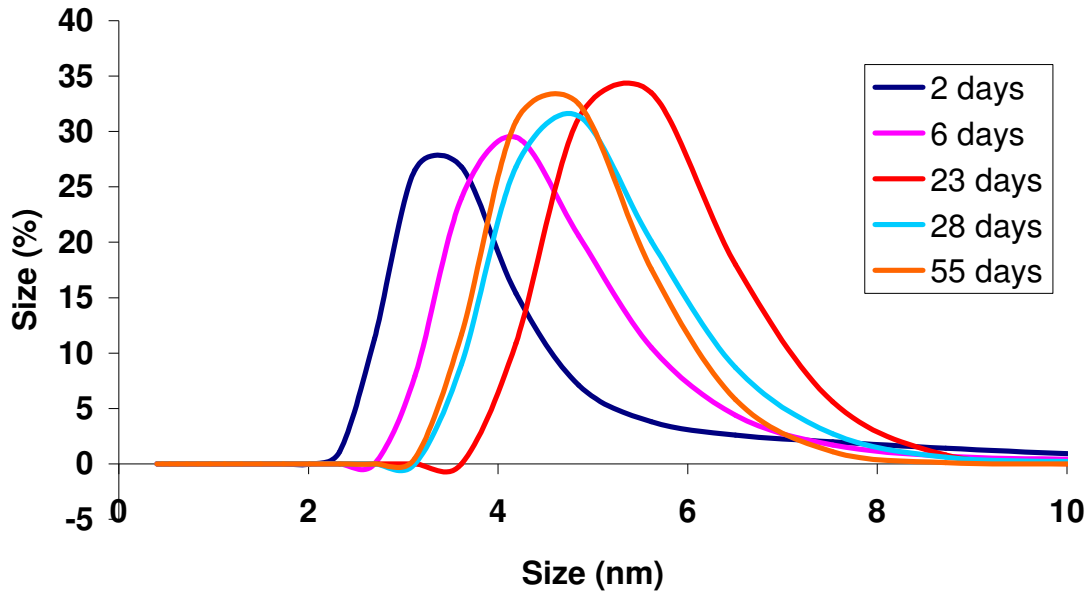

Figure A. 4. Size distriubution plot for Urea [0.2 M] fluorescence (05.06)

Urea with and without fluorescene (Figure A.3 and A.4, respectively), produce relatively monodisperse solution which is promising for producing uniform films.

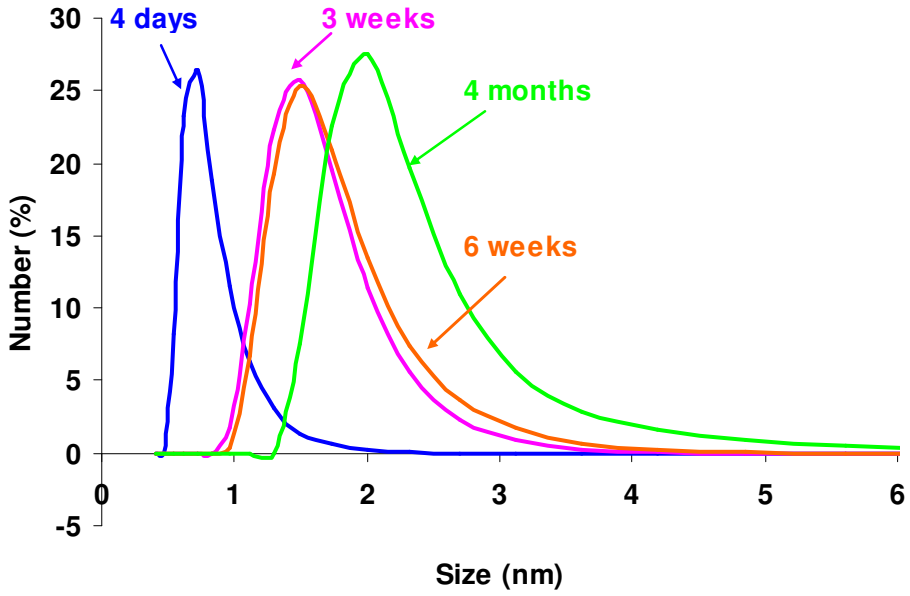

Figure A. 5. Size distriubution plot by number for BESO [2.0] (Sample II, insufficient water)

The sample prepared with insufficient water is relatively monodisperse, after 4 months the size distribution is between 1-6 nm. However, the growth rate is too slow for any practial use, i.e. industry.

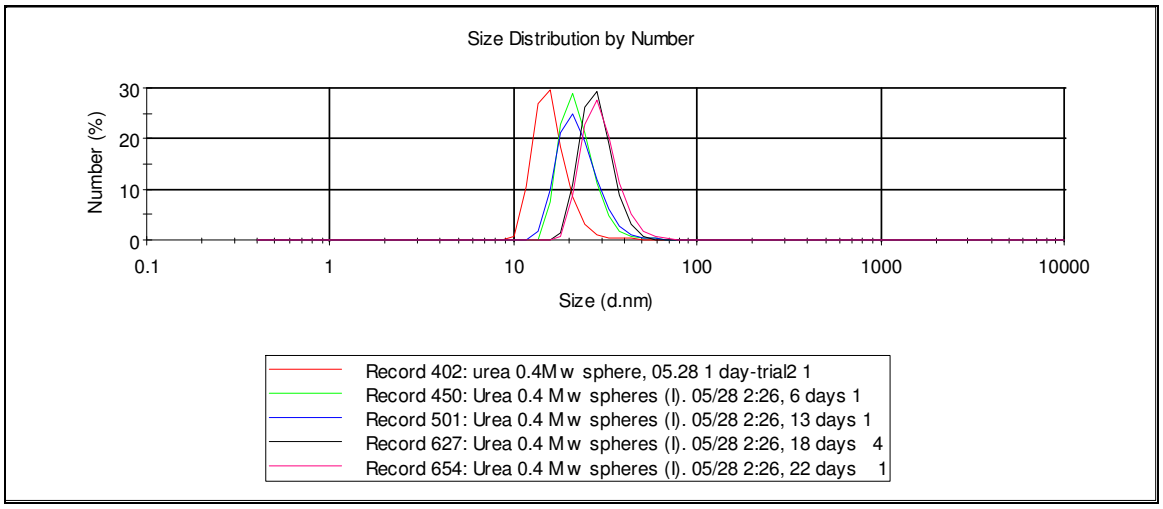

Figure A. 6. Size distribution plot by number for Urea [0.4 M] w fluoresence

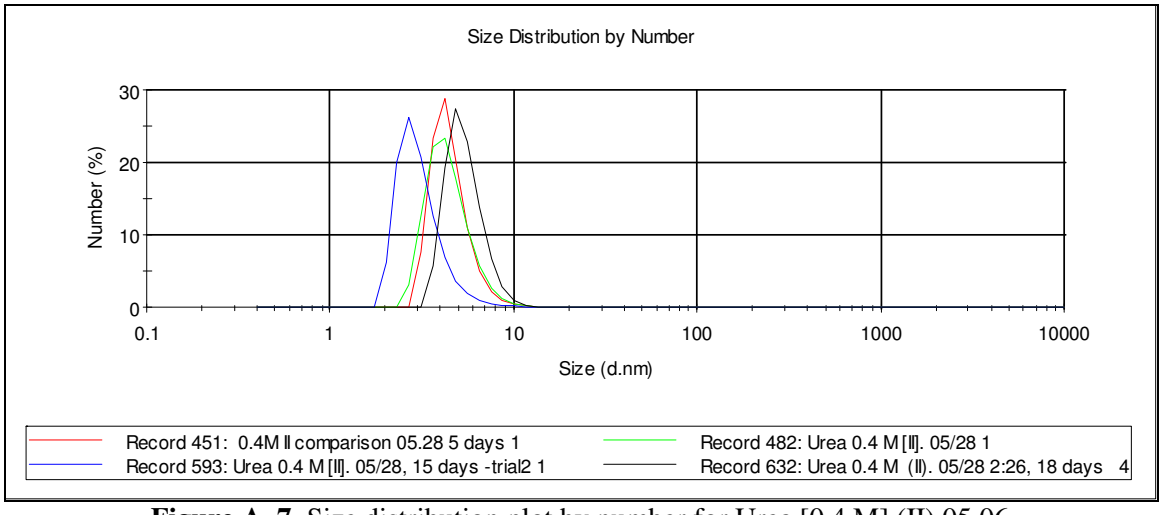

Figure A. 7. Size distribution plot by number for Urea [0.4 M] (II) 05.06

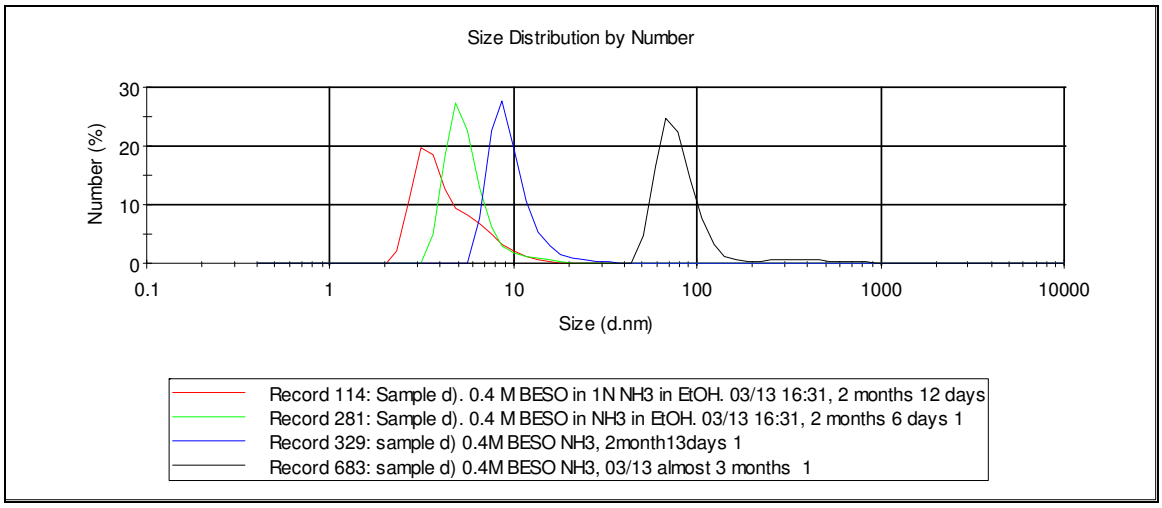

Figure A. 8. Size distribution plot by number for Sample d), BESO [0.4 M] w NH_3

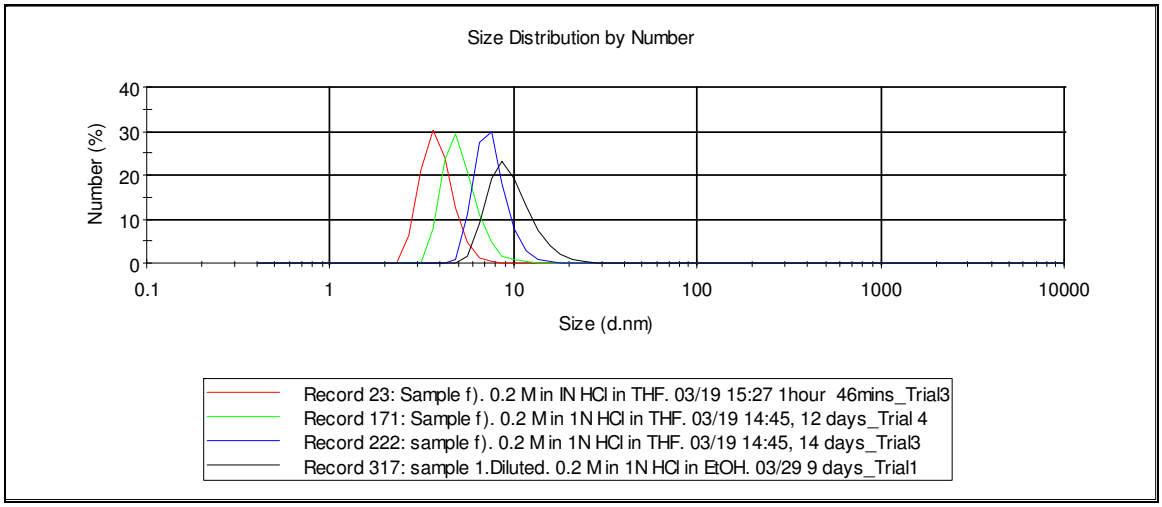

Figure A. 9. Size distribution plot by number for Sample f , BESO [0.2 M] in THF

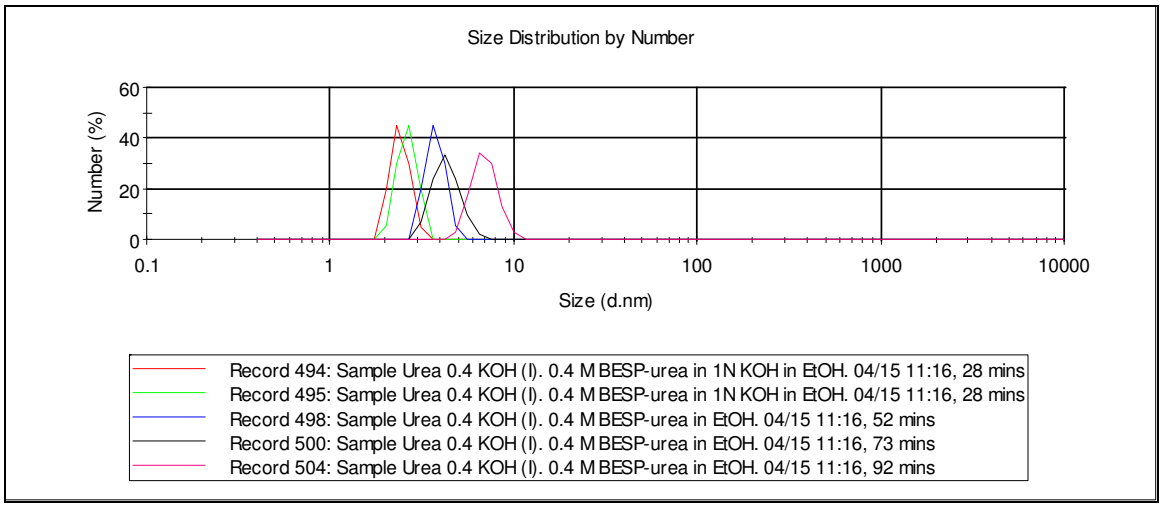

Figure A. 10. Size distribution plot by number for Urea [0.4M] KOH (05.15)

Appendix 6. Atomic Force Microscopy analysis

The atomic force microscopy size determination was done by section analysis of the horizontal distance (Figure A.13)

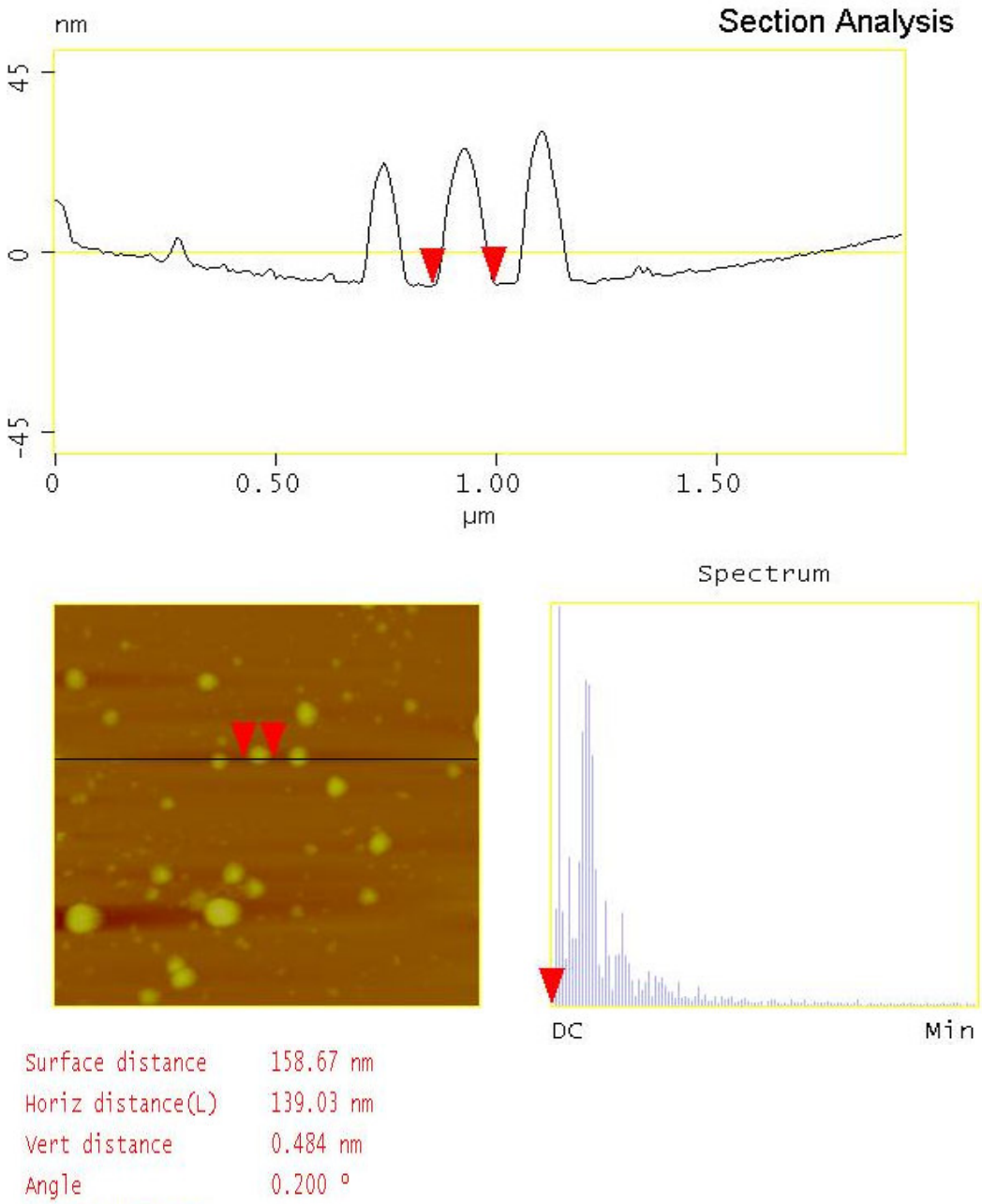

Figure A. 11. Atomic Force Microscopy size determination by section analysis of the horizontal distance